Evaluation of Autoregulated RUNX2 Suppression on Mesenchymal Stem Cell-based Cartilage Regeneration in Complex Pathological Environments

by

Gurcharan Kaur

A dissertation submitted in partial fulfillment
of the requirements for the degree of
Doctor of Philosophy
(Biomedical Engineering)
in the University of Michigan
2023

Doctoral Committee:

Associate Professor Rhima Coleman, Chair
Associate Professor Kelly Arnold
Assistant Professor Tristan Maerz
Professor Jan Stegemann

Gurcharan Kaur

gckaur@umich.edu

ORCID iD: 0000-0002-1000-4115

Dedication

To my husband, Antarpreet, for your unconditional love, support, and encouragement.

To my family, for your love, support and sacrifice that has brought me to where I am today.

To my *Guru*, the perfect master for his abundant love and grace.

Acknowledgements

First, I would like to thank my advisor Dr. Rhima Coleman for being a great mentor and giving me the opportunity to work in her lab. Thank you for believing in me and giving me the freedom to pursue my research interests. You taught me that it's okay to make mistakes and that failure is really a steppingstone towards success. I am grateful for the encouragement and outstanding mentorship you gave me that has resulted in the successful completion of this journey.

I would also like to thank my dissertation committee, Dr. Jan Stegemann, Dr. Kelly Arnold and Dr. Tristan Maerz for their time and effort devoted to the progress of my thesis. You provided great insights into my research and your thought-provoking feedback greatly improved the rigor and quality of my work. In addition to serving as my committee members, I also got to collaborate with Dr. Tristan Maerz and Dr. Jan Stegemann on various research projects. You encouraged me to be a conscientious researcher and helped develop critical thinking skills that deeply enriched my PhD experience.

Next, I want to thank the current and former members of the CHARM lab, Dr. Biming Wu, Ciara Davis, Dr. Tiana Wong, Dr. Yue Qin, Yuqian Yang, Lauren Terry, Amanda Liss, Dr. Ryan Rosario, Sunny Karnan and Justin Redmond for being great colleagues and friends and supporting me throughout my PhD. Especially to Ciara, Tiana, Yue and Lauren, I am grateful for every light and deep conversation we've had, all the laughs we shared and the hugs that made bad days a little better. I really appreciate your support in both good and challenging times of this tremendous journey.

In addition to my lab members, I was fortunate to collaborate with Nick Schott, Easton Farrell, Alexander Knights, Emily Margolis and Yadav Wagley on multiple exciting projects. I learnt a lot from working with and learning from all of you and your insights definitely increased the potential and impact of my work. In addition to a professional relationship, Nick and Emily also became my good friends and I am very grateful for their support and encouragement.

I am thankful to the BME staff, especially Maria Steele and Tonya Thompson who helped me with administrative requirements. I am also thankful to Rackham Graduate School for the Rackham Pre-doctoral Fellowship for funding me during the final year of my PhD.

Table of Contents

List of Tables

List of Figures

List of Appendices

Abstract

Articular cartilage has limited healing capability, resulting in cartilage injuries to often progress into post traumatic osteoarthritis (PTOA), a painful debilitating disease. Adult human mesenchymal stem cell (hMSC)-based tissue engineering strategies have been widely explored to achieve functional cartilage repair due to their ability to differentiate into chondrocytes and secrete cartilage matrix macromolecules collagen II and aggrecan. However, clinical application of MSC-based cartilage repair strategies faces two significant challenges. First, upon chondrogenic differentiation, MSC-derived chondrocytes (hMdChs) undergo hypertrophic maturation driven by master transcription factor RUNX2. Second, the inflammatory environment of the injured joint, established predominantly by pro-inflammatory macrophages, accelerates chondrocyte hypertrophy and matrix degradation, a process also mediated by RUNX2 activity. Inflammatory cytokines induce hMdChs to secrete further inflammatory and catabolic factors, establishing a positive feed forward loop that sustains the joint inflammation. This results in matrix loss which compromises the functionality of engineered cartilage.

The central objective of this thesis is to increase matrix accumulation and retention by hMdChs under hypertrophic and inflammatory conditions to improve cartilage regeneration. We hypothesize RUNX2 suppression can increase matrix accumulation by 1) maintaining the production of cartilage structural proteins, 2) protecting the cells from hypertrophy and inflammation induced matrix degradation by inhibiting matrix metalloproteinase (MMP) expression and, 3) inhibiting the pro-inflammatory crosstalk between hMdChs and M1 macrophages. To evaluate these hypotheses, we used a synthetic gene circuit that induces

autonomous and tunable RUNX2 suppression in hMdChs based on intracellular RUNX2 concentrations.

In Aim 1, I show that suppressing RUNX2 activity using our gene circuit increases matrix accumulation and inhibits matrix mineralization under hypertrophic conditions. Moreover, RUNX2 suppression stabilizes the expression of chondrogenic markers collagen II and aggrecan and inhibits the expression of hypertrophic markers MMP13 and collagen X in hMdChs under hypertrophic stimulus. These results indicate that the gene circuit increases the stability of hMdCh chondrogenic phenotype.

In Aim 2, I show that RUNX2 suppression protects hMdChs from inflammatory cytokine IL-1β induced cartilage matrix catabolism. Moreover, I show that under inflammatory stimulus, RUNX2 suppression in hMdChs increases matrix retention by preserving the expression of cartilage matrix macromolecules and inhibiting the expression of hypertrophic and catabolic markers.

In Aim 3, using a conditioned media-based co-culture model to recapitulate the injured joint environment, I show that RUNX2 suppression protects hMdChs from M1 conditioned media (M1CM) induced matrix catabolism partly by inhibiting MMP13 expression. Moreover, RUNX2 suppression abates the pro-inflammatory response of hMdChs to M1CM. Finally, pro-inflammatory M1 macrophages treated with the secretome of RUNX2 suppressing hMdChs exhibited downregulation of inflammatory markers and upregulation of anti-inflammatory markers indicating a shift towards anti-inflammatory phenotype.

This thesis reveals that RUNX2 mediates many pathological features of PTOA progression. Although the role of RUNX2 in mediating hypertrophy and cartilage matrix catabolism is well known, I demonstrate the application of autoregulated gene circuits to study the

RUNX2 mediated pro-inflammatory crosstalk between hMdChs and pro-inflammatory macrophages that reinforces macrophage inflammation, resulting PTOA progression. As demonstrated in this dissertation, the ability to concomitantly improve cartilage matrix accumulation and resolve joint inflammation utilizing autoregulated gene circuits, is a significant step towards clinical application of MSC-based tissue engineering strategies for cartilage regeneration

Chapter 1 Introduction

Articular cartilage, the connective tissue present at the end of long bones, facilitates transmission of high loads during joint movement[1]. However, due to its avascular nature, articular cartilage has limited healing capacity upon injury. Inadequate healing along with persistent mechanical stress due to joint movement often result in progression of a cartilage defect towards post-traumatic osteoarthritis (PTOA)[2,3]. Osteoarthritis is the 3rd most common musculoskeletal disease and 11th highest contributor to disability. PTOA cases make up 12% of more than 300 million worldwide cases of OA[4]. Therefore, exogenous intervention is often necessary for repair of injured/ damaged cartilage tissue. Furthermore, cartilage injury results in a hostile inflammatory joint environment that impedes the clinical success of cartilage repair strategies[5]. Current treatment options for cartilage defects, such as microfracture, subchondral bone transplantation or (matrix assisted-) articular chondrocyte implantation (M/ ACI) have shown limited success and still do not fully restore cartilage function[2,6]. Therefore, tissue engineering- based strategies have been explored to develop cartilage regeneration therapies[7,8].

Mesenchymal stem cells (MSCs) are an appealing cell source for cartilage tissue engineering as they can differentiate into chondrocytes and produce cartilage matrix molecules[9–11]. However, clinical application of MSC-based cartilage repair strategies faces significant challenges. First, upon chondrogenic differentiation, MSC-derived chondrocytes (MdChs) undergo hypertrophic maturation driven by the master transcription factor (TF) runt related transcription factor 2 or RUNX2, which decreases the expression of cartilage matrix

macromolecules and increases expression of matrix degrading enzymes like matrix metalloproteinases (MMPs)[12–15]. Therefore, there is a need for strategies that stabilize MdCh phenotype and inhibit hypertrophic maturation. Second, the inflammatory environment of the injured joint also accelerates, and exacerbates chondrocyte hypertrophy and matrix degradation by further inducing RUNX2 expression[16–19]. Macrophages are the predominant immune cell types in the synovium that mediate inflammation[20–23]. Inflammatory cytokines produced by pro-inflammatory M1-like macrophages also induce MdChs to further secrete more inflammatory and catabolic factors, establishing a positive feed forward loop that sustains the joint inflammation[20,21,24]. This results in matrix loss which compromises the functionality of the engineered cartilage. Therefore, strategies that can protect hMdChs from inflammation induced matrix loss while simultaneously attenuating inflammation are desirable.

1.1 Thesis Objectives

The overarching goal of this thesis is to improve MSC-based cartilage repair in complex pathological environments. The role of RUNX2 in driving hypertrophic maturation and mediating the catabolic effects of inflammation has been well established, making it an ideal target to achieve this objective. The central hypothesis is that RUNX2 suppression will increase cartilage matrix accumulation by human MdChs (hMdChs) by stabilizing the chondrogenic phenotype and inhibiting the expression of matrix degrading enzymes. Since RUNX2 is required for chondrogenesis, our lab previously developed RNAi strategies to target RUNX2 expression in hMdChs using synthetic gene circuits that allow temporal control over RUNX2 expression based on intracellular RUNX2 concentrations[25]. Using lentiviral transduction to modify MSCs with the gene circuits, we tested our hypothesis in the following Specific Aims:

Aim 1: To determine the effect of RUNX2 suppression on hMdCh matrix accumulation under hypertrophic conditions.

Studies have shown that T3 and βGP accelerate hypertrophic maturation of hMdChs and induce matrix mineralization[26–28]. Therefore, in this aim we utilized a combination of T3 and βGP to induce hypertrophic maturation in hMdChs. Utilizing unmodified WT and gene circuit modified MSCs, the objective was to analyze the effect of low and high levels of RUNX2 suppression on cartilage matrix accrual, matrix mineralization and expression of chondrogenic and hypertrophic markers in hMdChs under hypertrophic stimuli.

Aim 2: To determine the effect of RUNX2 suppression in hMdChs on inflammation induced cartilage matrix catabolism.

Inflammation is a key contributor towards progression of PTOA and multiple studies have implicated the inflammatory cytokines IL-1β and TNF-α in PTOA pathogenesis[5,29]. The objective of this study was to analyze the effect of RUNX2 suppression in hMdChs on the catabolic and hypertrophic effects of IL-1β and TNF-α. WT and gene circuit modified cells were treated with IL-1β or TNF-α and the effect on RUNX2 activity, cartilage matrix accumulation and expression of chondrogenic and hypertrophic markers was analyzed.

Aim 3: To determine the effect of RUNX2 suppression in hMdChs on pro-inflammatory crosstalk between hMdChs and M1 macrophages.

Pro-inflammatory M1 macrophages are the predominant immune cells that mediate inflammation in the knee joint post injury. These cells engage in pro-inflammatory crosstalk with chondrocytes, creating a vicious cycle that sustains joint inflammation[22–24]. The objective of this aim is to analyze the effect of RUNX2 suppression in hMdChs on their pro-inflammatory response towards macrophage inflammation. First, we investigated the effect RUNX2 suppression on matrix

accumulation and expression of chondrogenic, hypertrophic and inflammatory markers in hMdChs upon treatment with conditioned media from inflammatory M1-like macrophages. Second, we investigated the effect of the double conditioned media from M1CM treated hMdChs on the inflammatory macrophage phenotype to analyze the role of RUNX2 in mediating pro-inflammatory crosstalk between hMdChs and pro-inflammatory macrophages.

1.2 Preview of Thesis

This thesis is designed to provide a comprehensive background and motivation for the overall project followed by the background, methods, results, discussion, and conclusions for each specific aims. Finally, the overall conclusions and description of future directions for this work are laid out the final chapter. A summary of the chapters are as follows:

Chapter 2 provides a broad background of articular cartilage architecture, function, inadequate repair post injury and pathology of osteoarthritis. This chapter discusses the limitation of current treatments for articular cartilage repair and explores advancement in tissue engineering based articular cartilage repair strategies. Specifically, this chapter focuses on predominant challenges towards clinical application of MSC-based cartilage repair strategies, namely hypertrophic maturation, and inflammation. Furthermore, this chapter describes current approaches to address those challenges and proposes synthetic gene circuits as a viable method to improve MSC-based cartilage regeneration by simultaneously inhibiting hypertrophy and inflammation induced matrix catabolism.

Chapter 3 (Aim 1) investigates the effect of low and high levels of autoregulated RUNX2 suppression on hypertrophic maturation of hMdChs. This study revealed that both low and high levels of autoregulated RUNX2 suppression increases cartilage matrix accumulation by hMdChs under hypertrophic conditions. Moreover, RUNX2 suppression inhibited mineral deposition and

downregulated the expression of hypertrophic markers. This chapter demonstrates that synthetic gene circuits are a viable approach to regulate stem cell phenotype to achieve desirable cartilage tissue engineering outcomes.

Chapter 4 (Aim 2) investigates the effect of autoregulated RUNX2 suppression on matrix degradation by hMdChs indued by the inflammatory cytokines IL-1β and TNF-α. This study revealed that treatment with either IL-1β or TNF-α increase RUNX2 activity, which induced matrix catabolism in hMdChs. I show that autoregulated RUNX2 suppression in hMdChs successfully inhibited RUNX2 activity and increased matrix retention. Moreover, cells containing RUNX2 suppressing gene circuits also resisted IL-1β- induced increases in hypertrophic marker expression and maintained higher expression of chondrogenic markers. This chapter demonstrates the efficacy of autoregulated RUNX2 suppression to partially protect hMdChs from inflammation induced matrix catabolism and IL-1β induced hypertrophic maturation.

Chapter 5 (Aim 3) employs a condition media-based co-culture model to investigate the effect of RUNX2 suppression in hMdChs on the pro-inflammatory crosstalk between hMdChs and inflammatory M1 macrophages. This study revealed that M1 conditioned media (M1CM) induces RUNX2 activity and neocartilage degradation which was successfully resisted by RUNX2 suppression in hMdChs. Moreover, double conditioned media from M1CM-treated RUNX2 suppressing hMdChs attenuated macrophage inflammation and induced a pro-inflammatory to anti-inflammatory phenotype switch.

Chapter 6 summarizes the findings of this dissertation and describes the future directions for the utilization of synthetic gene circuits for cartilage repair. This chapter describes how the work done in this thesis addresses the significant challenges towards clinical application of MSC-based cartilage repair strategies. Although this thesis makes a compelling case for application of

autoregulated RUNX2 suppression to improve MSC-based cartilage regeneration invitro, future studies are needed to validate these findings using in vivo models of cartilage defect repair and PTOA.

Overall, this dissertation demonstrates that autoregulated RUNX2 suppression not only stabilizes hMdCh phenotype and protects hMdChs from inflammation induced matrix catabolism, but also inhibits the pro-inflammatory crosstalk between hMdChs and M1 macrophages to attenuate macrophage inflammation, creating an environment conducive to MSC-based cartilage healing.

Chapter 2 Background

Articular cartilage is the connective tissue present at the end of long bones that provides a smooth, low friction surface to facilitate the transmission of load during joint movement[1]. This load bearing function of articular cartilage is enabled by its unique extracellular matrix comprising of collagen II and aggrecan, which is deposited by native cartilage cells called chondrocytes (Fig 2-1). Collagen II is the predominant type of collagen found in cartilage ECM and creates a dense fibril network that maintains mechanical integrity of the tissue by providing the tensile strength required to resist swelling and tensile loads during joint movement[1,30]. Aggrecan is made up of negatively charged sulfated glycosaminoglycan side chains which attract water molecules from the synovial fluid to build up osmotic pressure required to resist compressive loads exerted on cartilage during regular joint movements[1,30].

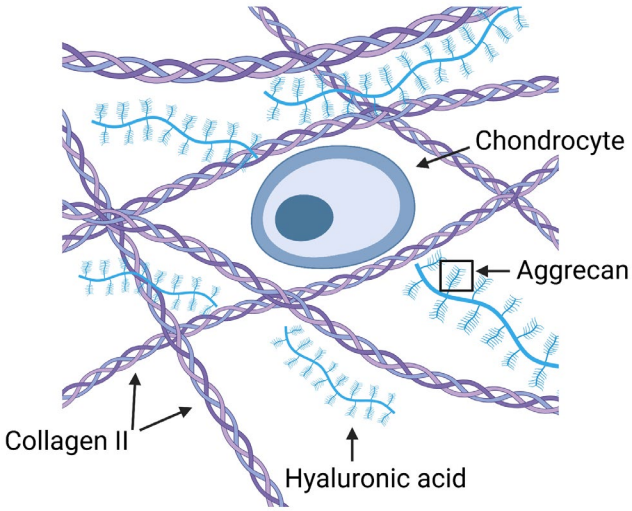

Figure 2-1 Schematic representation of chondrocyte embedded in cartilage ECM. Created with Biorender.com.

In addition to ECM composition, the zonal architecture of articular cartilage also contributes to its mechanical strength and function[31]. Articular cartilage is divided into four zones namely superficial, intermediate, deep, and calcified zones (Fig. 2-2). Each zone has specific cellular and ECM organization that protects chondrocytes from loading stresses and allows smooth transmission of loads during joint movement. Superficial zone consists of elongated flattened chondrocytes and thinner collagen fibers running parallel to the articulating surface. This zone provides tensile strength to resist shear forces experienced during joint movement[1,30–32]. The intermediate zone is comprised of thicker collagen fibers oriented randomly with circular chondrocytes embedded at relatively lower density. This zone provides resistance to compressive forces experienced during joint movement[1,30,31]. The deep zone contains thickest collagen fibers arranged perpendicularly to the articulating surface with columnar arrangement of chondrocytes parallel to collagen fibers. This zone provides maximum resistance to the compressive forces during joint movement[1,30,31]. Finally, the calcified zone anchors the collagen fibers to the subchondral bone to provide smooth integration thereby securing articular cartilage in place[1,30].

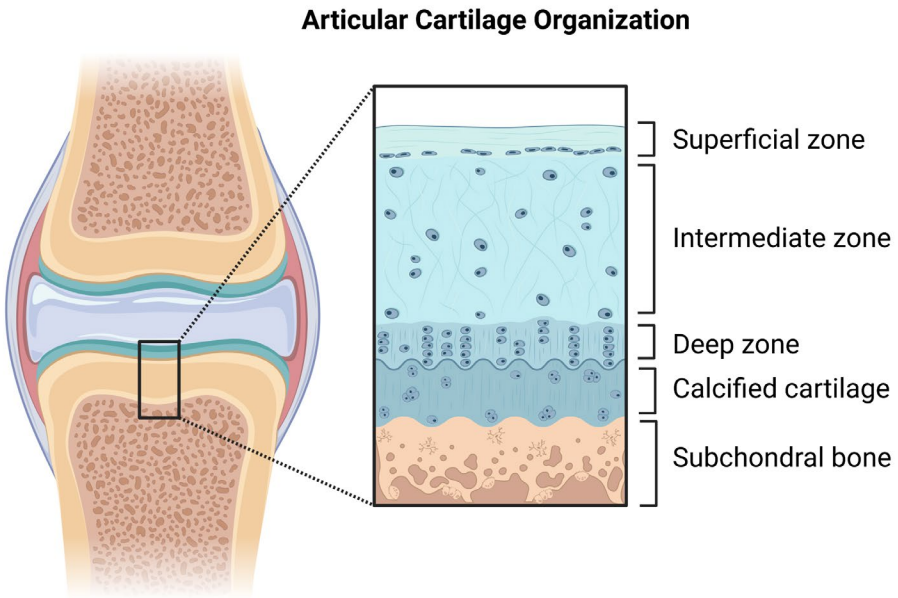

Figure 2-2 Schematic representation of the zonal organization of articular cartilage. Created with Biorender.com

2.1 Articular cartilage injury and pathology of PTOA

The synovial joint is comprised of multiple tissues like articular cartilage, meniscus, subchondral bone and synovium, which work together to maintain healthy joint function[33]. Articular cartilage is avascular and non-innervated with low cell density, resulting in limited healing capability during traumatic injuries[5,34]. Cartilage injury leads to release of degraded cartilage ECM fragments and cellular stress signals into the synovial fluid, which interact with the synovium to initiate inflammation. Synovial inflammation plays an important role in mediating PTOA progression. The synovial membrane lines the joint cavity and its main function is to secrete synovial fluid to lubricate joint movement. Upon injury, these degraded ECM molecules act as danger associated molecular patterns (DAMPs) and bind to the pathogen recognition receptors (PRRs) on synovial macrophages resulting in their activation into pro-inflammatory phenotype[22–24,35,36].

Classically, macrophages were broadly classified into either pro-inflammatory M1 or anti-inflammatory M2 phenotype. However, multiple studies in various disease contexts have shown that macrophages phenotype exists on a spectrum instead of these binary extremes. Exposure to inflammatory stimulus like lipopolysaccharides (LPS) or, interferon gamma (IFNγ)[37]. results in polarization of macrophages towards pro-inflammatory (M1-like) phenotype which secrete pro-inflammatory and catabolic mediators whereas anti-inflammatory (M2-like) macrophages are responsible for resolution of inflammation and promote tissue repair/healing response[37,38]. As mentioned before, this M1/M2 classification defines the extreme ends of a spectrum of phenotypes that can be acquired by macrophages in response to the environmental conditions[39,40]. Therefore, a ratio of inflammatory and anti-inflammatory markers is utilized to accurately identify macrophage phenotype state (Fig 2-3).

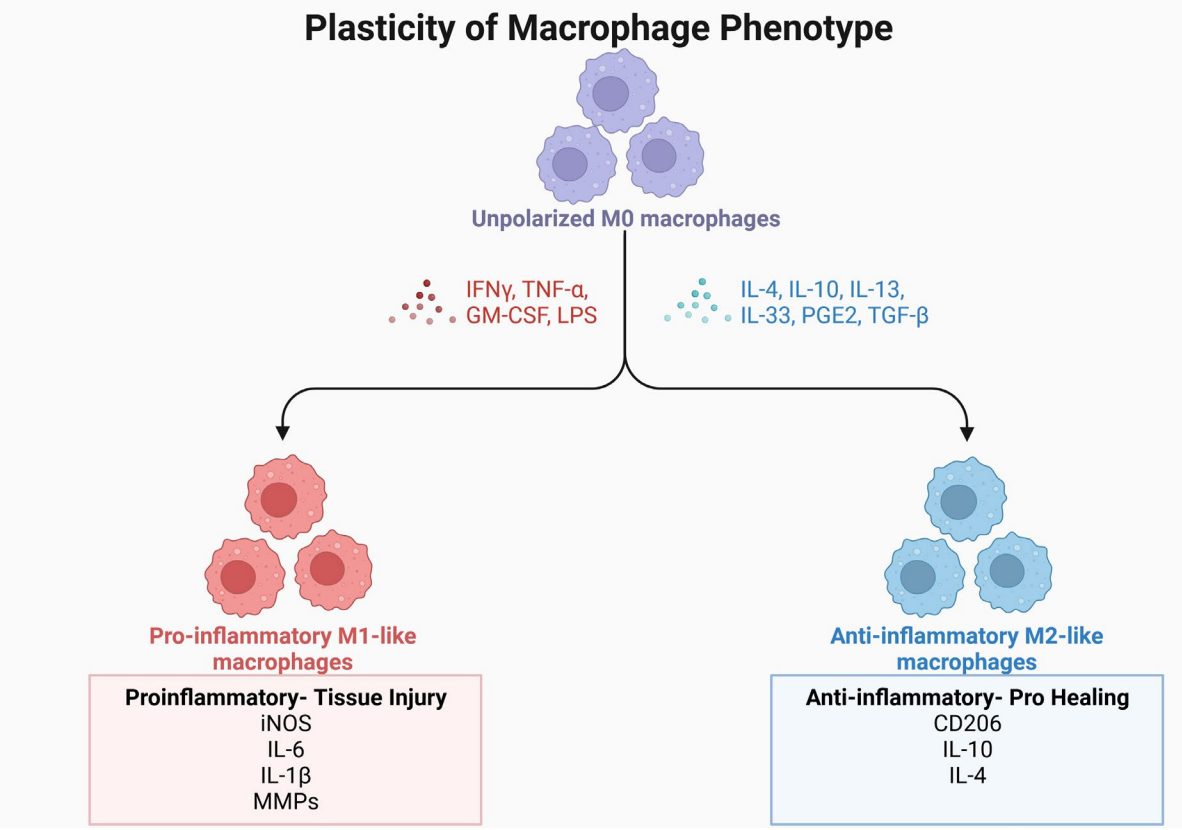

Figure 2-3 Pro-inflammatory and anti-inflammatory macrophage phenotype and markers. Macrophage phenotype can be determined by analyzing the expression of pro-inflammatory and anti-inflammatory markers. Image created using Biorender.com.

Activation of PRRs, especially toll like receptors (TLRs) by DAMPs results in pro-inflammatory polarization of synovial macrophages, which then secrete a cocktail of inflammatory cytokines such as IL-1, TNF-α and IL-6, chemokines like MCP-1, and catabolic mediators like MMPs that act via autocrine and paracrine signaling to maintain joint inflammation[21,24,36]. These inflammatory cytokines reinforce pro-inflammatory macrophage polarization and activate fibroblast-like synoviocytes to also produce inflammatory cytokines, nitric oxide, prostaglandins, and metalloproteinases[41–43]. Secretion of these factors by fibroblast like synoviocytes has been positively correlated with the severity of OA and result in cartilage degradation and inflamed synovium or synovitis[44].

These pro-inflammatory and catabolic mediators secreted by inflammatory M1-like macrophages and activated fibroblasts act on chondrocytes (Fig. 2-4), inducing them to secrete more inflammatory cytokines and matrix degrading enzymes[35,45,46]. This persistent cartilage degradation reinforces pro-inflammatory polarization of synovial macrophages, causing continued secretion of inflammatory cytokines, thereby creating a positive feed forward loop that sustains joint inflammation, resulting in the onset and progression of PTOA [29,47,48](Fig. 2-5).

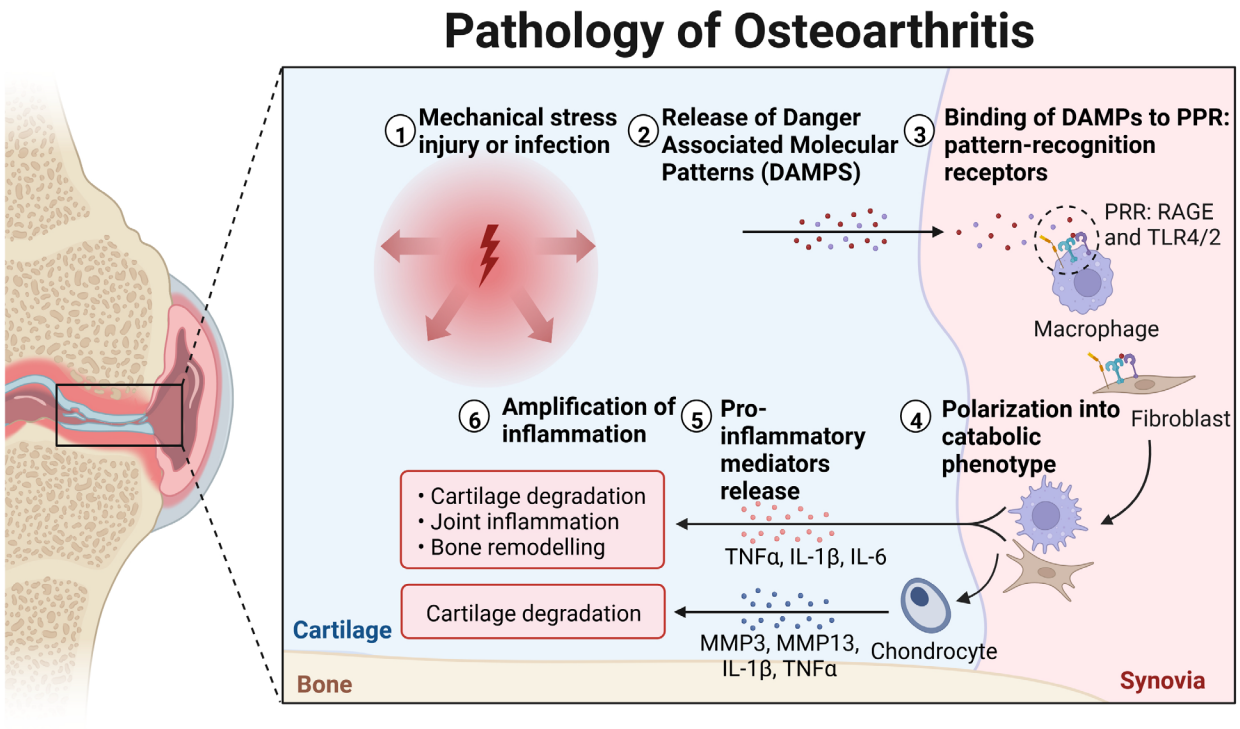

Figure 2-4 Pathology of post-traumatic osteoarthritis. Activation of synovial macrophages, fibroblast-like synoviocytes and chondrocytes into pro-inflammatory states after cartilage injury, ultimately causing joint inflammation and cartilage degradation. Image created using Biorender.com.

The balance of pro-inflammatory/anti-inflammatory macrophages is skewed towards pro-inflammatory phenotype during PTOA progression and studies have shown a therapeutic effect of macrophage ablation in animal models of PTOA due to reduced secretion of inflammatory cytokines and matrix metalloproteinases resulting in lesser and delayed cartilage damage[35,46,49]. Other studies investigating treatment with corticosteroids reported reduced cartilage damage and

osteophyte formation in PTOA models due to increased infiltration by anti-inflammatory macrophages[50–54]. Since macrophages are the predominant immune cell type in the synovial joint that mediates inflammation, therapies that repair injured cartilage as well as help regain the healthy pro-inflammatory/anti-inflammatory ratio in the joint could be a successful strategy to delay if not prevent the onset of PTOA[36,50].

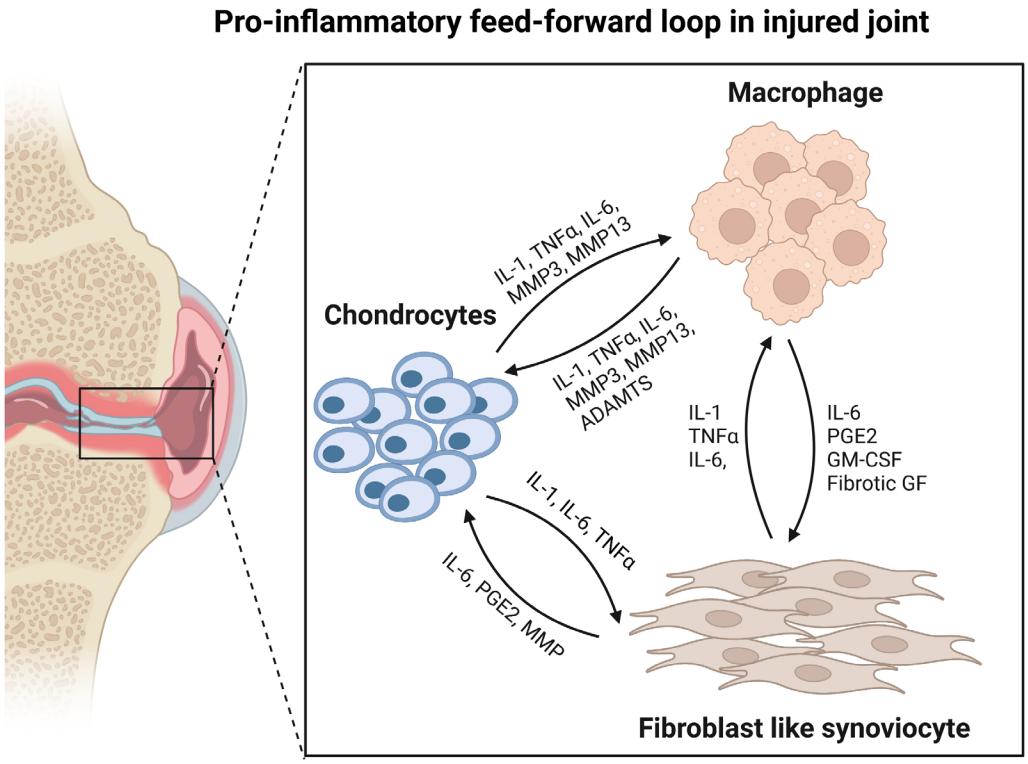

Figure 2-5 Joint injury establishes a pro-inflammatory feed-forward loop. Macrophages, fibroblast-like synoviocytes and chondrocytes secrete cytokines and chemokines that act via autocrine and paracrine mechanisms to sustain joint inflammation, thereby causing PTOA progression. Image created using Biorender.com.

2.2 Current treatment strategies for articular cartilage injuries

Three surgical treatment strategies are currently employed to repair articular cartilage focal defects, microfracture, osteochondral implantation and autologous chondrocyte implantation.

Microfracture: This procedure is commonly utilized to repair small cartilage defects (< 2cm^2). During this procedure, the defects are debrided, and subchondral bone is drilled through to create channels between cartilage and underlying bone marrow to facilitate recruitment of bone

marrow derived multipotent stem cells for cartilage repair[55]. Although this process is simple, economical, and has low recovery time, it often leads to formation of fibrocartilage instead of hyaline cartilage, which causes mismatch of mechanical properties as fibrocartilage is less stiff than hyaline cartilage[6,56,57]. The inferior mechanical properties of this tissue compromises it's load bearing function, ultimately leading to progression of PTOA[56].

Osteochondral transplantation: Also known as mosaicplasty, this procedure is used for small to intermediate defects[6]. Autograft or allograft osteochondral plugs are utilized to replace damaged cartilage. If autograft, single or multiple osteochondral plugs comprising of cartilage and subchondral bone are harvested from non-load bearing region of patient's own joint and implanted at the defect site[58]. However, this process causes donor site morbidity and can be limited by insufficient donor tissues. Furthermore, there is limited integration between the implant and the native tissue[59]. For larger defects (> $3cm^2$), allografts are used for repair. Allografts are also associated with challenges as they can initiate immune response in the host, cause disease transmission and result in thickness mismatches[6,60].

Autologous chondrocyte implantation: This is a twostep cell-based procedure often used to repair large cartilage defects. During first surgery, small pieces of healthy cartilage are harvested from non-load bearing region of patient's knee. The isolated cartilage is then digested to remove chondrocytes, which are then expanded invitro. A second surgery is carried out to inject the expanded chondrocytes into the defect and a periosteal patch is placed on top to contain cells in place[61]. Although this technique has shown positive long-term outcomes in younger patients, the regenerative potential of chondrocytes from aged patients varies significantly[62]. Moreover, ACI requires multiple invasive procedures and chondrocytes have been shown to dedifferentiate during in vitro expansion[63]. The use of periosteal patch has been linked with complications such as

hypertrophy and calcification. Therefore, matrix assisted autologous chondrocyte implantation (MACI) was developed to overcome some of these challenges[57,64]. During MACI, a scaffold embedded with expanded chondrocytes is implanted at defect site using fibrin glue. However, this procedure has similar limitations to ACI, as it also requires multiple invasive procedures and invitro expansion of chondrocytes, which causes their dedifferentiation and can result in formation of fibrocartilage instead of hyaline articular cartilage after implantation[65].

As discussed in this section, current treatment strategies for cartilage injuries do not fully restore cartilage function or resolve inflammation. Therefore, there is a need to develop cartilage repair strategies that restore cartilage function and serve as disease modifying treatment to prevent the onset of PTOA.

2.3 Tissue engineering based articular cartilage repair

Current clinical cartilage repair strategies are associated with significant challenges as described above. To overcome these challenges, tissue engineering strategies have been proposed as an appealing approach for cartilage regeneration[8,66]. By utilizing a combination of cells, scaffolds and growth factors, researchers have generated neocartilage tissues comprising of collagen II and aggrecan with similar structural and mechanical properties to articular cartilage[8,67].

Articular chondrocytes are the gold standard and the only FDA approved cell type for cartilage tissue engineering as they are currently used for ACI and MACI[64,65]. However, limited availability of chondrocytes necessitates invitro expansion to achieve cell numbers suitable for repair. Expansion in monolayer causes chondrocyte dedifferentiation resulting in downregulation of cartilage specific collagen II expression as well as proteoglycans like aggrecan and elevated collagen I expression[63,68–70]. Moreover, high variability in the regeneration potential of

chondrocytes isolated from younger vs. older patients limits their success for tissue engineering[62], as it restricts the application of chondrocyte-based engineered neocartilage to young patients.

Adult human mesenchymal stem cells (hMSCs) are an appealing cell source for cartilage tissue engineering applications as they can differentiate into chondrocytes and produce cartilage macromolecules collagen II and aggrecan[71–74]. Moreover, these cells are more abundant than chondrocytes as they can be isolated from multiple tissues in the body such as bone marrow, and adipose tissue, and they have higher proliferation potential that allows in vitro expansion. These cells can differentiate into multiple musculoskeletal lineages, such as bone, cartilage, muscle and adipose tissues[10,75,76]. hMSCs have been widely studied for cartilage tissue engineering applications and several growth factors and culture conditions have been explored to achieve chondrogenic differentiation to generate neocartilage tissues. Growth factors like bone morphogenic proteins (BMP)[9,72,77,78], transforming growth factor beta (TGF-β)[9,28,79,80] and insulin like growth factor (IGF)[81] have been shown to induce hMSC chondrogenesis and the accumulation of cartilage macromolecules by inducing the expression of SOX9, the master transcription factor for chondrogenesis. Moreover, supplementation with fibroblast growth factor (FGF-2) during hMSC expansion phase has been shown to improve chondrogenesis and cartilage matrix accumulation by hMSC derived chondrocytes (hMdChs)[82,83]. Strategies employing various combinations of scaffolds and growth factors have been also explored to achieve and maintain hMSC chondrogenesis. Scaffolds made from synthetic polymers like polyethylene glycol (PEG), poly lactic acid (PLA), and poly glycolic acid (PGA) and natural materials like agarose, gelatin, collagen, chitosan as well as decellularized articular cartilage matrix have been employed to support MSC chondrogenesis[32,84–88].

In addition to scaffolds and growth factors, different culture conditions have also been explored to induce hMSC chondrogenesis and improve cartilage matrix accumulation. Hypoxia has been shown to promote chondrogenic differentiation of hMSCs activating HIF1α signaling, which upregulates SOX9 expression[89–93]. Mechanical stimulation of hMSCs via dynamic loading and shear stress also promotes chondrogenic differentiation of hMSCs via activation of YAP/TAZ pathway[94]s and activation of TRPV4 ion channels[95–99].

2.4 Challenges towards MSC-based cartilage repair

Although a promising candidate for tissue engineering-based cartilage regeneration, clinical application of hMSC-based cartilage repair is impaired by two major challenges:

2.4.1 MSC-derived chondrocytes undergo hypertrophic maturation

While hMSCs can undergo chondrogenic differentiation and produce cartilage matrix macromolecules, the unstable chondrogenic phenotype of hMdChs is a major challenge. Upon chondrogenic differentiation, once hMSCs commit to chondrogenic lineage and differentiate into hMdChs, they continue down the endochondral ossification pathway by undergoing maturation into pre-hypertrophic and hypertrophic chondrocytes[18] as shown in Fig 2-6. During hypertrophic maturation, hMdChs downregulate SOX9 expression thereby downregulating the production of collagen II and aggrecan and start producing collagen type X[100–102]. Moreover, hypertrophic hMdChs initiate the expression of matrix degrading enzymes like matrix metalloproteinase-13 (MMP13) and a disintegrin and metalloproteinase with thrombospondin motifs-4/5 (ADAMTS 4/5), causing neocartilage degradation and compromising the integrity of engineered tissue[13,28,102]. Loss of collagen II and aggrecan via MMP activity leads to lower compressive and tensile strength of the engineered tissue, which compromises its function. This ECM remodeling lays the

foundation for cartilage matrix mineralization and blood vessel infiltration, preparing the tissue for vascularized bone formation[103]. This process is driven by runt related transcription factor 2 (RUNX2), the master transcription factor that drives chondrocyte hypertrophy during development. RUNX2 is the transcriptional regulator of hypertrophic markers and directly binds to the promoter region of *COL10a1*, *MMP13* and *VEGF* to initiate their transcription during hypertrophic maturation[14,15,101,104].

Therefore, **inhibition of hMdCh hypertrophy is a pre-requisite for successful clinical application of MSC-based cartilage repair strategies**.

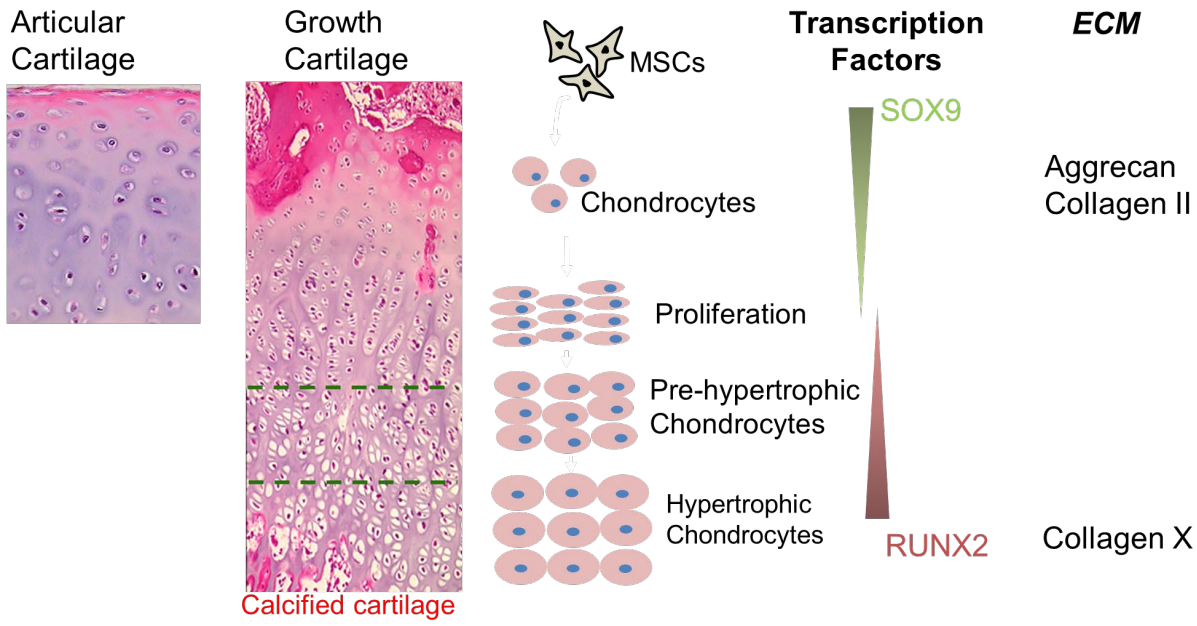

Figure 2-6 MSC chondrogenesis follows endochondral ossification pathway. H&E staining of articular cartilage and growth cartilage sections. Comparison of hMdCh hypertrophic maturation to corresponding growth cartilage phenotypes.

2.4.2 Inflammation induced neocartilage degradation

Traumatic joint injury leads to activation of synovial macrophages into the pro-inflammatory phenotype, which mediates the onset and progression of PTOA. Inflammatory cytokines, like IL-1β, TNF-α, and IL-6, inhibit hMSC chondrogenesis by suppressing SOX9 expression[105] and

induce hypertrophic maturation in hMdChs by upregulating RUNX2 expression, thereby upregulating MMP13 expression and causing cartilage matrix degradation[51,100]. Moreover, like chondrocytes, these cytokines induce hMdChs to also produce inflammatory and catabolic mediators to sustain joint inflammation[23,36,50,106].

Therefore, **successful application of hMSC-based cartilage repair necessitates the ability to resist the catabolic and pro-inflammatory influence of the inflamed joint and inhibition of the pro-inflammatory crosstalk between hMdChs and M1 macrophages**.

The **central objective** of this thesis is to *enhance the cartilage matrix accumulation by hMdChs under hypertrophic and inflammatory conditions for cartilage defect repair*. Since the transcription factor RUNX2 regulates chondrocyte hypertrophy and mediates the pro-inflammatory and catabolic response of hMdChs to inflammatory cytokines, we **hypothesize** that *suppression of the RUNX2 pathway in hMdChs can increase cartilage matrix accumulation by inhibiting hypertrophy and preventing inflammation-induced matrix catabolism.*

2.5 Synthetic gene circuit to improve MSC-based cartilage regeneration

RNA interference (RNAi) allows suppression of target genes without treatment with chemical inhibitors, hence reducing potential off-target effects mediated by broad-spectrum delivery of these factors [107]. RNAi utilizes small interfering RNA (siRNA), microRNA (miRNA) or short hairpin RNA (shRNA) with sequence complimentary to the mRNA of interest, which results in binding of siRNA to mRNA resulting in formation of dsRNA which activates the RNA-induced silencing complex (RISC)[108]. This results in either cleavage of target mRNA or inhibition of target mRNA translation by forming a “stuck” RISC, ultimately suppressing target protein synthesis.

Utilizing a doxycycline inducible vector to induce RUNX2 suppression, our lab has previously shown that RUNX2 is required during early chondrogenesis and constitutive RUNX2 suppression inhibits chondrogenesis by downregulating collagen II and aggrecan expression[25] (Fig. 2-7).

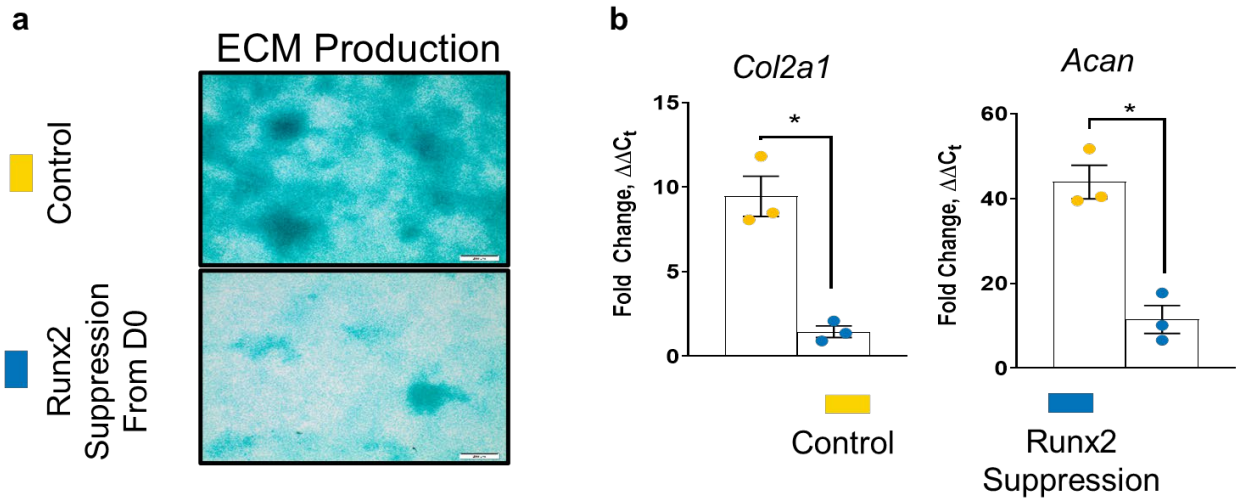

Figure 2-7 Constitutive RUNX2 silencing inhibits chondrogenesis. (a) Alcian blue staining for sGAG accumulation and (b) Col2a1 and Can gene expression in wildtype (control) and constitutively RUNX2 suppressing ATDC5 cells after 21-day chondrogenic culture. Figure modified with permission from Kaur G et.al., bioRxiv 2021.

To control the timing and level of RUNX2 suppression, our lab designed a gene circuit which targets RUNX2 by synthetically inducing a negative feedback loop in chondrogenic cells, to reduce the negative effect of hypertrophy without interfering with MSC chondrogenesis (Fig. 2-8). The circuit consists of an engineered COL10A1-like promoter with variable numbers of RUNX2 binding sites (cis-enhancers) upstream of the basal promoter to tune the sensitivity of the gene circuit. A shRNA targeting RUNX2 is placed downstream of the COL10A1-like promoter thereby allowing cells to regulate RUNX2 activity based on intracellular RUNX2 concentrations. We also added a luciferase reporter to track RUNX2 activity as a measure of luciferase activity in our circuits. Transduction controls were created by replacing the shRUNX2 sequence with a scrambled sequence that does not target any mRNAs[25].

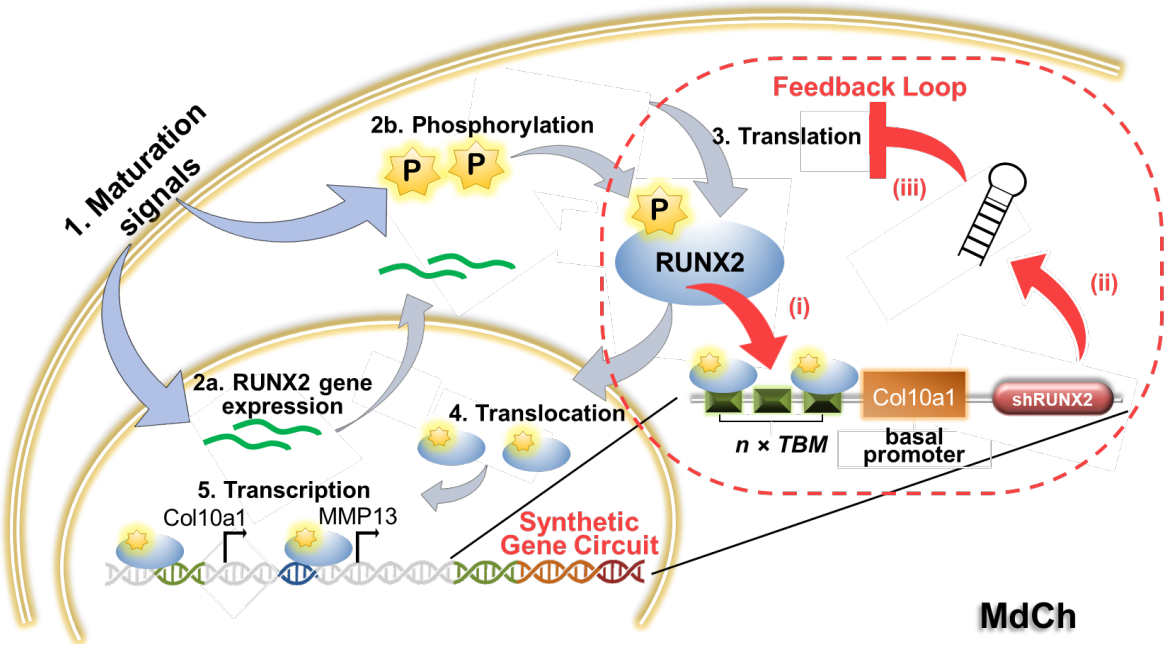

Figure 2-8 Biosynthetic strategy to regulate hMdCh phenotype. The endogenous intracellular process of RUNX2 transcription, translation, and DNA binding (1—5) is hijacked to activate a RUNX2–silencing gene circuit using an engineered Col10a1–like promoter to drive shRNA expression (i—iii).

To tune the sensitivity of the gene circuit, we created circuits containing 1,2 or 3 cis-enhancer sequences (Fig. 2-9a). We then tested the efficacy of the gene circuits to induce RUNX2 suppression in the ATDC5 chondroprogenitor cell line. We showed that based on the number of cis-enhancer sequences, we achieved RUNX2 suppression ranging from 18% in 1-*cis* circuit, 30% in 2-*cis* circuit to 77% in 3-*cis* circuit (Fig. 2-9b).

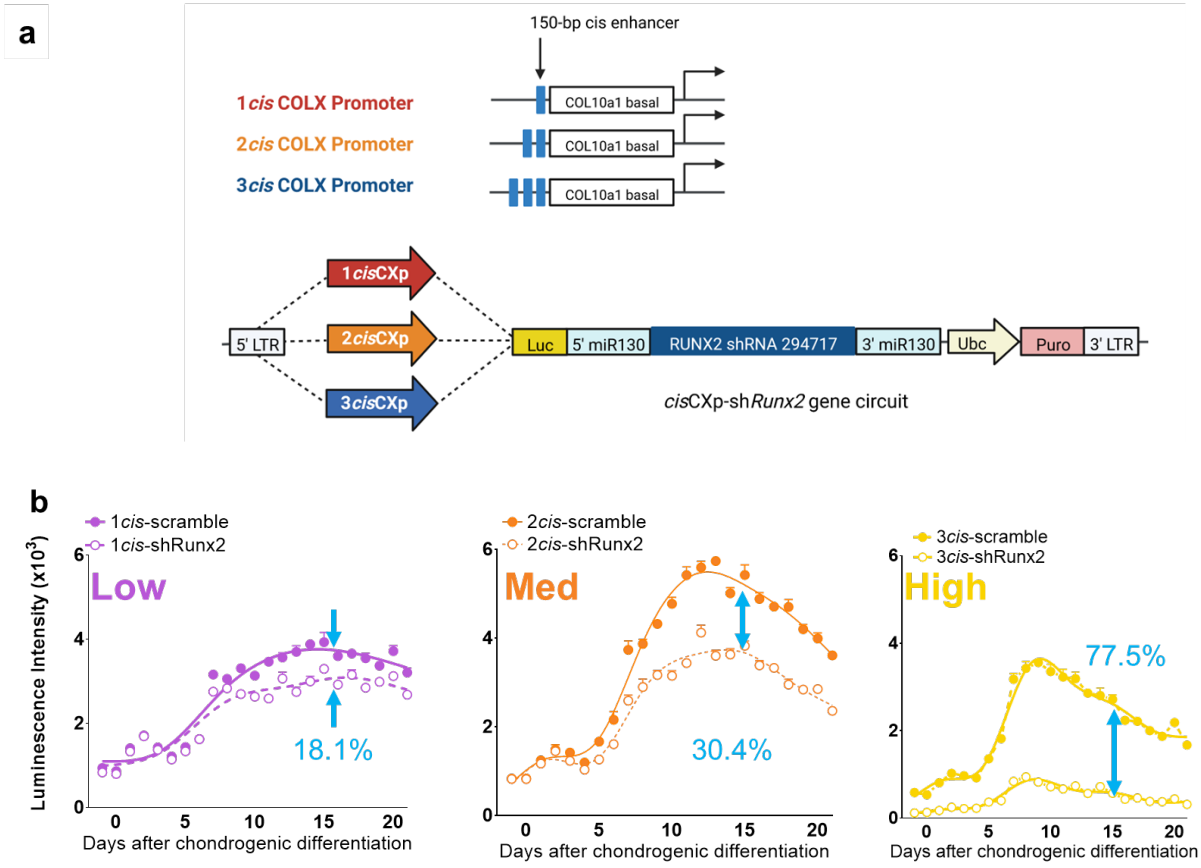

Figure 2-9 Tunable sensitivity of engineered autoregulatory RUNX2 suppressing gene circuit. (a) Map of RUNX2 suppressing gene circuits made of either 1, 2 or 3 cis-enhancer sequences. COL10a1 basal promoter provides chondrocyte specificity and number of cis enhancers provide tunability of the circuit to RUNX2 concentration. Luciferase provides reporter activity and miRNA30 sequences flanking the shRNA help in post transcriptional processing of shRNA. Downstream of Ubc constitutive promoter, there is puromycin selection marker. (b) Suppression of RUNX2 activity via gene circuits containing 1, 2 or 3 *cis*-enhancer sequences measured using luciferase reporter. Figure modified with permission from Kaur G et.al., bioRxiv 2021.

In this dissertation, we tested the efficacy of low and high levels of autoregulated RUNX2 suppression to increase chondrogenic phenotype stability and promote cartilage matrix accumulation by hMdChs under hypertrophic and inflammatory environments. We utilized gene circuits containing 1 and 3 cis-enhancers to achieve low and high levels of RUNX2 suppression respectively in hMdChs.

Chapter 3 Autoregulated RUNX2 suppression inhibits hMdCh hypertrophy

3.1 Abstract

Focal defects in articular cartilage often progress into post traumatic osteoarthritis (PTOA). Human mesenchymal stem cell (hMSC)-based tissue engineering is an appealing approach for treating cartilage defects due to their ability to differentiate into chondrocytes and secrete cartilage matrix macromolecule. However, their inability to maintain a stable chondrogenic phenotype remains a significant challenge and limit their potential for defect repair. Upon chondrogenic differentiation, hMSC derived chondrocytes (hMdChs) undergo hypertrophic maturation driven by master transcription factor (TF) RUNX2, which decreases the expression of cartilage matrix macromolecules and increases expression of matrix degrading enzymes like MMPs. This results in matrix loss which compromises the functionality of the engineered cartilage. We hypothesized that suppression of RUNX2 can increase matrix accumulation by hMdChs under hypertrophic stimuli by 1) maintaining the production of cartilage structural proteins and 2) reducing expression of proteases that degrade cartilage matrix. Using synthetic gene circuits that allow autonomous RUNX2 suppression in hMdChs, we investigated the effect of varying magnitudes of RUNX2 suppression on the response to hypertrophic stimuli hMSC chondrogenic pellets cultures. We show that RUNX2 suppression increases cartilage matrix accumulation, inhibits mineral deposition by hMdChs. Moreover, RUNX2-suppressing hMdChs retain higher expression of chondrogenic markers and resist the upregulation of hypertrophic markers compared to controls under

hypertrophic stimuli. This study demonstrates that synthetic gene circuits are a viable tool to regulate cell phenotype and improve MSC-based cartilage regeneration outcomes.

3.2 Introduction

Articular cartilage has limited healing capability, causing traumatic cartilage injuries to often progress into post-traumatic osteoarthritis (PTOA), a painful debilitating disease. Although treatment strategies exist for articular cartilage repair like microfracture, osteochondral implantation and (matrix assisted) autologous chondrocyte implantation, current treatments still do not fully restore cartilage function[109]. In recent years, tissue engineering and regenerative medicine community has made significant progress towards engineering articular cartilage. Efforts have included utilizing different cell types, scaffolding materials, growth factors and culture conditions either alone or in combination[9,83,87,110]. However clinical application of engineered articular cartilage still faces numerous challenges.

Articular chondrocytes are the primary cell type found in articular cartilage and are gold standard for cartilage tissue engineering. However, these cells tend to dedifferentiate during in-vitro expansion and chondrogenic capabilities of articular chondrocytes can vary greatly depending on donor age, presence of co-morbidities etc [70]. Therefore, additional cell types that have articular cartilage regeneration potential are highly desirable.

Adult mesenchymal stem cells (MSCs) have been extensively explored in the tissue engineering field as they can differentiate down multiple lineages, including osteoblasts, adipocytes, and chondrocytes. Therefore, adult MSCs are an appealing cell source for articular cartilage regeneration since they have the capability to undergo chondrogenesis and produce the desired cartilage extracellular matrix macromolecules, like aggrecan and collagen II which are important for cartilage function[9,72,74]. However, MSCs are limited in their ability to maintain a

stable chondrogenic phenotype. As MSCs undergo chondrogenesis they differentiate into MSC derived chondrocytes (hMdChs), a phenotype similar to articular chondrocytes in their ability to produce aggrecan and collagen II. However, hMdChs continue down the endochondral ossification pathway and undergo hypertrophic maturation[98,102,111], a process orchestrated by runt-related transcription factor 2 (RUNX2)[101,112,113], the master transcription factor for chondrocyte hypertrophy. During hypertrophic maturation, RUNX2 downregulates the expression of collagen II and aggrecan and drives the expression of matrix metalloproteinases like MMP13 and aggrecanases like ADAMTS4,5. This results in neocartilage degradation which compromises the mechanical integrity of engineered cartilage[14,114].

The ability to maintain chondrogenic phenotype is one of the predominant challenges towards clinical application of adult MSC-based cartilage regeneration. Decades of research by regenerative community has explored different strategies to stabilize hMdCh phenotype and increase cartilage matrix accumulation. In tibial explants, hypoxia has been shown to increase cartilaginous epiphysis, length of resting zone and increase the expression of chondrogenic markers[115]. In MSC derived chondrocytes as well as osteoarthritic chondrocytes, hypoxia was shown to inhibit hypertrophic maturation and reduce calcification by downregulating the expression of hypertrophic markers and upregulating expression of chondrogenic markers[70,92,116–120]. Additionally, mechanical loading has been shown to improve MSC chondrogenesis and decrease matrix metalloproteinase expression. Furthermore, dynamic loading of engineered cartilage constructs during chondrogenesis has been shown to improve matrix accumulation and retention[95,98]. However, all these methods have had limited success in stabilizing chondrogenic phenotype of hMdChs.

Since RUNX2 is the master transcription factor that drives chondrocyte hypertrophy, we **hypothesized** that RUNX2 suppression can enhance cartilage accumulation by hMdChs by stabilizing their chondrogenic phenotype and downregulating expression of matrix metalloproteinases. However, RUNX2 is required for MSCs to undergo chondrogenesis and constitutive RUNX2 suppression has been shown to inhibit MSC chondrogenesis. Therefore, we required a sophisticated system that allows spatial-temporal control over RUNX2 expression. To address this, we developed a gene circuit that allows the cells to suppress RUNX2 based on intracellular RUNX2 concentrations by creating a negative feed-back loop inside the cells[25]. In this study we test the efficacy of RUNX2 suppressing gene circuits to increase the stability of hMdCh's chondrogenic phenotype and increase cartilage matrix accumulation.

3.3 Methods

3.3.1 Synthesis of gene circuits

All vectors were constructed as previously described[25] and incorporated into lentiviruses by the University of Michigan Vector Core. The shRNA sequence for shRUNX2 was selected from the Hannon Elledge library (RNAi codex). Using the pINDUCER plasmid[121], a Tet-on inducible system was modified to synthesize tet-on-Luc-mir30-shRUNX2. Next, the COL10a1 basal promoter (-220 to 110 bp) and cis-enhancers (-4296 to- 4147) were synthesized using IDT technology using gBlocks gene fragments service and assembled into pLenti-CMVtight-Egfp-Puro vector[101]. Finally, the Tet-on promoter in pINDUCER was replaced by COL10a1 promoter containing varying number of cis-enhancers to obtain 1cis-luc-mir30-shRUNX2 and 3cis-luc-mir30-shRUNX2. Scramble controls were created by using the same gene circuit backbone and scrambling shRUNX2 sequence to create a non-specific oligonucleotide sequence which doesn't target any genes.

3.3.2 Cell culture

Cell Expansion: Human bone marrow derived mesenchymal stem cells (hMSCs) were obtained from our collaborators at Case Western Reserve University and expanded in Low Glucose DMEM with 10% Fetal Bovine Serum and 10ng/ml FGF-2[83].

Lentiviral Transduction: hMSCs were plated at density of 10,000 cells/cm^2 and transduced with lentiviruses containing low and high RUNX2 suppressing gene circuits at moieties of infection (MOI) = 5. Twenty-four hours post-transduction, media was replaced with expansion media described above. Transduced cells were selected by treatment with 1µg/ml Puromycin treatment.

MSC chondrogenesis: Wildtype and gene circuit transduced hMSCs were trypsinized using 0.05% Trypsin-EDTA and resuspended in chondrogenic media at 125000 cells/ml. Chondrogenic media consisted of High Glucose DMEM (Gibco, Cat # 11965-092), supplemented with 1 % (v/v) insulin-transferrin-selenium (Corning, Cat # 354350), 1 % (v/v) non-essential amino acids (Gibco, Cat # 11-140-050) 40 μg/mL L-proline (Sigma, cat # P-0380), 50 μg/mL L-ascorbic acid-2-phosphate (Sigma, Cat # A8960), 0.1 μM dexamethasone (Sigma, Cat # D4902), and 10 ng/mL TGF-β1 (Shenandoah Biotechnology, cat # 100-39). hMSC pellets were formed by dispensing 200µl of cell suspension per well of 96 well plate followed by centrifugation at 1640 rpm for 5 minutes. Cells were incubated at 37℃, 5% CO_2, 95% humidity and allowed to condense into tight pellets for 3 days after which fresh chondrogenic media was supplied every other day.

Hypertrophic induction: To induce hMdCh hypertrophy, we utilized the protocol developed by Tuan et.al. by treatment with T3 and beta-glycerophosphate[28,102]. Thyroid hormone T3 is a precursor for thyroxine (T4) which has been shown to promote chondrocyte hypertrophy by downregulating SOX9 expression and upregulating expression of hypertrophic markers COLX

and ALP[26,28,122]. Beta-glycerophosphate has previously been shown to induce hypertrophic maturation of hMdChs[28,102]. Both TGF-β1 and dexamethasone has been shown to inhibit chondrocyte hypertrophy[28,79,80,102,122] hence after 14 days of chondrogenic stimulation, they were removed from hypertrophy induction medium.After 14 days of chondrogenic culture, human MSC derived chondrocytes (hMdChs) were treated with hypertrophic media for one week to induce hypertrophic maturation. Hypertrophic media consisted of chondrogenic media without TGFβ1 and dexamethasone, supplemented with 10nM tri-iodo-thyronine (T3) and 10mM beta-glycerophosphate (βGP)[28]. hMdChs treated with chondrogenic media without TGFβ1, and dexamethasone were used as controls. A schematic representing the experimental outline is shown below.

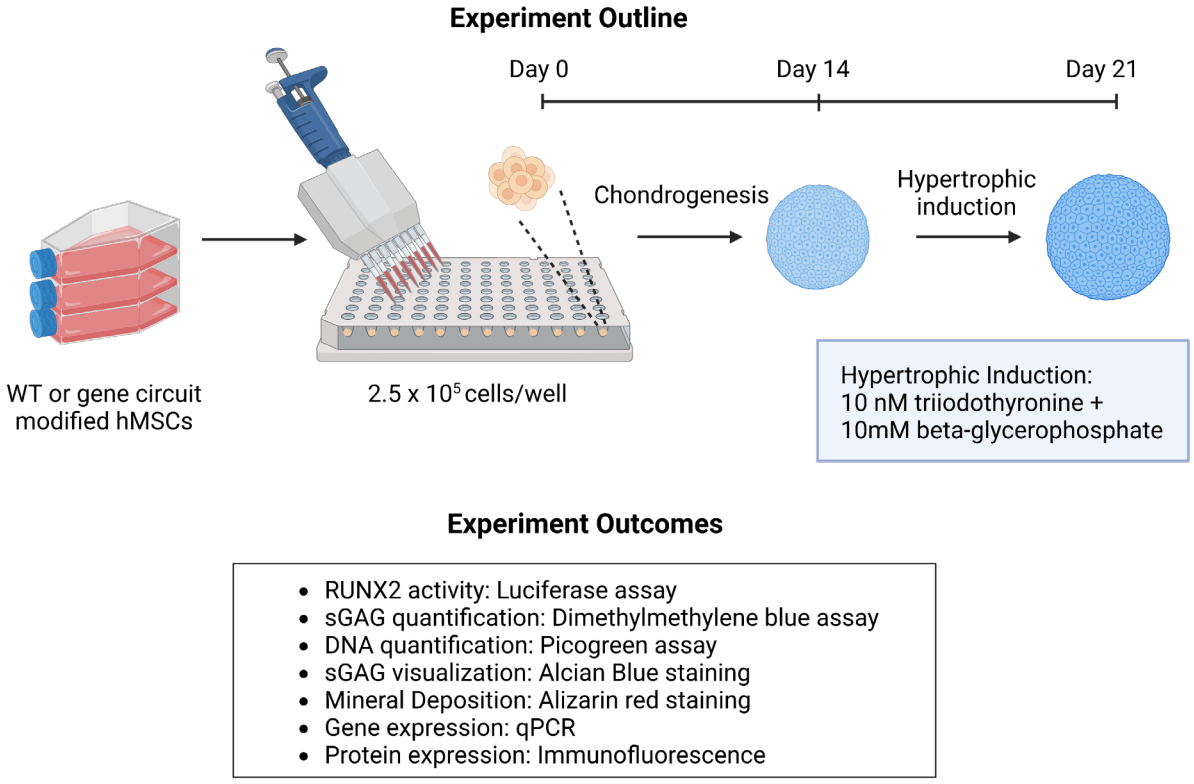

Figure 3-1 Hypertrophic induction of hMSC derived chondrocytes. Created using Biorender.com.

3.3.3 RNA extraction and qPCR

RNA extraction: After completion of treatments, hMdCh pellets were washed with PBS and flash frozen in liquid nitrogen and stored at -80℃ till ready for processing. For RNA extraction, frozen pellets were homogenized using pestles in Trizol. Following homogenization, bromoanisol was added for phase separation and RNA was precipitated using isopropanol. Purified RNA was resuspended in Ultrapure DI water and concentration was quantified using nanodrop.

cDNA synthesis and qPCR: Following RNA extraction, cDNA was synthesized using High Capacity cDNA Reverse Transcription kit (Applied Biosystems, Cat # 4368814) using 1µg RNA/sample and following the manufacturer's protocols. Gene expression of chondrogenic (ACAN, COL2A1, SOX9) and hypertrophic (COL10A1, RUNX2, MMP13) markers was analyzed using Fast SyBr Green master mix (Applied Biosystems, Cat # 4385612) on Applied Biosystems real time 7500 Fast qPCR machine. Primers sequences of the genes are listed in Table 3.1 below. GUS and TBP were used as housekeeping genes. Relative expression was calculated using $\Delta\Delta C_t$ method and fold change was calculated as $2^{-\Delta\Delta Ct}$.

Table 1 Primer sequences for qPCR

Gene	Forward Primer	Reverse Primer
GUSB	GACTGAACAGTCACCGACGA	ACTTGGCTACTGAGTGGGGA
TBP	GTGGGGAGCTGTGATGTGAA	TGCTCTGACTTTAGCACCTGT
ACAN	GGAGTGGATCGTGACCCAAG	AGTAGGAAGGATCCCTGGCA
COL2A1	CTCCAATGGCAACCCTGGAC	CAGAGGGACCGTCATCTCCA
SOX9	GCTCTGGAGACTTCTGAACGA	CCGTTCTTCACCGACTTCCT
RUNX2	CCGGAATGCCTCTGCTGTTA	AGCTTCTGTCTGTGCCTTCTGG
COL10A1	GAACTCCCAGCACGCAGAATC	TGTTGGGTAGTGGGCCTTTT
MMP13	TTGCAGAGCGCTACCTGAGA	CCCCGCATCTTGGCTTTTTC

Abbreviations: GUSB, glucuronidase beta; TBP, tata binding protein; ACAN, aggrecan; COL2A, collagen II; SOX9, SRY-Box transcription factor 9; RUNX2, runt related transcription factor 2; COL10A1, collagen X; MMP13, matrix metalloproteinase 13

3.3.4 Biochemical Analysis

Samples were digested in papain buffer made of papain, EDTA and sodium phosphate, overnight at 65℃. Dimethyl methylene blue (DMMB) assay was used to quantify sGAG concentrations as previously described[27]. Standard curve was generated using known concentrations of chondroitin-6-sulfate. 10µl of sample was added per well followed by 200 µl of DMMB dye. After adding the dye, absorbance was immediately read using Synergy H1 plate reader at 425nm and 495nm. sGAG concentrations were normalized to DNA content using PicoGreen DNA assay kit (Thermo Fisher). 10µl of samples and λDNA standards were added to black 96 well plate followed by Picogreen dye. Fluorescence was measured using Synergy H1 plate reader at excitation wavelength of 498nm and emission wavelength of 528nm and compared to the standard curve.

3.3.5 Histological Analysis

hMdCh pellets were washed with Phosphate Buffered Saline (PBS) and fixed using 10% Neutral Buffered Formalin for 30 minutes. After fixing cells were washed with PBS and stored in 70% ethanol until ready to process. hMdCh pellets were then dehydrated using graded series of ethanol (70-100%), cleared with Xylene, embedded in paraffin wax and sectioned into 7µm thick sections. The sections were then cleared in Xylene, rehydrated, stained with alcian blue (1% in 3% acetic acid, Poly Scientific) and counter stained with Nuclear Fast Red (Electron Microscopy Sciences) to visualize sGAG deposition. To visualize mineral deposition, rehydrated sections were stained with 2% alizarin red solution.

3.3.6 Immunofluorescence

The hMdCh pellet sections were cleared and rehydrated as explained above. Peroxidase activity of the pellets was blocked using 3% hydrogen peroxide followed by antigen retrieval using BD Retreivagen Antigen Retrieval kit (Thermofisher). Samples were permeabilized using 0.5%Triton-X-100 in TBS and incubated with blocking buffer consisting of 10% goat serum and 1% (w/v) bovine serum albumin in 0.1% TBS-TX100 (1XTBS with 0.1% Triton-X-100). Samples were then incubated overnight with primary antibody of ACAN (AbClonal, A8536, 1:500), COLX (AbClonal, A6889,1:100), RUNX2 (AbClonal, A2851, 1:100), MMP13 (AbClonal, A16920, 1:100) or COLII (Abcam, ab34712, 1:150) at 4℃. Samples were then stained with secondary antibody (IgG anti-rabbit, 488, 1:500, Invitrogen, A11034) for one hour followed by 5-minute incubation with 4', 6-diamidino-2-phenylindol (DAPI, Sigma, 300 nM). Anti-fade was used to coverslip the slides and images were taken on a Olympus microscope.

3.3.7 Statistical Analysis

All the data is presented as mean $\pm$ standard deviation (SD). All statistical analysis is performed using GraphPad Prism 8.3 software (GraphPad, San Diego, CA). One-way or two-way ANOVA was used with Tukey's multiple comparison post-hoc test. P-value < 0.05 was considered statistically significant.

3.4 Results

3.4.1 RUNX2 suppressing gene circuit does not inhibit chondrogenesis

As previously shown by our lab in mouse chondroprogenitor ATDC5 cells, we observed that 3cis-shRUNX2 gene circuit causes higher inhibition of RUNX2 activity (~70%) compared to 1cis-shRUNX2 gene circuits (~30%) as measured via luciferase activity (Fig.3-2a). Hence, we

labelled 3cis-shRUNX2 as high suppression and 1cis-shRUNX2 as low suppression circuits for the rest of this study. We observed that both low and high level of RUNX2 suppression did not inhibit chondrogenesis as observed by abundant matrix accumulation in sGAG quantification assay (Fig. 3-2b) as well as sGAG staining (Fig. 3-2c). Histological staining also shows that the number of hypertrophic cells in pellet cultures is reduced with either levels of RUNX2 suppression as highlighted in red (Fig. 3-2c).

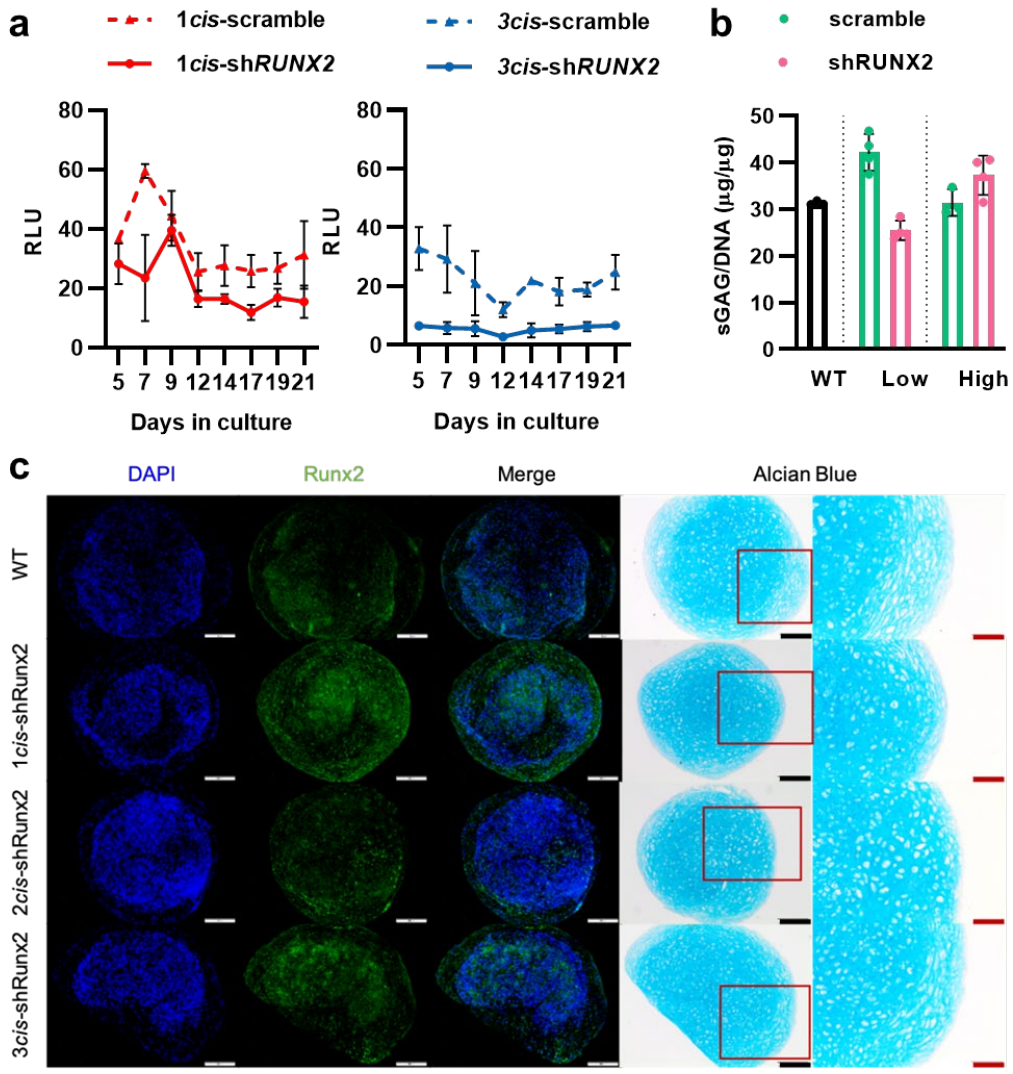

Figure 3-2 Effect of autoregulated RUNX2 suppression on MSC chondrogenesis. (a) Relative RUNX2 activity of gene circuit modified hMdChs over 21 days under chondrogenic culture (n=3-4) (b)Quantification of sGAG accumulation using DMMB assay demonstrating that gene circuit does not affect cartilage matrix accumulation (n =3-4) (c) RUNX2 immunofluorescence (green) to visualize RUNX2 protein expression and alcian blue staining (blue) of hMdCh pellet sections to visualize sGAG accumulation after 21-day chondrogenesis. Scale bar: 50µm

3.4.2 RUNX2 suppression promotes cartilage matrix accumulation under hypertrophic stimuli

Under hypertrophic stimuli, hMdChs pellets with both low and high levels of RUNX2 suppression accumulated significantly higher amount of sGAG compared to WT or scramble controls (Fig 3-3a,b). Upon analyzing mineral deposition using alizarin red staining, we observed no mineral deposition in untreated hMdCh pellets as there is no source of phosphate in the media. However, in hypertrophic induction group, we observed lower mineral deposition by RUNX2 suppressing hMdCh pellets compared to controls (Fig. 3-3c). This data indicates that both low and high levels of RUNX2 suppression significantly increases cartilage matrix accumulation and reduced mineral deposition under hypertrophic stimuli.

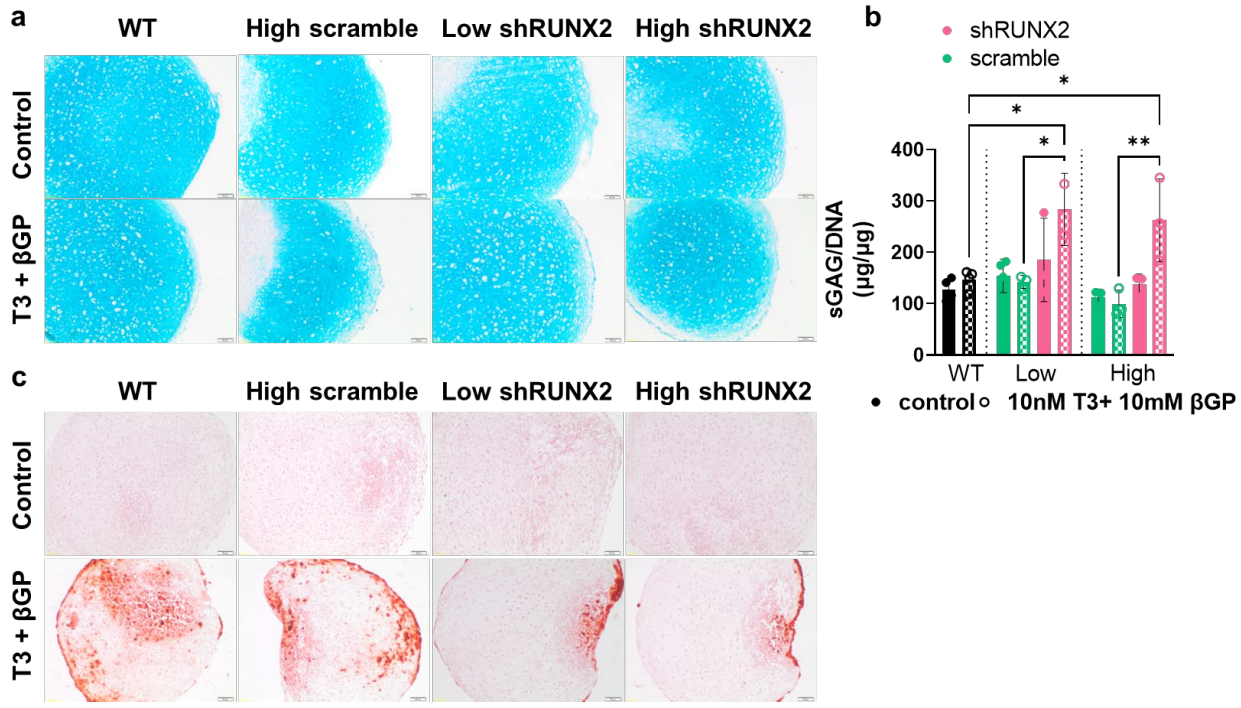

Figure 3-3 RUNX2 suppression increases cartilage matrix accumulation under hypertrophy. Visualization of (a) sGAG deposition via alcian blue staining (b) quantification of sGAG accumulation via DMMB assay (n=3-4) and (c) mineral deposition via alizarin red staining by control and hypertrophy induced WT and gene circuit modified hMdCh pellets. Scale bar: 50µm. The graphs are represented as mean ± S.D where significance is indicated by *p<0.05 and **p<0.01.

3.4.3 RUNX2 suppression increases expression of chondrogenic markers

Gene expression analysis revealed a significant downregulation of *ACAN* and *COL2A1* expression in WT hMdChs. However, both low and high level RUNX2 suppressing hMdChs retained higher levels of *ACAN* and *COL2A1* (Fig. 3-4a, b). Similarly, hypertrophic induction significantly downregulated SOX9 expression in WT hMdChs whereas RUNX2 suppressing hMdChs exhibited no changes in *SOX9* expression (Fig. 3-4c). Immunofluorescence analysis revealed higher ACAN protein expression in hMdChs with both low and high levels of RUNX2 suppression compared to controls under hypertrophic stimuli (Fig. 3-4e). Similarly, higher protein expression of COLII was also observed in RUNX2 suppressing hMdChs compared to WT and scramble controls (Fig. 3-4d).

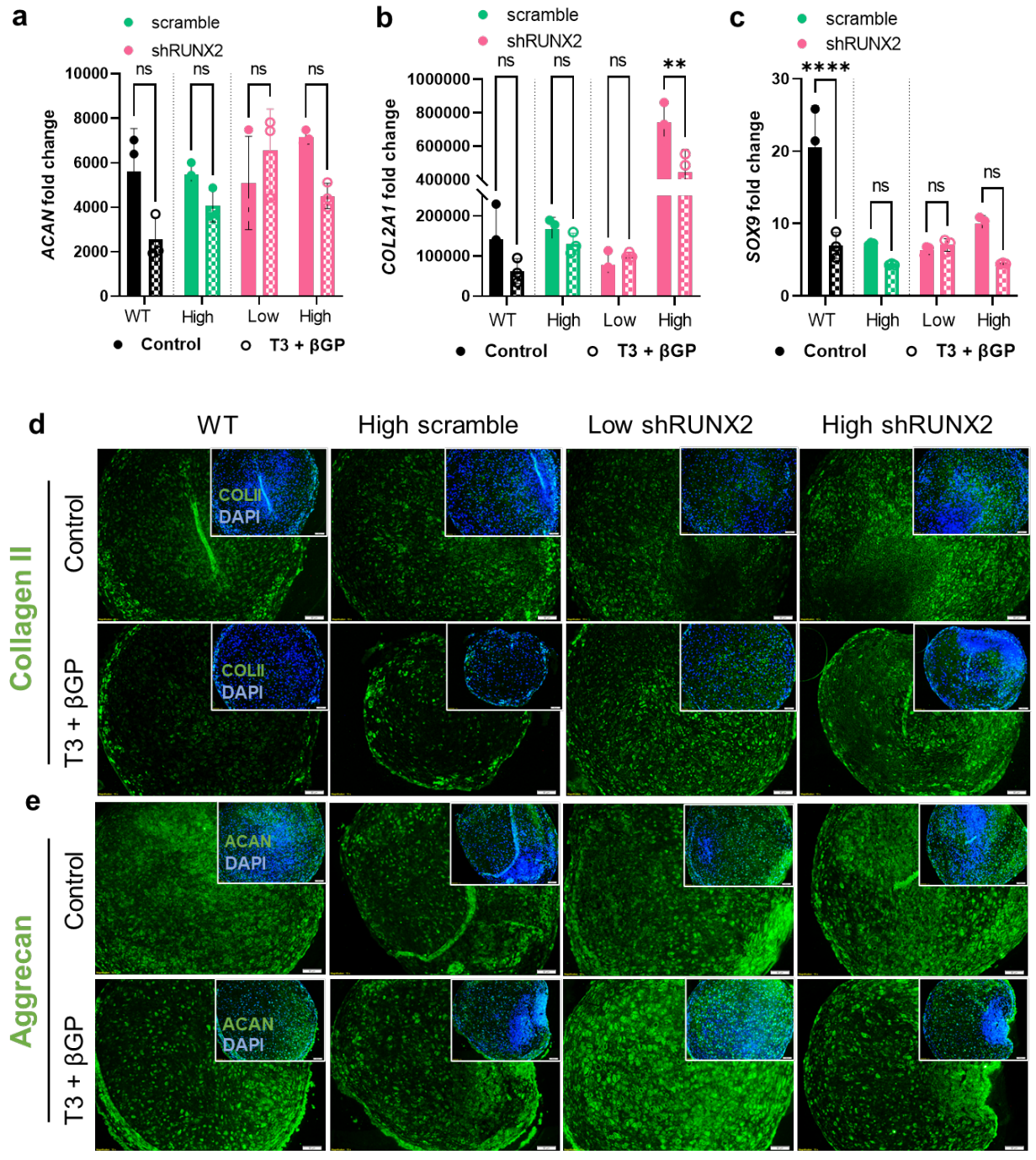

Figure 3-4 Effect of auto regulated RUNX2 suppression on chondrogenic marker expression in hMdChs. (a-c) qPCR gene expression analysis of chondrogenic markers ACAN, COL2A1 and SOX9 in hypertrophy induced hMdChs. Gene expression is normalized to day 0 for each cell type. Immunufluorescence analysis of (d) Collagen II (green) and (e) Aggrecan (green) protein expression in control and hypertrophy induced hMdCh pellets. Inset is merged image with counterstain DAPI (blue). Scale bar: 50µm. The graphs are represented as mean ± S.D where significance is indicated by *p<0.05 , **p<0.01 and ****p<0.001.

3.4.4 RUNX2 suppression decreases expression of hypertrophic markers

While hypertrophic induction did not change the COL10A1 gene expression, hypertrophy induced WT and scramble hMdCh pellets showed higher COLX protein expression than both low and high level RUNX2 suppressing hMdChs (Fig. 3-5a). Hypertrophic induction significantly increased both gene and protein expression of MMP13 in WT pellets which was successfully resisted by RUNX2 suppressing hMdChs (Fig. 3-5b). Interestingly, hypertrophic induction appears to upregulate *RUNX2* gene expression in RUNX2 suppressing hMdChs (Fig. 3-5c). However, immunofluorescence analysis revealed successful inhibition of COLX, MMP13 and RUNX2 protein expression in both low and high level RUNX2 suppressing hMdChs while their expression is upregulated in both WT and scramble hMdChs upon hypertrophic induction (Fig. 3-5d-f).

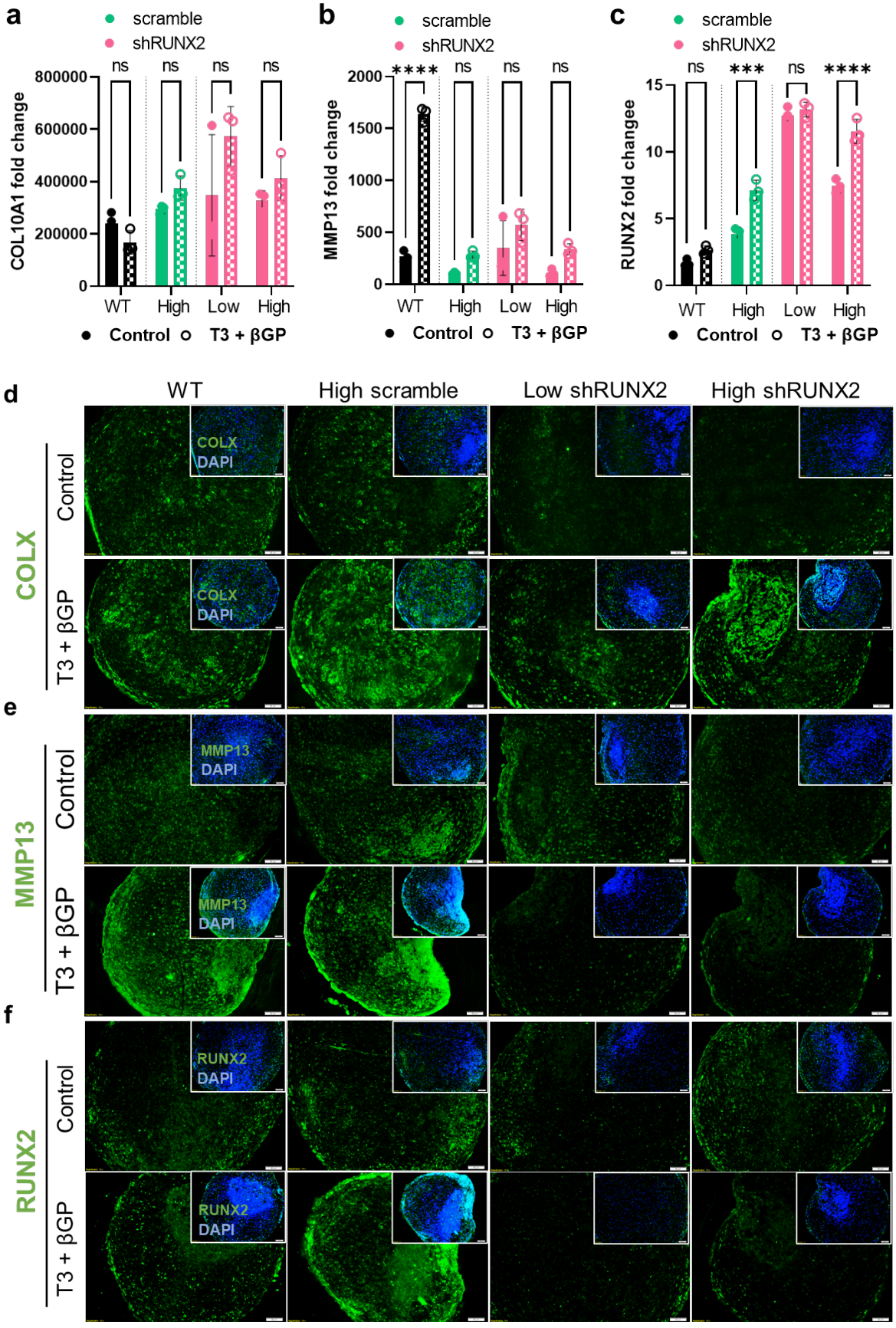
a
scramble
shRUNX2
COL10A1 fold change
800000
600000
400000
200000
0
ns
ns
ns
ns
WT
High
Low
High
Control
T3 + βGP
b
scramble
shRUNX2
MMP13 fold change
2000
1500
1000
500
0
****
ns
ns
ns
WT
High
Low
High
Control
T3 + βGP
c
scramble
shRUNX2
RUNX2 fold changee
15
10
5
0
ns
***
ns
****
WT
High
Low
High
Control
T3 + βGP
d
WT
High scramble
Low shRUNX2
High shRUNX2
COLX
Control
T3 + βGP
COLX
DAPI
e
MMP13
Control
T3 + βGP
MMP13
DAPI
f
RUNX2
Control
T3 + βGP
RUNX2
DAPI

Figure 3-5 Autoregulated RUNX2 suppression inhibits hypertrophic marker expression. (a-c) Gene expression analysis of hypertrophic markers COL10A1, MMP13 and RUNX2 in hypertrophy induced hMdChs (n=3). For each cell type, gene expression is normalized to respective day 0 values. Immunofluorescence for protein expression of hypertrophic markers (d) COLX (green), (e) MMP13 (green) and (f) RUNX2 (green) in hMdChs. Insets contain merge images with counterstain DAPI (blue). Scale bar: 50μm. The graphs are represented as mean ± S.D where significance is indicated by *p<0.05, **p<0.01, ***p<0.001 and ****p<0.001.

3.5 Discussion

Increasing the stability of hMdCh's chondrogenic phenotype has been a long-standing goal of cartilage regeneration community towards clinical application of MSC-based therapies for cartilage repair. Although RUNX2 drives hypertrophic maturation of hMdChs, we have previously shown that RUNX2 is also essential for early chondrogenesis, thus inhibiting chondrogenesis if suppressed constitutively[25]. In this study we show that auto regulated RUNX2 suppression via our gene circuits does not inhibit MSC chondrogenesis. Moreover, we demonstrate that both low and high levels of RUNX2 suppression increases cartilage matrix accumulation by hMdChs under hypertrophic stimuli of T3 and βGP. Additionally, both low and high levels of RUNX2 suppression successfully inhibit mineral deposition by hMdChs upon hypertrophic induction. We further show that RUNX2 suppressing hMdChs retained higher expression of chondrogenic markers under hypertrophic induction compared to WT hMdChs. Finally, we demonstrate that RUNX2 suppressing hMdChs successfully suppress the expression of hypertrophic markers compared to WT and scramble controls under hypertrophic induction. Taken together, this data suggests that auto regulated RUNX2 suppression in hMdChs successfully attenuates hypertrophy and increases cartilage matrix accumulation upon treatment with hypertrophic stimuli.

Since majority of RUNX2 suppression starts to occur when cells have successfully undergone chondrogenesis and are in pre-hypertrophic stage, our gene circuit can successfully suppress RUNX2 without compromising chondrogenesis. Moreover, considering the heterogeneous nature of human MSCs, the gene circuit allows each cell to self-regulate RUNX2 expression based on intracellular RUNX2 concentrations by establishing a negative feedback loop,

without the need for any exogenous interference. Luciferase reporter verified the low and high levels of RUNX2 activity suppression with 1cis-shRUNX2 and 3cis-shRUNX2 gene circuits respectively. Although 1cis-shRUNX2 gene circuits successfully suppressed RUNX2 activity compared to 1cis-scramble, the RUNX2 activity was consistently higher than 3cis-shRUNX2 gene circuits throughout chondrogenesis. This data is parallel to our previous observations in mouse chondroprogenitor ATDC5 cell line[25].

Hypertrophic maturation of hMdChs is similar to that of growth plate chondrocytes[28]. Although one week of hypertrophic induction does not seem to affect cartilage matrix accumulation in wildtype and scramble hMdChs, both low and high RUNX2 suppressing hMdChs accumulated higher cartilage matrix upon treatment with hypertrophic stimuli. This suggests a synergistic effect of RUNX2 suppression and treatment with T3 and βGP on hMdChs matrix accumulation. Previously, our lab has shown the biphasic effect of phosphate on cartilage matrix accumulation by ATDC5 cells where moderate Pi abundance enhanced chondrogenic markers and cartilage matrix production during early chondrogenesis while inducing hypertrophy during late chondrogenesis[27]. Here, treatment with βGP combined with RUNX2 suppression seems to favor the pro-chondrogenic function of Pi while inhibiting hypertrophy induction, validated by increase in sGAG accumulation and inhibition of mineral deposition.

During hypertrophic maturation, the expression of chondrogenic markers is downregulated and RUNX2 drives the expression of hypertrophic markers COL10 and MMP13. In present study, although treatment with T3 and βGP did not significantly downregulate *ACAN* gene expression, low level RUNX2 suppressing hMdChs retained higher ACAN protein expression compared to WT and scramble hMdChs. Moreover, hMdChs with high level RUNX2 suppression retained significantly higher *COL2A1* expression compared to controls under hypertrophic induction.

Consistent with previously studies[26], hypertrophic stimuli caused significant downregulation of SOX9 expression in wildtype hMdChs. Although hypertrophic induction did not change SOX9 gene expression both scramble and RUNX2 suppressing hMdChs, gene circuit modified hMdChs generally expressed lower levels of SOX9 compared to WT.

Analysis of hypertrophic markers reveals interesting patterns. While hypertrophic induction does not change *COL10A1* gene expression, we observed a distinct increase in COLX protein expression in wildtype and scramble hMdChs which was successfully resisted by both low and high RUNX2 suppressing cells. Hypertrophic induction also led to a significant increase in *MMP13* gene expression on wildtype hMdChs which was not observed in either scramble or RUNX2 suppressing hMdChs. However, both wildtype and scramble hMdChs showed increase in MMP13 protein expression upon hypertrophic induction while both low and high level RUNX2 suppressing hMdChs resisted this increase. Since cartilage accumulation is the net sum of cartilage matrix production and degradation, inhibition of MMP13 expression provides additional justification for higher cartilage matrix accumulation by RUNX2 suppressing hMdChs under hypertrophic stimuli. Interestingly, RUNX2 suppressing hMdChs showed highest levels of *RUNX2* gene expression compared to WT and scramble controls. However, immunofluorescence analysis showed successful suppression of RUNX2 protein expression by both low and high RUNX2 suppressing hMdChs while increase in RUNX2 expression in wildtype and scramble hMdChs upon chondrogenic induction. Our gene circuit utilizes RNA interference to induce RUNX2 suppression which can occur via either incorporating RISC complex to cause mRNA cleavage or by causing translational inhibition followed by exonucleotic decay[107,108,123,124]. This data indicates that our gene circuit affects the post-transcriptional processing of RUNX2, causing translational inhibition, where lack of RUNX2 protein under hypertrophic stimuli causes increased

transcription of RUNX2 mRNA while it's translation is continually blocked by the shRUNX2 gene circuit. While this data successfully demonstrates the efficacy of the gene circuit to inhibit RUNX2 protein expression, future studies investigating RNA interference pathways employed by the gene circuit would be important to understand it's function.

There does not appear to be a significant difference between the efficacy of low and high RUNX2 suppressing hMdChs to resist T3 and βGP induced hypertrophic maturation. Both low and high RUNX2 suppressing hMdChs accumulated similar amounts of cartilage matrix and deposited lower mineral under hypertrophic induction. Moreover, both low and high RUNX2 suppressing hMdChs showed increased expression of chondrogenic markers and decreased expression of hypertrophic markers under hypertrophic induction. This study suggests that low levels of RUNX2 suppression is sufficient to increase the stability of hMdChs chondrogenic phenotype and increase cartilage matrix accumulation under hypertrophic stimuli. In addition to matrix accumulation, zonal architecture of articular cartilage is also important for its optimal function. Therefore, future studies that incorporate attaining articular cartilage architecture along with increasing matrix accumulation are important. Furthermore, the efficacy of our auto regulated RUNX2 suppressing gene circuits need to be tested in vivo to validate our results in animal models of cartilage defect repair.

3.6 Conclusion

Clinical application of MSC- based cartilage repair strategies is dependent on the ability of hMdChs to resist hypertrophic maturation and continue producing cartilage extracellular matrix. In this study, we demonstrate the applicability of synthetic biology tools like autoregulated gene circuits to improve MSC-based cartilage regeneration. We show that auto regulated RUNX2 suppression does not affect MSC chondrogenesis and inhibits T3 and βGP induced hypertrophic

maturation, with RUNX2 suppressing hMdChs showing higher chondrogenic activity than unmodified wildtype cells. We also found that low levels of RUNX2 suppression is sufficient to increase the stability of hMdCh chondrogenic phenotype. Our results exhibit that synthetic gene circuits are a valid approach to regulate and determine cell fate without the need for exogenous cues that can have potential off-target effects.

Chapter 4 RUNX2 suppression protects hMdChs from inflammation-induced matrix catabolism and hypertrophic maturation

4.1 Abstract

There is evidence that inflammatory factors like interleukin-1 (IL-1) and tumor necrosis factor α (TNF-α) increase in the joint following traumatic cartilage injury. These cytokines cause degradation of cartilage matrix by inducing expression of catabolic enzymes like MMP13 through upregulation of RUNX2, the master transcription factor that orchestrates chondrocyte hypertrophy during endochondral ossification. Exposing human mesenchymal stem cells (hMSCs) to inflammatory cytokines drives their hypertrophy, thereby decreasing accumulation of extracellular matrix (ECM) components and the mechanical properties of engineered cartilage and resulting in subpar repair of cartilage injuries. We hypothesized that suppressing RUNX2 activity would protect nascent cartilage tissue produced by MSC derived chondrocytes (hMdChs) from catabolic effects of inflammatory cytokines. However constitutive silencing of RUNX2 has been shown to inhibit chondrogenesis. To control the timing and level of RUNX2 suppression, we created a gene circuit which targets RUNX2 by synthetically inducing a negative feedback loop in chondrogenic cells to reduce the negative effect of hypertrophy without interfering with MSC chondrogenesis. We investigated the effect of RUNX2 suppression on the response to inflammatory factors in hMSC chondrogenic pellets cultures. We show that autoregulated RUNX2 protects hMdChs from inflammation-induced hypertrophy, increases cartilage matrix retention and increases expression of chondrogenic markers under inflammatory stimuli.

4.2 Introduction

Articular cartilage is avascular, resulting in limited healing ability which often causes traumatic cartilage injuries to progress into post-traumatic osteoarthritis. Inflammation is a key mediator of osteoarthritis and one of the fundamental challenges towards successful cartilage repair[29,47]. Within hours of traumatic injury, the levels of inflammatory cytokines like IL-1β, IL-1α, IL-6, TNFα etc. and catabolic mediators begin to increase in the joint milieu[125]. Current treatment strategies for cartilage injury result in sub-optimal repair and do not resolve inflammation. Microfracture, a method to bring progenitor cells to the defect site for healing results development of fibrocartilage as compared to hyaline cartilage, resulting in a mismatch of mechanical properties, which compromises joint function[109]. Use of osteochondral allografts is limited by donor site morbidity and insufficient donor tissue[126]. In autologous chondrocyte implantation (ACI), chondrocytes are isolated, expanded in vitro and implanted at the defect site to heal the defect. Although it provides good clinical outcomes, harvesting chondrocytes without further damaging the tissue is a challenge. Furthermore, the inconsistency in chondrocyte quality in younger vs. older patients makes it harder to use for all patients[62,127]. Therefore, tissue engineering-based strategies have been widely explored to repair articular cartilage and prevent progression of injury towards PTOA.

Adult human mesenchymal stem cells (hMSC) are an appealing cell source to engineer cartilage due to their ability to differentiate into chondrocytes[9,12]. This process is carried out by chondrogenic transcription factor SOX9[128–131]. Like chondrocytes, hMSC-derived chondrocytes (hMdChs) can produce the articular cartilage matrix macromolecules collagen II and aggrecan, which are important for supporting the compressive loading on articular cartilage. Collagen II forms the fibrillar network and provide tensile strength while negatively charged sulfated

glycosaminoglycan (sGAG) molecules in aggrecan attract water molecules to generate osmotic pressure and provide compressive strength[30]. However, the chondrogenic phenotype of hMdChs is unstable which limits the applicability of MSC based repair of cartilage defects. As discussed in the previous chapter, following chondrogenesis, hMdChs undergo hypertrophic maturation orchestrated by the master transcription factor of RUNX2 and follow developmental pathway of endochondral ossification[18,28,101]. RUNX2 decreases the expression of cartilage macromolecules collagen II and aggrecan and increases the expression of collagen X, altering matrix composition. Moreover, RUNX2 induces expression of matrix degrading enzymes like MMP13 and ADAMTS 4/5 which degrade collagen II and aggrecan and compromise the hydrostatic loading capability of the engineered cartilage[13,101,132]. Various methods have been employed to increase matrix accumulation by hMdChs like growth factor treatments, mechanical loading[95,96], induction of hypoxia[90,115,133]. However, these methods have had limited success in preventing cartilage matrix loss in long term cultures.

Inflammation further abrogates the applicability of hMdChs for cartilage repair. Inflammatory cytokines (IL-1, TNF-α, IL-6 etc) inhibit MSC chondrogenesis by activating of NFκB pathway causing suppression of SOX9[105,134]. Furthermore, activation of NFκB pathway upregulates RUNX2 in already differentiated hMdChs[17,135]. These cytokines also upregulate MEF2C expression[18,111], which is a TF that drives RUNX2 expression, hence activating RUNX2 expression via multiple signaling pathways, resulting in cartilage matrix degradation due to expression of catabolic enzymes like MMPs. Therefore, to successfully engineer viable cartilage, hMdChs need to be protected from inflammation-induced matrix catabolism. Multiple studies have been performed aiming to resolve inflammation. Researchers have used 3D scaffolds to deliver anti-inflammatory drugs, however it is difficult to achieve sustained release for prolonged time

periods[53,136]. Genetic engineering approaches have been employed to induce expression of IL-1 receptor antagonists to prevent IL-1 induced response, but it does not protect cells from other inflammatory factors[84,88,137–139]. Hence there is a need for novel strategies to prevent inflammation induced matrix catabolism in hMdChs.

The primary objective of this project is to increase matrix accrual by hMdChs under inflammatory conditions to generate mechanically functional cartilage tissue for focal defect repair. As mentioned before, RUNX2 plays a pivotal role in mediating the catabolic effects of inflammatory cytokines by increasing the expression of matrix degrading enzymes like MMP13 and ADAMTS4/5. Therefore, we **hypothesized** that silencing RUNX2 in hMdChs would decrease matrix catabolism and increase accretion of cartilage matrix macromolecules under inflammatory conditions. This would be due to both reduction in protease expression that causes matrix degradation and maintenance of chondrogenic marker expression that produces these matrix macromolecules. Using a novel closed loop gene circuit previously developed in our lab, we induced RUNX2 suppression and analyzed the effect on hMdChs cartilage matrix accumulation under inflammatory conditions.

4.3 Methods

4.3.1 Synthesis of gene circuits

All vectors were constructed as previously described[25] and incorporated into lentiviruses by the UM Vector Core. The shRNA sequence for shRUNX2 was selected from the Hannon Elledge library (RNAi codex). Using the pINDUCER plasmid[121], a Tet-on inducible system was modified to synthesize tet-on-Luc-mir30-shRUNX2. Next, the COL10a1 basal promoter (-220 to 110 bp) and cis-enhancers (-4296 to- 4147) were synthesized using IDT technology using gBlocks gene fragments service and assembled into pLenti-CMVtight-Egfp-Puro vector[101]. Finally, the

Tet-on promoter in pINDUCER was replaced by COL10a1 promoter containing varying number of cis-enhancers to obtain 1cis-luc-mir30-shRUNX2, 2cis-luc-mir30-shRUNX2 and 3cis-luc-mir30-shRUNX2. Scramble controls were created by using the same gene circuit backbone and scrambling shRUNX2 sequence to create a non-specific oligonucleotide sequence which doesn't target any genes.

4.3.2 Cell culture

Cell Expansion: Human bone marrow derived mesenchymal stem cells (hMSCs) were obtained from our collaborators at Case Western Reserve University and expanded in Low Glucose DMEM with 10% Fetal Bovine Serum and 10ng/ml FGF-2[83].

Lentiviral Transduction: hMSCs were plated at density of 10,000 cells/cm^2 and transduced with lentiviruses containing low and high RUNX2 suppressing gene circuits at moieties of infection (MOI) = 5. Twenty-four hours post-transduction, media was replaced with expansion media described above. Transduced cells were selected by treatment with 1µg/ml Puromycin treatment.

MSC chondrogenesis: Wildtype and gene circuit transduced hMSCs were trypsinized using 0.05% Trypsin-EDTA and resuspended in chondrogenic media at 125000 cells/ml. Chondrogenic media consisted of High Glucose DMEM (Gibco, Cat # 11965-092), supplemented with 1 % (v/v) insulin-transferrin-selenium (Corning, Cat # 354350), 1 % (v/v) non-essential amino acids (Gibco, Cat # 11-140-050) 40 μg/mL L-proline (Sigma, cat # P-0380), 50 μg/mL L-ascorbic acid-2-phosphate (Sigma, Cat # A8960), 0.1 μM dexamethasone (Sigma, Cat # D4902), and 10 ng/mL TGF-β1 (Shenandoah Biotechnology, cat # 100-39). hMSC pellets were formed by dispensing 200µl of cell suspension per well of 96 well plate followed by centrifugation at 1640 rpm for 5

minutes. Cells were incubated at 37℃, 5% CO_2, 95% humidity and allowed to condense into tight pellets for 3 days after which fresh chondrogenic media was supplied every other day.

Inflammation treatment: After 21 days of chondrogenic culture, human MSC derived chondrocytes (hMdChs) were treated with individual inflammatory cytokines for 72 hours to provide inflammatory stimulus. The culture media consisted of chondrogenic media without TGFβ1 and dexamethasone, supplemented with either 0.1ng/ml IL-1β or 0.1ng/ml TNF-α. hMdChs maintained in chondrogenic media without TGFβ1, and dexamethasone were used as controls.

4.3.3 Biochemical Analysis

Samples were digested in papain buffer made of papain, EDTA and sodium phosphate, overnight at 65℃. Dimethyl methylene blue (DMMB) assay was used to quantify sGAG concentrations as previously described[27]. Standard curve was generated using known concentrations of chondroitin-6-sulfate. 10µl of sample was added per well followed by 200 µl of DMMB dye. After adding the dye, absorbance was immediately read using Synergy H1 plate reader at 425nm and 495nm. sGAG concentrations were normalized to DNA content using PicoGreen DNA assay kit (Thermo Fisher). 10µl of samples and λDNA standards were added to black 96 well plate followed by Picogreen dye. Fluorescence was measured using Synergy H1 plate reader at excitation wavelength of 498nm and emission wavelength of 528nm.

4.3.4 Histological Analysis

hMdCh pellets were washed with Phosphate Buffered Saline (PBS) and fixed using 10% Neutral Buffered Formalin for 30 minutes. After fixing cells were washed with PBS and stored in 70% ethanol untill ready to process. hMdCh pellets were then dehydrated using graded series of

ethanol (70-100%), cleared with Xylene, embedded in paraffin wax and sectioned into 7µm thick sections. The sections were then cleared in Xylene, rehydrated, stained with alcian blue (1% in 3% acetic acid, Poly Scientific) and counter stained with Nuclear Fast Red (Electron Microscopy Sciences) to visualize sGAG deposition.

4.3.5 Immunofluorescence

The hMdCh pellet sections were cleared and rehydrated as explained above. Peroxidase activity of the pellets was blocked using 3% hydrogen peroxide followed by antigen retrieval using BD Retreivagen Antigen Retrieval kit (Thermofisher). Samples were then incubated overnight with primary antibody of ACAN (AbClonal, A8536, 1:500), COLX (AbClonal, A6889,1:100), RUNX2 (AbClonal, A2851, 1:100), MMP13 (AbClonal, A16920, 1:100) or COLII (Abcam, ab34712, 1:150) at 4°C. Samples were then stained with secondary antibody (IgG anti-rabbit, 488, 1:500, Invitrogen, A11034) for one hour followed by 5-minute incubation with 4', 6-diamidino-2-phenylindol (DAPI, Sigma, 300 nM). Anti-fade was used to coverslip the slides and images were taken using Olympus microscope.

4.3.6 Luciferase Analysis

RUNX2 activity in hMdChs was measured using luciferase reporter in the gene circuit. Six hours after treatment with inflammatory cytokines, D-luciferin was added to the culture media. After 20-minute incubation period, luminescence was measured using Synergy H1 plate reader. Following luciferase measurement, fresh culture media was added to the wells and plates were put back in incubators.

4.3.7 Statistical Analysis

All the data is presented as mean ± SD. All statistical analysis is performed using GraphPad Prism 8.3 software (GraphPad, San Diego, CA). One-way or two-way ANOVA was used with Tukey's multiple comparison post-hoc test. P-value < 0.05 was considered statistically significant.

4.4 Results

4.4.1 shRUNX2 modified hMdChs inhibit inflammation-induced increase in RUNX2 activity

Treatment with IL-1β increased RUNX2 activity in scramble hMdChs while shRUNX2 hMdChs were successfully able to resist this increase (Fig. 4-1a). Treatment with TNF-α also induced a significant increase in RUNX2 activity in scramble hMdChs, while shRUNX2 hMdChs resist this increase (Fig. 4-1b). This data successfully demonstrates that treatment with inflammatory cytokines upregulate RUNX2 activity in hMdChs which is successfully suppressed by shRUNX2 hMdChs.

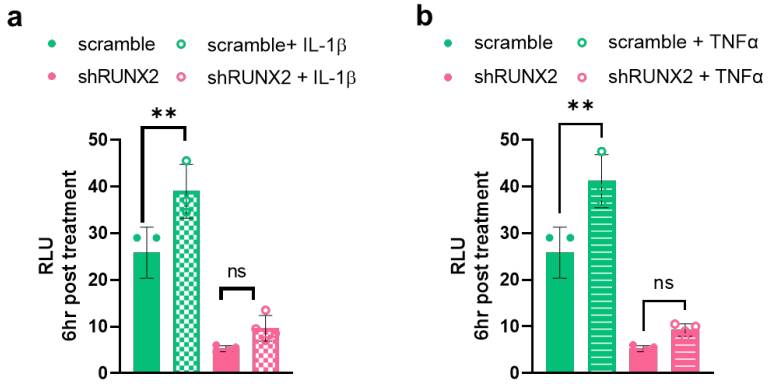

Figure 4-1 Treatment with inflammatory cytokines increase RUNX2 activity in hMdChs. RUNX2 activity of scramble and shRUNX2 modified hMdChs after six hour treatment with (a) 0.1ng/ml IL-1β (n=3-4) (b) 0.1ng/ml TNF-α (n=3-4) measured as relative luminescence units (RLU). The graphs are represented as mean ± S.D where statistical significance was determined using one way ANOVA and indicated by *p<0.05 and **p<0.01.

4.4.2 RUNX2 suppression protects hMdChs from inflammation-induced cartilage matrix loss

Next, we analyzed the effect of RUNX2 suppression on inflammation mediated neocartilage degradation in hMdChs. Treatment with IL-1β induced significant matrix loss in hMdChs however shRUNX2 hMdChs retained higher amounts of sGAG compared to WT or

scramble controls (Fig. 4-2 a,b). shRUNX2 hMdChs also retained higher amounts of sGAG upon treatment with TNF-α (Fig. 4-2 a,b). Taken together, this data suggests that RUNX2 at-least partially mediates the catabolic effects of pro-inflammatory cytokines and RUNX2 suppression in hMdChs increases cartilage matrix retention upon treatment with IL-1β.

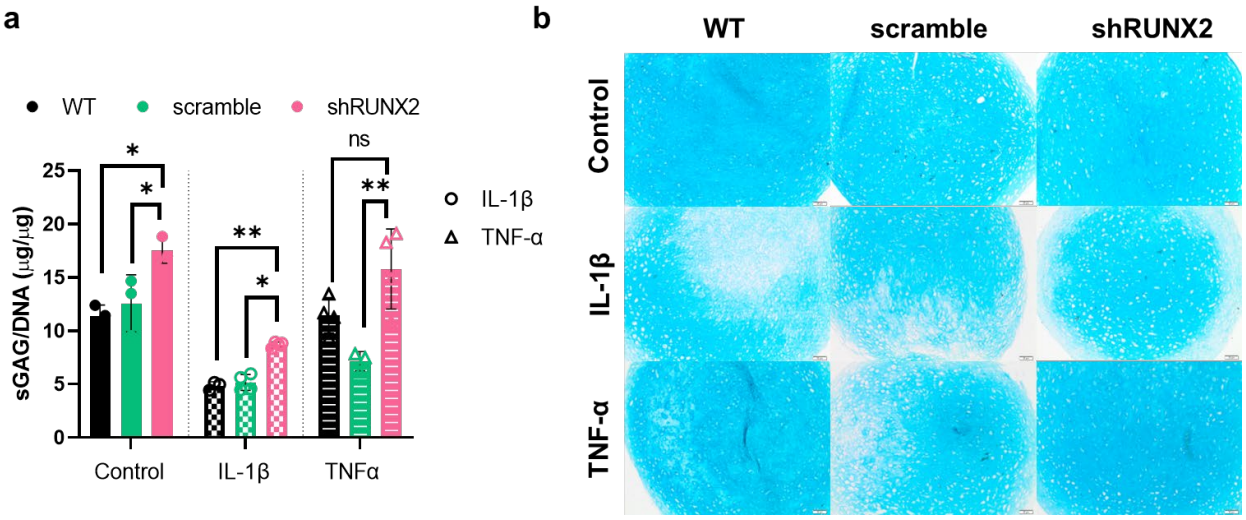

Figure 4-2 RUNX2 suppression decreases inflammation-induced neocartilage degradation in hMdChs. (a) sGAG quantification (n=3-4) and (b) alcian blue staining for sGAG visualization by wildtype, scramble and shRUNX2 modified hMdChs after 72-hour treatment with IL-1β or TNF-α. Scale bar: 50μm. The graphs are represented as mean ± S.D where significance is indicated by *p<0.05 and **p<0.01.

4.4.3 RUNX2 suppressing hMdChs maintain expression of chondrogenic markers under inflammation

To determine how RUNX2 suppression increases sGAG retention in hMdChs, we analyzed the protein expression of chondrogenic markers in hMdCh pellets treated with 0.1ng/ml IL-1β using immunofluorescence. shRUNX2 hMdChs retained higher expression of chondrogenic markers ACAN (Fig. 4-3a) and COLII (Fig. 4-3b) when treated with IL-1β while considerable loss was observed in WT and scramble hMdChs.

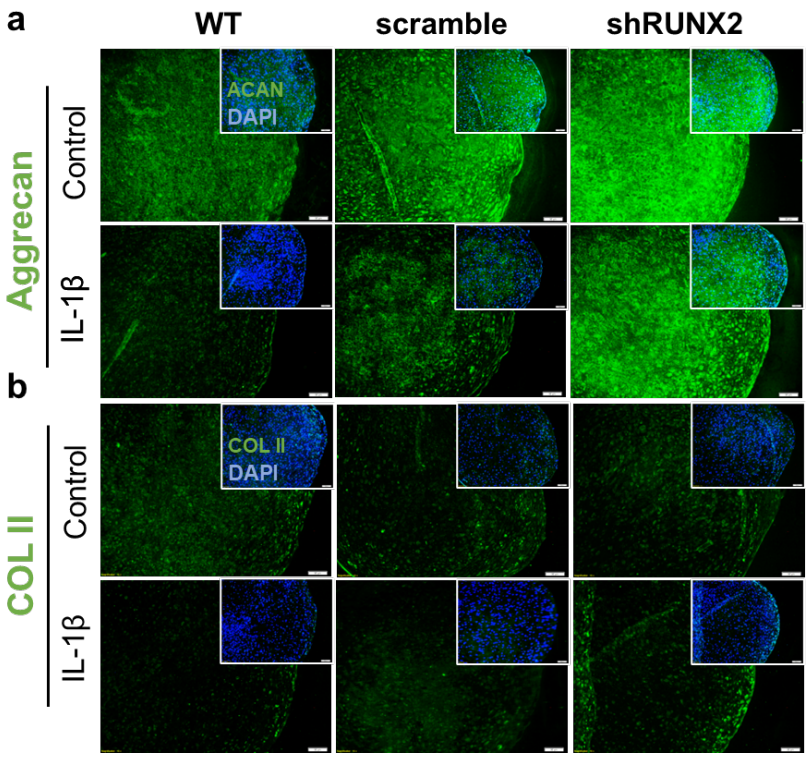

Figure 4-3 RUNX2 suppression protects hMdChs from inflammation induced downregulation of chondrogenic markers. Immunofluorescence analysis of chondrogenic markers (a) ACAN, green and (b) COLII, green untreated (control) and IL-1β treated hMdCh pellets. Insets are merged images of protein of interest and nuclear stain DAPI (blue). Scale bar: 50μm.

4.4.4 RUNX2 suppression attenuates inflammation-induced hypertrophy in hMdChs

Treatment with IL-1β increased RUNX2 protein expression in WT and scramble hMdChs which was suppressed by shRUNX2 hMdChs (Fig. 4-4a). IL-1β also increased the expression of hypertrophic marker COLX in both WT and scramble pellets which was also suppressed by shRUNX2 hMdChs (Fig. 4-4b). Moreover, IL-1β induced expression of catabolic marker MMP13 in WT and scramble pellets while shRUNX2 hMdChs resisted this increase (Fig. 4-4c).

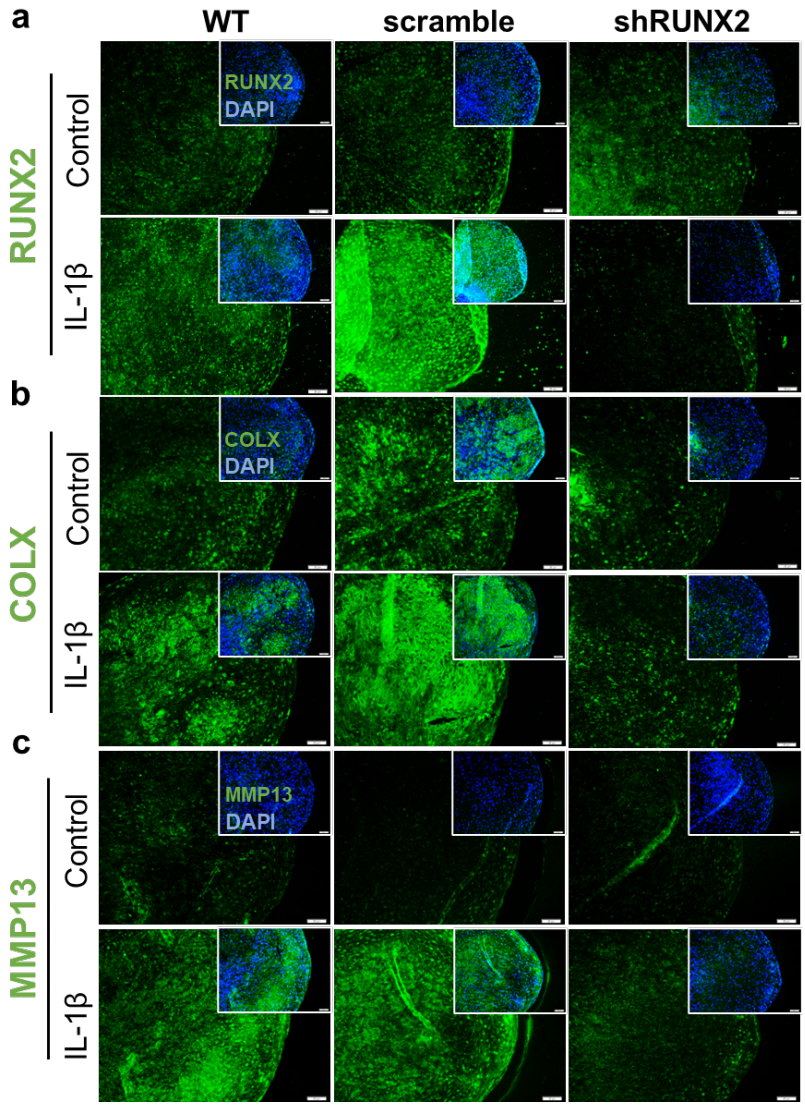

Figure 4-4 RUNX2 suppression inhibits IL-1β-induced increase in hypertrophic marker expression in hMdChs. Immunofluorescence analysis wildtype, scramble and shRUNX2 modified hMdChs either untreated (control) or treated with 0.1ng/ml IL-1β for the expression of hypertrophic proteins (a) RUNX2 and (b) Collagen type X, and catabolic marker (c) MMP13. Insets represent merged images with protein of interest in green and nuclear stain DAPI in blue. Scale bar: 50µm.

4.5 Discussion

Inflammation mediates the progression of cartilage injury towards PTOA[29,140,141]. Furthermore, the catabolic effects of inflammatory cytokines in the joint milieu present a major challenge towards clinical application of MSC-based cartilage repair strategies[142,143]. In this study

we found that treatment with inflammatory cytokines IL-1β and TNF-α increases RUNX2 activity in hMdChs, which is successfully suppressed by shRUNX2 modified hMdChs. IL-1β induced significant neocartilage degradation in hMdChs and we found that RUNX2 suppression protected hMdChs from IL-1β mediated cartilage matrix catabolism. Upon further investigating the effect of IL-1β on hMdChs, we observed that treatment with IL-1β increased the protein expression of hypertrophic markers RUNX2, COLX and MMP13 and decreased the expression of chondrogenic markers ACAN and COLII in WT as well as scramble modified hMdChs, which was resisted by shRUNX2 modified hMdChs.

Inflammatory cytokines are important signaling molecules that act in autocrine and paracrine fashion to influence a multitude of physiological processes. There is little evidence that immune cells infiltrate into the cartilage tissue upon injury[144], indicating that pro-inflammatory function of immune cells is primarily mediated by the secretome of immune cells in the synovium, predominantly via cytokines and chemokines[144–146]. IL-1β and TNF-α are the most well studied cytokines known to mediate progression of post-traumatic osteoarthritis, hence we chose these cytokines to mimic joint inflammation. Since inflammatory cytokines act via multiple pathways, we decided to utilize 3cis-shRUNX2 gene circuits which induces maximum RUNX2 suppression to investigate the role of RUNX2 in mediating the effect of inflammatory cytokines. In line with previous studies[105,147,148], we observed that treatment with both IL-1β and TNF-α increase RUNX2 activity in hMdChs as measured by luciferase reporter. Furthermore, we demonstrate that shRUNX2 gene circuits successfully suppress RUNX2 activity in both IL-1β and TNF-α treated hMdChs indicating that the gene circuit is active and responds predictably to these exogenous cues. Furthermore, we observed that treatment with IL-1β induced significant neo-cartilage degradation in hMdCh pellets, where RUNX2 suppressing hMdChs retained significantly higher amounts of

matrix compared to WT and scramble controls when treated with IL-1β. This result indicates that the catabolic effects of IL-1β are at least partially mediated by RUNX2. Interestingly, treatment with TNF-α did not cause matrix loss in either WT or shRUNX2 modified hMdChs but caused significant matrix loss in scramble hMdChs. Although the concentrations of these cytokines were chosen based on the synovial fluid concentrations of osteoarthritis knees[142,143,149], 0.1n/ml TNF-α might be insufficient to induce cartilage degradation in 72 hours. Therefore, future studies with higher concentrations and longer treatment times would be useful to conclusively determine the role of RUNX2 in mediating the catabolic and pathological effects of TNF-α on articular cartilage.

IL-1β has been shown to induce cartilage matrix degradation by inducing the expression of matrix metalloproteinases, and transcription factor RUNX2 is a known inducer of hypertrophic and catabolic markers like COLX and MMP13 in chondrocytes. Since RUNX2 suppression partially rescued hMdChs from IL-1β induced matrix catabolism, we analyzed the expression of hypertrophic, catabolic and chondrogenic markers in hMdChs to understand its mechanism. As expected, treatment with IL-1β increased the expression of RUNX2 and its downstream targets COLX and MMP13 in wildtype and scramble hMdCh pellets. However, shRUNX2 modified hMdChs successfully resisted this increase in RUNX2 protein and inhibited COLX and MMP13 expression. Moreover, protein expression analysis of chondrogenic markers revealed that shRUNX2 hMdChs retained higher expression of aggrecan and collagen II upon treatment with IL-1β compared to wildtype and scramble hMdChs. Since collagen II and proteoglycans like aggrecan are degraded by MMP13, it appears that RUNX2 suppression protects the neocartilage from inflammation-induced matrix catabolism by downregulating MMP13 expression, resulting in enhanced cartilage matrix retention.

This study provides important evidence towards the efficacy of auto regulated RUNX2 suppression to improve clinical application of MSCs for cartilage defect repair under inflammation. However, the inflammatory microenvironment in the injured joint is highly complex, comprising of multiple cell types interacting via autocrine, paracrine, and direct cell-cell contact[5,140]. As a result, utilizing individual cytokines like IL-1β and TNF-α does not completely recapitulate the complex pathological environment of the injured joint. Therefore, future in vitro studies that capture the complex multicellular interactions in the injured joint as well as in vivo studies using cartilage defect repair, and PTOA models are highly desirable to validate the efficacy of the gene circuit to improve MSC based cartilage repair.

4.6 Conclusion

Inflammation-induced hypertrophic maturation of hMdChs and neocartilage degradation is a major challenge towards clinical application of MSC-based cartilage repair strategies. In this study we demonstrate that auto regulated RUNX2 suppression improves MSC-based cartilage regeneration under inflammatory environments. We show that RUNX2 suppression via our gene circuit supported chondrogenic activity of hMdChs and inhibited hypertrophic maturation under inflammatory stimulus. Overall, this study demonstrates the application of synthetic biology tools like closed loop gene circuits to improve tissue engineering outcomes under hostile culture environments.

Chapter 5 Autoregulated RUNX2 suppression modulates crosstalk between hMdChs and pro-inflammatory macrophages

5.1 Abstract

Macrophages, the predominant inflammatory cell in the joint, secrete a cocktail of inflammatory cytokines to induce cytokine and proteinase secretion by chondrocytes in injured cartilage in the joint. These cytokines synergistically increase inflammation in both cell types creating a positive feedforward loop and maintaining a high level of inflammation that drives early osteoarthritis (OA) onset. Although adult human mesenchymal stem cell (hMSC) based cartilage regeneration therapies could be used for cartilage repair, inflammatory cytokines in injured joint inhibit their ability to undergo chondrogenesis and induce hypertrophic maturation in hMSC derived chondrocytes (hMdChs). This process is orchestrated, in part, by upregulation of RUNX2, the master transcription factor of chondrocyte hypertrophy, which decreases the expression of cartilage matrix molecules and increases the expression of cartilage degrading metalloproteinases (MMPs). We hypothesize that RUNX2 suppression in hMdChs can 1) increase cartilage matrix accumulation by protecting engineered tissue from catabolic effects of inflammatory cytokines and 2) disrupt the pro-inflammatory crosstalk between hMdChs and inflammatory macrophages. Using a conditioned media-based co-culture model, we show that autoregulated RUNX2 suppression not only protects hMdChs from M1 conditioned media (M1CM) induced hypertrophy and cartilage matrix catabolism but also inhibits the pro-inflammatory crosstalk between hMdChs and pro-inflammatory macrophages, resulting in attenuation of macrophage inflammation.

5.2 Introduction

Inflammation is a key contributor towards progression of traumatic cartilage injury into post traumatic osteoarthritis (PTOA), a painful debilitating disease[29]. Macrophages, the predominant immune cells present in the synovium, are the primary contributor towards inflammation post joint injury.[21,140] Traumatic cartilage injury initiates the release of damage associated molecular patterns (DAMPs) like S100A8, S100A9 and HMGB-1 which interact with toll like receptors (TLRs) on macrophage surface to induce pro-inflammatory M1-like phenotype via activation of NFκB and STAT1 pathways[20,21,36]. These pro-inflammatory macrophages are responsible for protecting the body from invading pathogens and recruiting progenitor cells to initiate healing. In other tissues of the human body, the inflammation phase then transitions into the remodeling phase due secretion of anti-inflammatory cytokines and growth factors like IL-4, IL-10, and TGF which causes trans differentiation and/or recruitment of anti-inflammatory or inflammation resolving M2-like macrophages[37,38]. However, inadequate healing of articular cartilage and continued use of the injured joint causes sustained release of DAMPs in the synovial fluid resulting in persistent pro-inflammatory polarization of synovial macrophages[21].

Inflammatory macrophages produce a cocktail of inflammatory cytokines that activate fibroblast like synoviocytes to secrete inflammatory cytokines, chemokines, and prostaglandins[24,150]. Furthermore, inflammatory macrophages secrete a combination of matrix degrading enzymes like matrix metalloproteinases (MMPs) resulting in articular cartilage degradation which leads to sustained release of DAMPs, reinforcing pro-inflammatory phenotype in macrophages. This disturbs the intricate pro-inflammatory/anti-inflammatory macrophage balance in the synovium, resulting in OA propagation[49]. The cytokines secreted by inflammatory macrophages also induce chondrocytes to produce more inflammatory cytokines and MMPs,

hence establishing a feed-forward loop that sustains joint inflammation, ultimately causing progression of the injury into PTOA[20,21,36,49,50]. Therefore, success of cartilage repair strategy relies on the ability to regenerate cartilage under hostile environmental conditions. Current cartilage repair strategies like microfracture, osteochondral implantation and (matrix assisted) autologous chondrocyte implantation are focused on repairing cartilage tissue, but do not resolve inflammation.

Adult human mesenchymal stem cell (hMSC)-based cartilage regeneration is an appealing strategy due to their ability to differentiate into chondrocytes and produce cartilage matrix molecules like collagen II and aggrecan. However, the inflammatory cytokines secreted by pro-inflammatory macrophages impair the regeneration potential of hMSCs. These inflammatory cytokines suppress MSC chondrogenesis by inhibiting SOX9[105], the master transcription factor for chondrogenesis. Moreover, inflammatory cytokines induce hypertrophy in MSC-derived chondrocytes (henceforth called hMdChs) by inducing expression of RUNX2 (runt related transcription factor 2), which results in cartilage matrix degradation by upregulation of matrix metalloproteinases in hMdChs[16,17]. Therefore, strategies that can overcome joint-wide inflammation and hypertrophic maturation of hMdChs will drastically improve their efficacy as a repair method for cartilage injury, as well as a PTOA preventative measure. Genetic modification of stem cells and chondrocytes to regulate phenotype and target inflammation gives us the opportunity to overcome these limitations by simultaneously targeting multiple aspects of OA onset.

In the present study, we employ autoregulated gene circuits to improve hMSC-based cartilage repair and attenuate macrophage inflammation. Since inflammatory cytokines appear to induce cartilage matrix catabolism partially by upregulating RUNX2 expression in hMdChs, we

hypothesized that by suppressing RUNX2 expression, we can engineer hMdChs that are resistant to inflammation mediated matrix degradation and disrupt their pro-inflammatory crosstalk with pro-inflammatory M1-like macrophages. We investigated the effect of RUNX2 suppression on hMdChs matrix accumulation in conditioned media-based co-culture with THP-1 derived pro-inflammatory M1-like macrophages. We show that RUNX2 suppressing hMdChs resist M1 conditioned media (M1CM)- induced RUNX2 activity and that high levels of RUNX2 suppression is necessary to resist M1CM- induced matrix catabolism. Moreover, we show that treatment of pro-inflammatory macrophages with secretome of RUNX2 suppressing hMdChs attenuates macrophage inflammation and induces a shift towards anti-inflammatory phenotype.

5.3 Methods

5.3.1 Synthesis of gene circuits

All vectors were constructed as previously described[25] and incorporated into lentiviruses by the UM Vector Core. Briefly, the shRNA sequence for shRUNX2 was selected from the Hannon Elledge library (RNAi codex). Using the pINDUCER plasmid[121], a Tet-on inducible system was modified to synthesize tet-on-Luc-mir30-shRUNX2. Next, the COL10a1 basal promoter (-220 to 110 bp) and cis-enhancers (-4296 to- 4147) were synthesized using IDT technology using gBlocks gene fragments service and assembled into pLenti-CMVtight-Egfp-Puro vector[101]. Finally, the Tet-on promoter in pINDUCER was replaced by COL10a1 promoter containing varying number of cis-enhancers to obtain 1cis-luc-mir30-shRUNX2 and 3cis-luc-mir30-shRUNX2. Scramble controls were created by using the same gene circuit backbone and scrambling shRUNX2 sequence to create a non-specific oligonucleotide sequence which doesn't target any genes. Luciferase reporter was used to monitor RUNX2 activity in the scramble and shRUNX2 modified cells.

5.3.2 Cell culture

Cell Expansion: Human bone marrow derived mesenchymal stem cells (hMSCs) were obtained from our collaborators at Case Western Reserve University and expanded in Low Glucose DMEM with 10% Fetal Bovine Serum and 10ng/ml FGF-2[83].

THP-1 monocytic leukemia cell line was obtained from ATCC (Cat# TIB-202) and maintained in THP-1 growth media comprising of ATCC modified RPMI (Gibco, Cat# A1049101) supplemented with 10% Fetal Bovine Serum and 0.05 mM betamercaptoethanol (Sigma, Cat# M3148).

Lentiviral Transduction: hMSCs were plated at density of 10,000 cells/cm^2 and transduced with lentiviruses containing low and high RUNX2 suppressing gene circuits at moieties of infection (MOI) = 5. Twenty-four hours post-transduction, media was replaced with expansion media described above. Transduced cells were selected by treatment with 1µg/ml Puromycin treatment.

MSC chondrogenesis: Wildtype and gene circuit transduced hMSCs were trypsinized using 0.05% Trypsin-EDTA and resuspended in chondrogenic media at 125000 cells/ml. Chondrogenic media consisted of High Glucose DMEM (Gibco, Cat # 11965-092), supplemented with 1 % (v/v) insulin-transferrin-selenium (Corning, Cat # 354350), 1 % (v/v) non-essential amino acids (Gibco, Cat # 11-140-050) 40 μg/mL L-proline (Sigma, cat # P-0380), 50 μg/mL L-ascorbic acid-2-phosphate (Sigma, Cat # A8960), 0.1 μM dexamethasone (Sigma, Cat # D4902), and 10 ng/mL TGF-β1 (Shenandoah Biotechnology, cat # 100-39). hMSC pellets were formed by dispensing 200µl of cell suspension per well of 96 well plate followed by centrifugation at 1640 rpm for 5 minutes. Cells were incubated at 37°C, 5% CO_2, 95% humidity and allowed to condense into tight pellets for 3 days after which fresh chondrogenic media was supplied every other day.

THP-1 differentiation and polarization: THP-1 cells were differentiated into macrophages using treatment with 150 nM phorbol 12-myristate 13-acetate (PMA, Sigma, P8139) for 24 hours followed by 24-hour incubation in THP-1 growth media[151]. Differentiated macrophages were then polarized into pro-inflammatory M1 macrophages by treatment with 10pg/ml lipopolysaccharide (LPS, Sigma, Cat# L7770) and 20ng/ml interferon gamma (IFN-γ, Biolegend, Cat# 713906) for 24 hours[151]. M1 polarized macrophages were then washed with PBS and maintained in THP-1 growth media for conditioned media collection. M1 conditioned media (M1CM) was collected every 24 hours for 72 hours total post M1 polarization.

Inflammatory challenge: After 21 days of chondrogenic culture, human MSC derived chondrocytes (hMdChs) were treated with M1CM for 72 hours, with fresh media supplementation every 24 hours to provide inflammatory stimulus and double conditioned media was collected at every media change. The culture media consisted of equal parts chondrogenic media without TGFβ1 and dexamethasone, and M1CM. hMdChs maintained in chondrogenic media without TGFβ1, and dexamethasone were used as controls.

hMdCh-M1 macrophage crosstalk: THP-1 cells were differentiated and polarized into pro-inflammatory M1-like macrophages as described above. M1 macrophages were then treated with DCM from M1CM treated WT and gene circuit modified hMdChs for 72 hours with fresh DCM provided every 24 hours. After treatment, samples were processed for gene expression or immunofluorescence analysis.

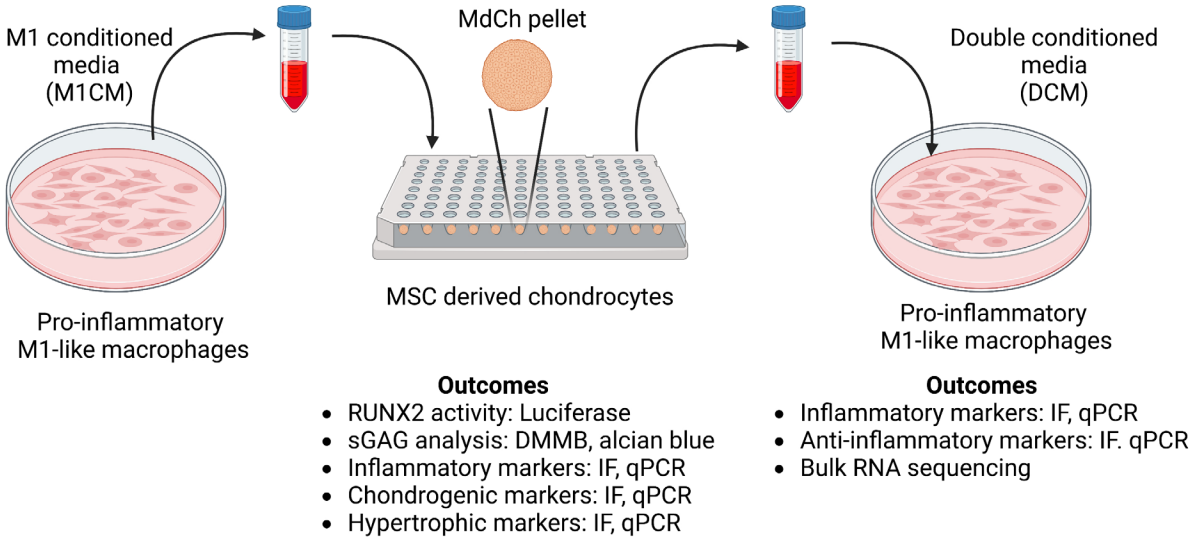

Figure 5-1 Experiment plan for conditioned media-based co-culture to study crosstalk between hMdChs and pro-inflammatory macrophages. Image created using Biorender.com.

5.3.3 Biochemical Analysis

Samples were digested in papain buffer made of papain, EDTA and sodium phosphate, overnight at 65°C. Dimethyl methylene blue (DMMB) assay was used to quantify sGAG concentrations as previously described[27]. Standard curve was generated using known concentrations of chondroitin-6-sulfate. Sample absorbance were read using Synergy H1 plate reader at 425nm and 495nm. sGAG concentrations were normalized to DNA content using PicoGreen DNA assay kit (Thermo Fisher. Fluorescence was measured using Synergy H1 plate reader at excitation wavelength of 498nm and emission wavelength of 528nm. DNA concentrations were determined by comparing to the standard curve.

5.3.4 Histological Analysis

hMdCh pellets were washed with Phosphate Buffered Saline (PBS) and fixed using 10% Neutral Buffered Formalin for 30 minutes. After fixing cells were washed with PBS and stored in 70% ethanol until ready to process. hMdCh pellets were then dehydrated using graded series of ethanol (70-100%), cleared with xylene, embedded in paraffin wax and sectioned into 7µm thick

sections. The sections were then cleared in xylene, rehydrated, stained with Alcian Blue (1% in 3% acetic acid, Poly Scientific) and counter stained with Nuclear Fast Red (Electron Microscopy Sciences) to visualize sGAG deposition.

5.3.5 Immunofluorescence

The hMdCh pellet sections were cleared and rehydrated as explained above. Peroxidase activity of the pellets was blocked using 3% hydrogen peroxide followed by antigen retrieval using BD Retreivagen Antigen Retrieval kit (Thermofisher). Samples were then permeabilized using 0.5%Triton-X-100 in TBS and incubated with blocking buffer consisting of 10% goat serum and 1% (w/v) bovine serum albumin in 0.1% TBS-TX100 (1XTBS with 0.1% Triton-X-100). Samples were then incubated overnight with primary antibody of ACAN (AbClonal, A8536, 1:500), COLX (AbClonal, A6889,1:100), RUNX2 (AbClonal, A2851, 1:100), MMP13 (AbClonal, A16920, 1:100), COLII (Abcam, ab34712, 1:150) at 4℃. Samples were then stained with secondary antibody (IgG anti-rabbit, 488, 1:500, Invitrogen, A11034) for one hour followed by 5-minute incubation with 4', 6-diamidino-2-phenylindol (DAPI, Sigma, 300 nM). Anti-fade was used to coverslip the slides and images were taken using Olympus microscope. For macrophage immunofluorescence, THP-1 cells were polarized in 8-well chamber slides and given appropriate treatments. Cells were then fixed using 10% neutral buffered formalin and permeabilized using 0.3% Triton-X-100 in PBS (PBS-T). After blocking the samples in 10% goat serum in PBS-T for one hour, they were incubated with the primary antibody for CD68 (AbClonal, A6554, 1:100), iNOS (AbClonal, A14031, 1:100) or CD206 (AbClonal, A8301, 1:100) at 4℃ overnight. Samples were then washed thrice with 0.05% Tween20 in PBS and incubated with secondary antibody at room temperature for 1 hour. Finally, samples were counterstained with DAPI nuclear stain, coversliped using anti-fade and imaged.

5.3.6 Luciferase Analysis

RUNX2 activity in hMdChs was measured using luciferase reporter in the gene circuit. Six hours after treatment with inflammatory cytokines, D-luciferin was added to the culture media. After 20-minute incubation period, luminescence was measured using Synergy H1 plate reader. Following luciferase measurement, fresh culture media was added to the wells and plates were put back in incubators.

5.3.7 RNA sequencing Analysis

Total cellular RNA of pooled samples (n=2) was isolated using the Total RNA Purification Plus Kit (Norgen) for mRNA sequencing. Library construction and sequencing was be performed by LC Sciences. Poly(A) RNA sequencing library was prepared following Illumina's TruSeq-stranded-mRNA sample preparation protocol. RNA integrity was checked with Agilent Technologies 2100 Bioanalyzer. Poly(A) tail-containing mRNAs were purified using oligo-(dT) magnetic beads with two rounds of purification. After purification, poly(A) RNA was fragmented using divalent cation buffer in elevated temperature. Quality control analysis and quantification of the sequencing library were performed using Agilent Technologies 2100 Bioanalyzer High Sensitivity DNA Chip. Paired-ended sequencing was performed on Illumina's NovaSeq 6000 sequencing system. Firstly, Cutadapt and perl scripts in house were used to remove the reads that contained adaptor contamination, low quality bases and undetermined bases[152]. Then sequence quality was verified using FastQC. HISAT2 was used to map reads to the genome of homo sapiens[153]. The mapped reads of each sample were assembled using StringTie[154]. Then, all transcriptomes were merged to reconstruct a comprehensive transcriptome using perl scripts and gffcompare. Matrix count files were uploaded to the pcaExplorer Shiny application[155] for principle component analysis to identify outliers in data. After these outliers are removed, count files of data

from two experimental conditions and their associated conditional matrix files were input into the DESeq2[156] R package version 1.33.452 to identify differentially-expressed genes (DEGs, padj < 0.05, based on Wald test with BH-adjustment) between conditions by calculating FPKM (FPKM=[total_exon_fragments / mapped_reads (millions) × exon_length (kB)). Various combinations of conditions will be compared using this method. Lowly-expressed genes (row sums < 10) were removed prior to running the DESeq function. Gene IDs and log 2-fold change values from DESeq results were input into the Panther Classification System[157,158] to compute differential gene ontologies (GOs). GOs were identified according to the Panther statistical enrichment test with the GO biological process complete annotation set. Select GOs from this analysis were represented in figures generated with other R packages.

5.3.8 RNA extraction and qPCR

RNA extraction: After completion of treatments, hMdCh pellets were washed with PBS and flash frozen in liquid nitrogen and stored at -80℃ till ready for processing. For RNA extraction, frozen pellets were homogenized using pestles in Trizol. Following homogenization, bromoanisol was added for phase separation and RNA was precipitated using isopropanol. Purified RNA was resuspended in Ultrapure DI water and concentration was quantified using nanodrop. For macrophages, cells in monolayer were lysed using Trizol and RNA was isolated as described for pellets.

cDNA synthesis and qPCR: Following RNA extraction, cDNA was synthesized using High-Capacity cDNA Reverse Transcription kit (Applied Biosystems, Cat # 4368814) using 1µg RNA/sample and following the manufacturer's protocols. Gene expression of inflammatory (IL-6, IL-1β, TNF-α, NFκB) and catabolic (MMP13) markers was analyzed using Fast SyBr Green master mix (Applied Biosystems, Cat # 4385612) on Applied Biosystems real time 7500 Fast

qPCR machine. Primers sequences of the genes are listed in Table 3.1 below. GUS and TBP were used as housekeeping genes. Relative expression was calculated using $\Delta\Delta C_t$ method and fold change was calculated as $2^{-\Delta\Delta Ct}$.

Table 2 Primer sequences for qPCR

Gene	Forward Primer	Reverse Primer
GUS	GACTGAACAGTCACCGACGA	ACTTGGCTACTGAGTGGGGA
TBP	GTGGGGAGCTGTGATGTGAA	TGCTCTGACTTTAGCACCTGT
IL-1β	ACGATGCACCTGTACGATCA	TCTTTCAACACGCAGGACAG
TNF-α	CCAAAGTAGACCTGCCCAGA	AACCTCCTCTCTGCCATCAA
NFκB	GGCTACTCTGGCGCAGAAAT	CTGTACCCCCAGAGACCTCA
IL-6	TTCGGTCCAGTTGCCTTCTC	TACATGTCTCCTTTCTCAGGGC
MMP13	TTGCAGAGCGCTACCTGAGA	CCCCGCATCTTGGCTTTTTC

Abbreviations: GUSB, glucuronidase beta; TBP, tata binding protein; IL-1β, interleukin 1 beta; TNF-α, tumor necrosis factor alpha; NFκB, nuclear factor kappa B; IL-6, interleukin 6; MMP13, matrix metalloproteinase 13

5.3.9 Statistical Analysis

All the data is presented as mean $\pm$ SD. All statistical analysis is performed using GraphPad Prism 8.3 software (GraphPad, San Diego, CA). One-way or two-way ANOVA was used with Tukey's multiple comparison post-hoc test. P-value < 0.05 was considered statistically significant.

5.4 Results

5.4.1 Successful polarization of THP-1 cells into pro-inflammatory macrophages

Both non-polarized M0 macrophages as well as pro-inflammatory M1-like macrophages stained positively for macrophage marker CD68 (Fig 5-2a) indicating successful differentiation. Moreover, pro-inflammatory M1-like macrophages exhibited upregulated IL-6 gene expression

compared to M0 macrophages (Fig 5-2b). We also analyzed the protein expression of inflammatory marker inducible nitric oxide synthase (iNOS) and observed upregulated iNOS expression in M1-like macrophages compared to M0 controls. Taken together, this data suggests successful polarization of THP-1 monocytes into pro-inflammatory macrophages.

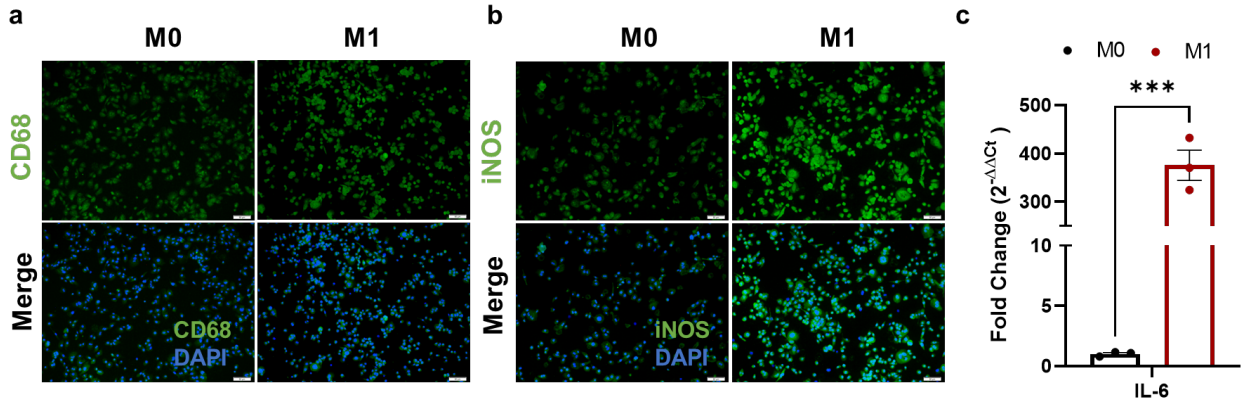

Figure 5-2 Differentiation and polarization of THP-1 cells into pro-inflammatory macrophages. Immunofluorescence analysis for (a) macrophage marker CD68 and (b) M1 marker iNOS in non-polarized M0 and M1-like macrophages. Merged images are an overlay of protein of interest (green) and DAPI (blue) nuclear stain. Scale: 50µm (c) IL-6 gene expression in M0 and M1-like polarized macrophages (n=3). Significance is indicated by ***p<0.001 analyzed using two tailed t-test.

5.4.2 RUNX2 suppression protects hMdChs from M1CM-induced matrix catabolism

After 21-day chondrogenic culture, WT and gene circuit modified hMdCh pellets were treated with M1CM for 72 hours. M1CM upregulated RUNX2 activity in scramble hMdChs while hMdChs modified with both low and high level RUNX2 suppressing gene circuits resisted this increase (Fig. 5-3a). Moreover, treatment with M1CM also induced significant cartilage matrix catabolism in WT and scramble hMdChs as seen by both sGAG quantification and Alcian Blue staining. hMdChs modified with low RUNX2 suppressing gene circuits also showed significant cartilage matrix loss, however, hMdChs modified with high RUNX2 suppressing circuits resisted M1CM-induced matrix catabolism (Fig 5-3b, c), suggesting that high levels of RUNX2 suppression is required to resist M1 macrophage induced neocartilage degradation.

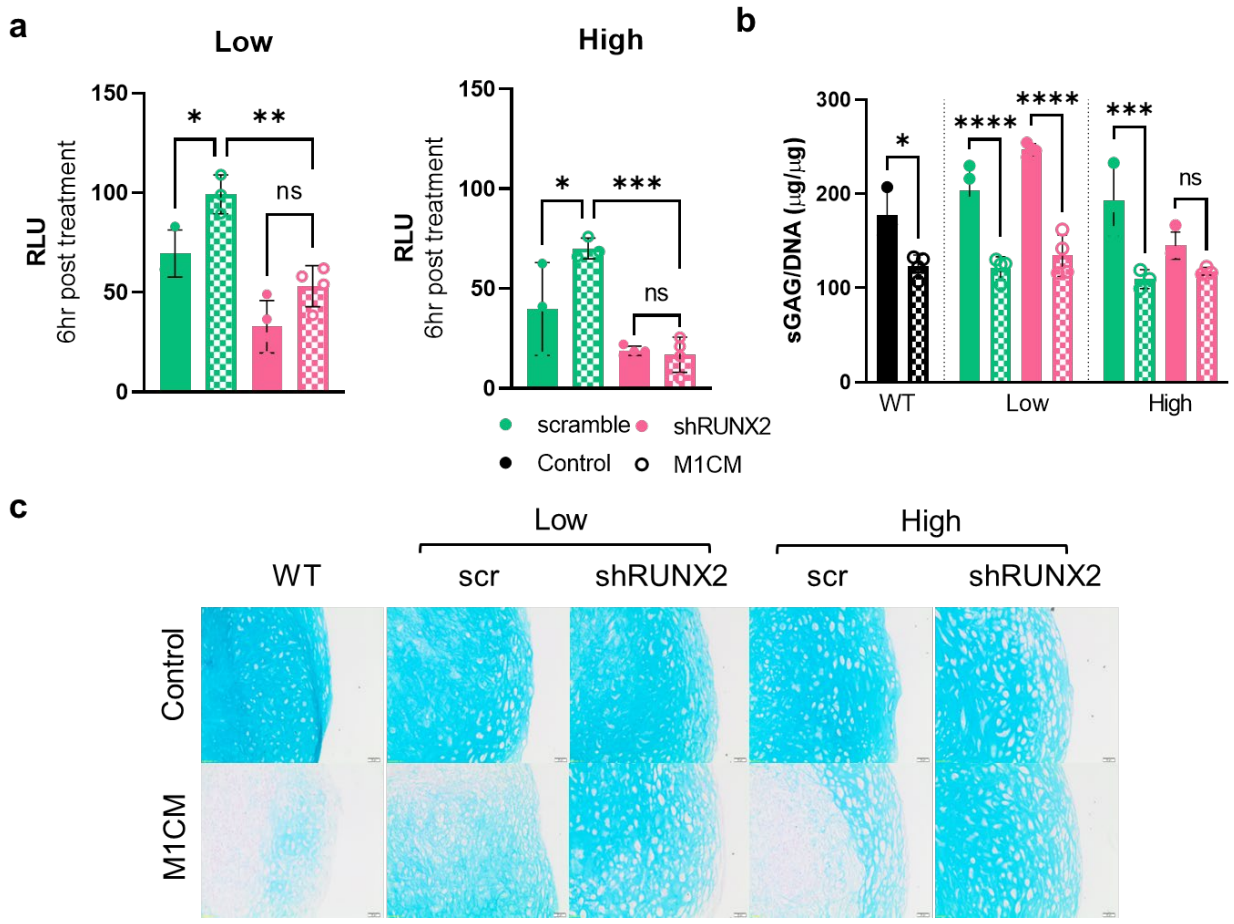

Figure 5-3 RUNX2 suppression protects hMdChs from M1CM-induced cartilage matrix catabolism. (a) RUNX2 activity in M1CM treated scramble or shRUNX2 modified hMdChs measured using the luciferase reporter (n=3-4). (b) sGAG quantification (n=3-4) and (c) Alcian blue staining for sGAG in WT, low and high shRUNX2 and scramble hMdChs treated with M1CM for 72 hours. Scale bar: 50µm. Significance is indicated by * $p<0.05$, ** $p<0.01$, *** $p<0.001$ and **** $p<0.0001$ analyzed using one way ANOVA with tukey's multiple comparison.

5.4.3 M1CM induces pro-inflammatory and hypertrophic response in hMdChs

We analyzed the expression of inflammatory, catabolic, and hypertrophic markers to understand the effect of RUNX2 suppression on the response of hMdChs towards M1CM treatment. Since high RUNX2 suppressing gene circuit protected hMdChs from matrix loss, we proceeded with WT and high RUNX2 suppressing hMdChs for this analysis. Gene expression analysis revealed upregulation of IL-6 and NFκB expression in WT hMdChs upon treatment with M1CM which was successfully resisted by RUNX2 suppressing cells (Fig. 5-4). Moreover, M1CM

also induced expression of catabolic marker MMP13 in WT hMdChs but not in RUNX2 suppressing hMdChs (Fig. 5-4).

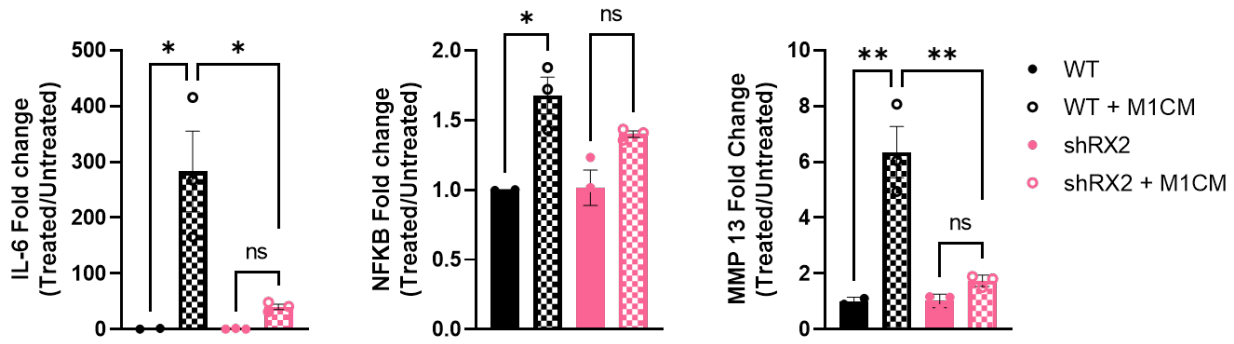

Figure 5-4 M1CM induced the expression of inflammatory and catabolic markers in hMdChs. Gene expression analysis for WT and high RUNX2 suppressing hMdChs for inflammatory markers IL-6 and NFκB, and catabolic marker MMP13 upon treatment with M1CM (n=3). Significance is indicated by * $p<0.05$, **$p<0.01$, analyzed using one way ANOVA with tukey's multiple comparisons.

Treatment with M1CM also upregulated protein expression of hypertrophic markers RUNX2 (Fig. 5-5a), COLX (Fig. 5-5b) and MMP13 (Fig. 5-5c) in WT and scramble hMdChs, which was suppressed by RUNX2 suppressing hMdChs.

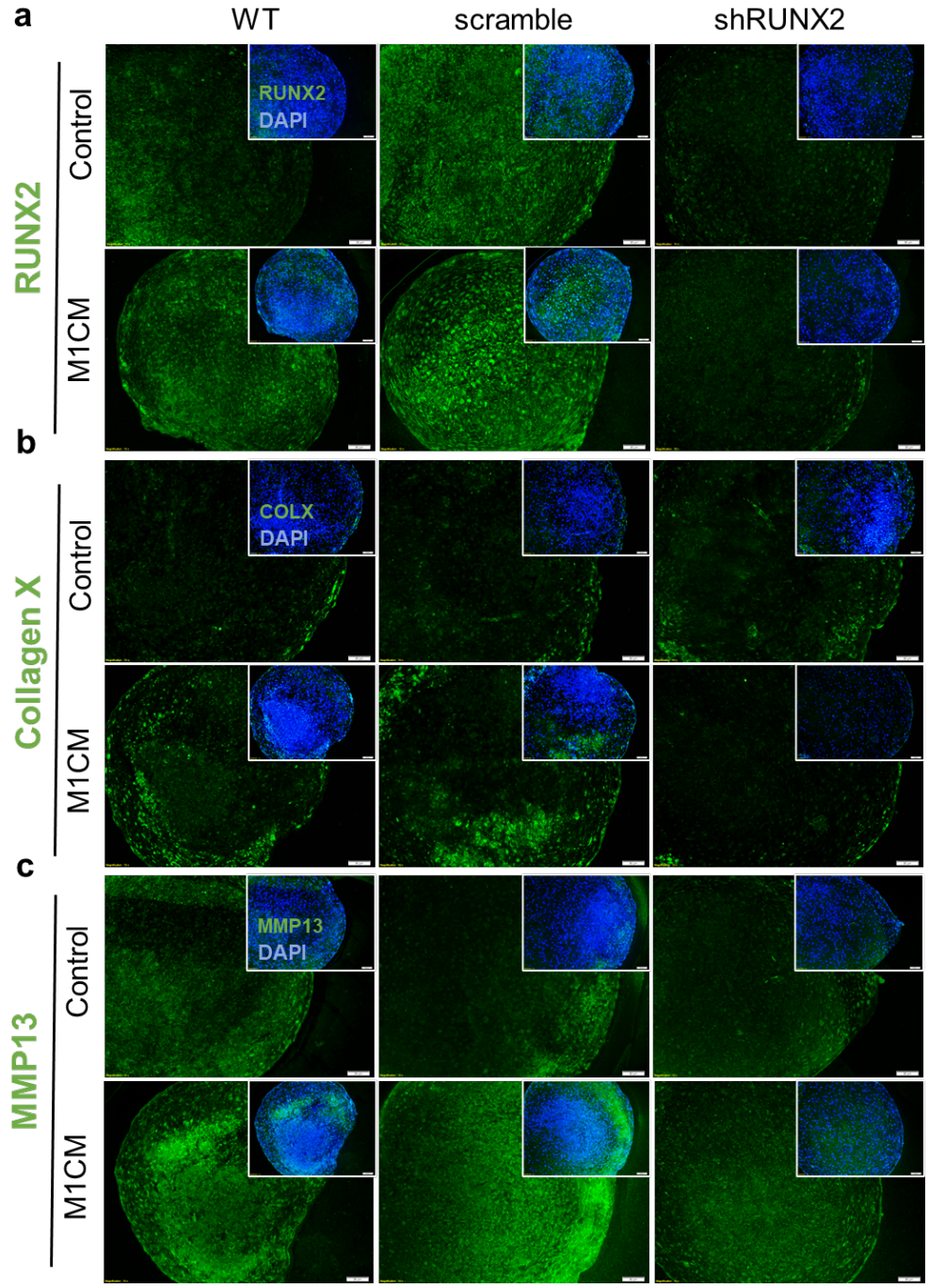

Figure 5-5 M1CM induces expression of hypertrophic markers in hMdChs. Immunofluorescence analysis for protein expression of hypertrophic markers (a) RUNX2, green (b) Collagen X, green (c) MMP13, green in untreated (control) and M1CM treated hMdChs. Insets are merged images of protein of interest (green) with nuclear stain DAPI (blue). Scale: 50μm.

5.4.4 RUNX2 suppression stabilizes the expression of chondrogenic markers under M1CM treatment

To further understand how RUNX2 suppression protects hMdChs from M1CM induced matrix catabolism, we analyzed the expression of chondrogenic markers. Immunofluorescence analysis revealed that M1CM induces downregulation of ACAN and COLII expression in WT and scramble hMdChs. However, RUNX2 suppressing hMdChs were able to maintain the expression of ACAN and COLII when treated with M1CM (Fig. 5-6).

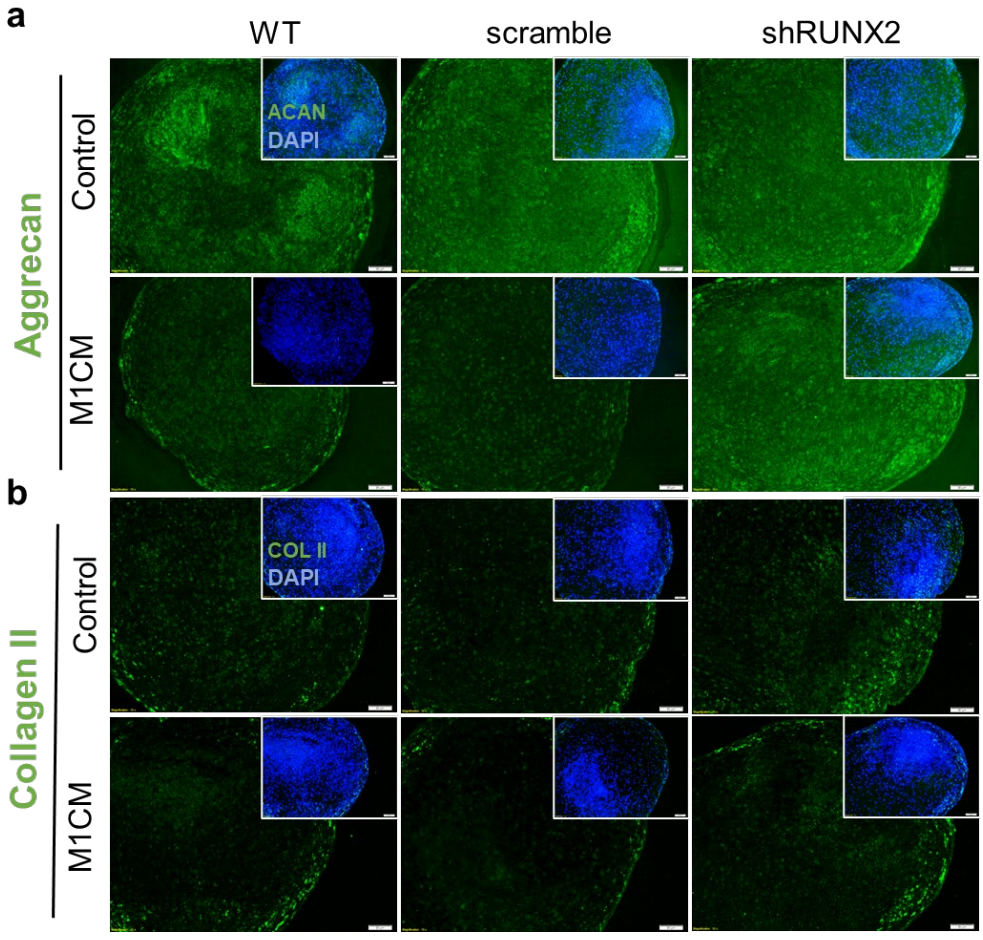

Figure 5-6 RUNX2 suppressing hMdChs retain higher expression of chondrogenic markers upon M1CM treatment. Immunofluorescence analysis for protein expression of chondrogenic markers (a) Aggrecan (green) and (b) Collagen II (green) in WT, scramble and high shRUNX2 hMdChs treated with M1CM for 72 hours. Insets are merged images of protein of interest (green) and nuclear stain DAPI (blue). Scale bar: 50μm.

5.4.5 Double conditioned media from RUNX2 suppressing hMdChs attenuates macrophage inflammation

Next, analyzed the effect of RUNX2 suppression in hMdChs on the pro-inflammatory crosstalk between hMdChs and inflammatory M1-like macrophages. To address this, pro-inflammatory macrophages were treated with double conditioned media (DCM) collected from M1CM treated hMdCh pellets for 72 hours. Treatment of pro-inflammatory macrophages with DCM from RUNX2 suppressing hMdChs (shRX2 DCM) decreased the expression of inflammatory marker iNOS compared to WT DCM (Fig. 5-7a). Moreover, pro-inflammatory macrophages treated with shRX2 DCM exhibited increased expression of anti-inflammatory marker CD206 compared to WT DCM (Fig. 5-7b).

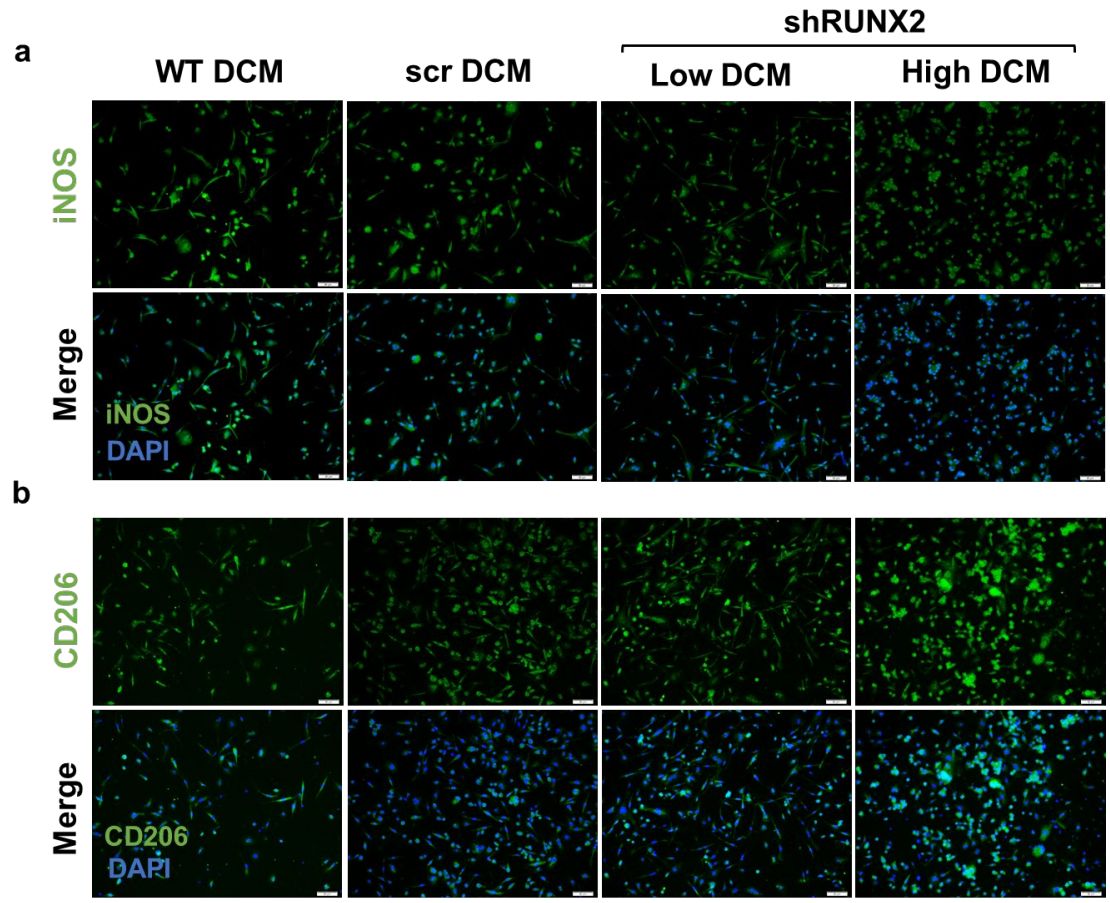

Figure 5-7 DCM from shRUNX2 hMdChs attenuates macrophage inflammation. (a) Immunofluorescence for protein expression of inflammatory marker iNOS and (b) anti-inflammatory marker CD206 in DCM treated pro-inflammatory M1-like macrophages. Merged images are an overlay of the protein of interest (green) and nuclear stain DAPI (blue). Scale bar: 50μm.

5.4.6 DCM from shRUNX2 hMdChs induces macrophage phenotype shift

To further investigate this phenotype shift in macrophages, we performed RNAseq analysis of control and shRX2 DCM-treated inflammatory M1-like macrophages. Gene ontology analysis revealed downregulation of GO terms corresponding to inflammatory response, chemotaxis, and innate immune response inflammatory macrophages treated with shRX2 DCM (Fig. 5-8a). Moreover, we observed significant downregulation in FPKM values of genes involved in macrophage chemotaxis, inflammation and catabolic markers and upregulation in expression of anti-inflammatory markers in shRX2 DCM treated inflammatory macrophages (Fig. 5-8b). Gene expression analysis via qPCR also revealed a significant downregulation of NFκB and TNF-α expression in shRX2 DCM treated inflammatory macrophages. IL-1β expression was also downregulated but was statistically insignificant (Fig. 5-8c).

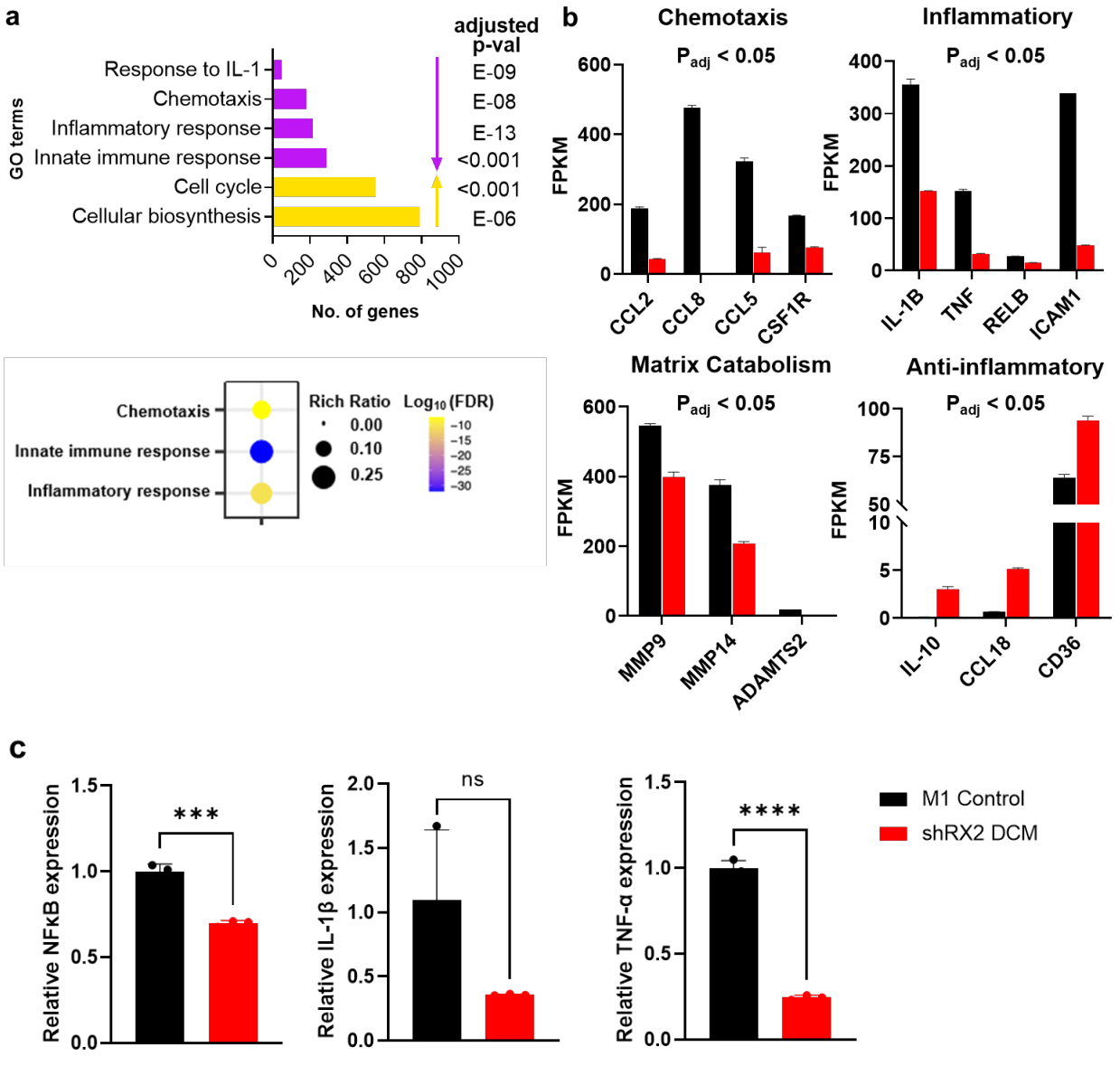

Figure 5-8 Treatment with shRUNX2 DCM downregulates inflammation and induces anti-inflammatory response from inflammatory macrophages. (a) Gene ontology analysis of shRUNX2 DCM treated inflammatory M1-like macrophages compared to control inflammatory macrophages (b) RNAseq FPKM analysis for expression of catabolic, inflammatory, chemotaxis and anti-inflammatory markers in control and shRUNX2 DCM treated pro-inflammatory M1-like macrophages (c) qPCR analysis for gene expression of inflammatory markers NFκB, IL-1 and TNF-α in control and shRX2 DCM treated inflammatory M1-like macrophages. Significance is indicated by * $p<0.05$, **$p<0.01$, analyzed using two tailed t-test.

5.5 Discussion

Pro-inflammatory macrophage-mediated inflammation is a key contributor towards PTOA pathogenesis. Therefore, clinical success of MSC-based cartilage repair requires not only increasing cartilage matrix accumulation under inflammation, but also resolving inflammation to create a conducive joint environment that allows for cartilage healing. In this study we show that M1CM increases RUNX2 activity in hMdChs which is successfully suppressed by hMdChs modified with either low or high RUNX2 suppressing gene circuits. As expected, treatment with M1CM caused significant cartilage matrix catabolism in hMdCh pellets and we found that high levels of RUNX2 suppression is required to protect hMdChs from M1CM induced neocartilage degradation. Moreover, M1CM induced expression of inflammatory markers IL-6 and NFκB, and catabolic markers MMP13 in WT hMdChs but failed to do so in RUNX2 suppressing hMdChs. RUNX2 suppressing hMdChs also maintained higher expression of chondrogenic markers ACAN and COLII and inhibited the expression of hypertrophic markers RUNX2 and COLX compared to WT hMdChs. Finally, we found that RUNX2 suppression in hMdChs inhibits their pro-inflammatory crosstalk with inflammatory macrophages, where treatment of inflammatory macrophages with DCM from shRUNX2 hMdChs attenuates macrophage inflammation and increases the expression of anti-inflammatory markers.

Pro-inflammatory macrophages secrete a cocktail of cytokines as well as catabolic and inflammatory mediators, resulting in degradation of cartilage extracellular matrix[5,159]. In this study, treatment with M1CM increased RUNX2 activity in hMdChs, indicating that RUNX2 plays a role in mediating the pro-inflammatory response of hMdChs towards M1CM. This observation is consistent with the existing literature as inflammatory cytokines such as IL-1 and TNFα that are secreted by inflammatory macrophages have previously been shown to upregulate NFκB pathway

in chondrocytes during osteoarthritis[160,161]. Furthermore, NFκB pathway has been shown to upregulate RUNX2 expression in OA chondrocytes[162] and to regulate RUNX2 activity by activating HIF2α signaling, another known inducer of RUNX2[135,163]. Taken together, our data demonstrates that both low and high RUNX2 suppressing gene circuits are actively suppressing RUNX2 in response to exogenous stimuli.

During PTOA progression, pro-inflammatory macrophages induce cartilage matrix catabolism by secreting catabolic mediators like MMPs into the synovial fluid. In our study, treatment with M1CM also induced significant neocartilage degradation in hMdCh pellets. Interestingly, we observed that high levels of RUNX2 suppression were required to inhibit M1CM mediated cartilage matrix loss as significant matrix degradation was observed in hMdChs modified with low shRUNX2 gene circuits. It is well documented that inflammatory cytokines secreted by M1 macrophages induce chondrocytes to secrete MMPs that degrade cartilage matrix. Both MMP13 and ADAMTS4/5, the key enzymes that degrade cartilage matrix macromolecules Collagen II and Aggrecan respectively are regulated by RUNX2 in chondrocytes. This is a possible explanation for why RUNX2 suppressing hMdChs resist M1CM induced cartilage matrix catabolism. However, M1CM would contain additional MMPs and cytokines that act via multiple signaling pathways to affect chondrocyte phenotype. Since the gene circuit is specific to RUNX2 expression, it is not surprising that high levels of RUNX2 suppression was essential for hMdChs to resist the effects of M1CM. Future studies investigating the effect of RUNX2 suppression during long-term treatment with M1CM would be useful to analyze the efficacy of the gene circuit under chronic inflammatory conditions.

It is well documented that inflammatory stimulus induces a pro-inflammatory and catabolic response in chondrocytes. Studies have shown upregulation of inflammatory and catabolic markers

in IL-1β and TNF-α treated bovine cartilage explants[5]. Moreover, osteoarthritis chondrocytes co-cultured with pro-inflammatory macrophages were shown to express higher levels of catabolic markers MMP-1, MMP-3, MMP-9, MMP-13 and inflammatory markers IL-1β, TNF-α, IL-6, IL-8, and IFN-γ compared to control osteoarthritic chondrocytes demonstrating that pro-inflammatory macrophages exacerbate the catabolic and pro-inflammatory response to chondrocytes[45]. Interestingly we observed that RUNX2 suppressing hMdChs resisted this upregulation in the expression of inflammatory and catabolic markers upon treatment with M1CM indicating that RUNX2 plays an important role in mediating this pro-inflammatory response to hMdChs to M1CM. Moreover, treatment with M1CM downregulated the expression of chondrogenic markers COLII and ACAN in WT and scramble hMdChs while RUNX2 suppressing hMdChs maintained their expression. During late chondrogenesis, RUNX2 inhibits SOX9 expression, and we have shown that M1CM induces RUNX2 activity, therefore, it is possible that RUNX2 suppressing hMdChs are able to maintain SOX9 expression upon treatment with M1CM, resulting in maintenance of chondrogenic markers compared to controls since SOX9 drives the expression of COLII and ACAN. Therefore, it is desirable to analyze SOX9 expression in these hMdChs in response to M1CM treatment.

As stated before, pro-inflammatory macrophages secrete inflammatory cytokines into the synovium that act in autocrine and paracrine manner to mediate cartilage degradation and induce hMdChs to produce additional inflammatory cytokines, establishing a positive feed forward loop that sustains joint inflammation. Since we observed that RUNX2 suppression inhibits the pro-inflammatory response of hMdChs to M1CM, we investigated the effect of DCM from M1CM treated hMdChs on pro-inflammatory macrophage phenotype. We observed that treatment with shRUNX2 DCM attenuated macrophage polarization as indicated by downregulation of

inflammatory marker iNOS and upregulation of anti-inflammatory marker CD206 expression. One possible explanation could be the secretion of TGF-β, which is produced by hMdChs to maintain cartilage production, and has been shown to induce anti-inflammatory or inflammation resolving polarization in macrophages[164,165]. Therefore, shRX2 DCM should be analyzed for the presence of TGF-β and other anti-inflammatory cytokines in comparison to WT DCM. RNAseq analysis of control and shRUNX2 DCM treated inflammatory macrophages also revealed downregulation genes and pathways corresponding to inflammation, chemotaxis and matrix catabolism and upregulation of anti-inflammatory response in shRUNX2 DCM treated macrophages, indicating a switch towards inflammation resolving phenotype. Since RUNX2 suppression inhibits MMP13 expression in hMdChs, the DCM from shRUNX2 hMdChs will not contain the DAMPs that are required to reinforce the pro-inflammatory M1-like polarization of macrophages.

We show that RUNX2 suppression inhibits the pro-inflammatory response of hMdChs to M1CM treatment by downregulating NFκB pathway. Furthermore, MSCs and MSC-derived exosomes have been shown to have immunomodulatory effects in the context of cartilage injury and osteoarthritis via secretion of anti-inflammatory cytokines like IL-4, IL-10 and growth factors like TGF-β, FGF etc[166]. One study showed that MSCs challenged with IL-1β, TNF-α and IFN-γ secrete chondroprotective factors like tissue inhibitor of metalloproteinases (TIMPs) and produce exosomes containing miRNAs (miR-24-3p, miR-222-3p and miR-193b-3p) that switch synovial macrophage polarization from M1 to M2 type[166–168]. In another study, MSCs challenged with TNF-α and IFN-γ shuttled miR-34a-5p, miR21, miR146a-5p via exosomes to attenuate macrophage polarization[169]. It is possible that in the absence of NFκB activation, the response of hMdChs to M1CM resembles the anti-inflammatory response of MSCs. Therefore, future studies investigating the cytokine, growth factor as well as exosome composition of shRUNX2 DCM are desirable to

understand the mechanism of shRUNX2 DCM mediated attenuation of macrophage inflammation. In this study we demonstrate the efficacy of autoregulated RUNX2 suppression in protecting hMdChs from M1CM induced matrix catabolism and inhibiting the pro-inflammatory feed-forward loop between hMdChs and inflammatory macrophages. However, these results need to be validated in vivo using defect repair and PTOA models to support our in vitro findings.

5.6 Conclusion

The regenerative community needs to uncover novel pathways that can be targeted to resolve multiple aspects of the healing environment, namely tissue regeneration and chronic inflammation. This work utilizes an interdisciplinary approach, combining the fields of tissue engineering, synthetic biology, and immunology to expand the potential use of MSCs to both mitigate the effect of inflammation in multiple joint tissues and prompt repair, delaying the progression of PTOA. In this study we found a novel role of RUNX2 in mediating the pro-inflammatory crosstalk between hMdChs and inflammatory macrophages. We demonstrate that RUNX2 suppression in hMdChs not only protects hMdChs from inflammation induced matrix degradation but also disrupts the pro-inflammatory feedforward loop by attenuating macrophage inflammation. This study is an important step towards the clinical application of MSC-based cartilage regeneration therapies in complex pathological environment of the injured joint.

Chapter 6 Conclusions and Future Directions

Articular cartilage injuries often progress into post traumatic osteoarthritis (PTOA), a painful debilitating disease[5]. Mesenchymal stem cells-based cartilage repair is an appealing treatment strategy due to their ability to differentiate into chondrocytes and secrete cartilage matrix macromolecules like collagen II (COLII) and aggrecan (ACAN)[9,72]. However, clinical application of MSC-based cartilage repair strategies faces two main challenges, namely hypertrophic maturation of MSC derived chondrocytes[13,28,102,111] and inflammation mediated catabolism of the engineered neocartilage[5,45,140,170]. The overarching aim of this dissertation was to increase matrix accumulation and retention by hMdChs under hypertrophic and inflammatory conditions to achieve functional cartilage regeneration. Transcription factor RUNX2 mediates hypertrophic maturation and pro-inflammatory and catabolic effects of inflammation in hMdChs[15,17,101,171]. Therefore, we utilized a synthetic gene circuit that allows autoregulated RUNX2 suppression in hMdChs to achieve this aim[25]. First, we investigated the efficacy of autoregulated RUNX2 suppression to inhibit hMdCh hypertrophy under hypertrophic stimuli. Next, we analyzed the effect of autoregulated RUNX2 suppression on inflammation mediated matrix catabolism by treating hMdChs with individual inflammatory cytokines. Finally, we explored the effect of RUNX2 suppression on the pro-inflammatory crosstalk between hMdChs and inflammatory macrophages using a conditioned media-based co-culture model. The following discussion summarizes the key findings from the specific aims, impact of this dissertation and explores next steps and potential research avenues in the Future Directions section.

6.1 Summary

6.1.1 Aim 1: RUNX2 suppression stabilizes chondrogenic phenotype under hypertrophic stimuli

To improve MSC-based cartilage repair, we first investigated the efficacy of varying magnitudes of autoregulated RUNX2 suppression on hypertrophic maturation of hMdChs upon treatment with hypertrophic stimuli T3 and βGP[28,102]. We observed that hMdChs modified with either low or high RUNX2 suppressing gene circuit accumulated higher amounts of cartilage matrix and deposited lower mineral compared to unmodified or scramble controls. To understand the mechanism behind increased matrix accumulation by gene circuit modified cells, we investigated the expression of chondrogenic and hypertrophic markers in hMdChs. We observed that hMdChs modified with either gene circuit maintain higher expression of ACAN and COL II under hypertrophic stimuli compared to controls. Moreover, treatment with hypertrophic stimuli increases expression of hypertrophic markers COLX and MMP13 in control hMdChs which is successfully suppressed by gene circuit modified hMdChs. Since matrix turnover is the net summation of matrix production and degradation, inhibition of the predominant cartilage matrix degrading enzyme MMP13 could be a potential contributor towards increased matrix accumulation by gene circuit modified cells under hypertrophic stimuli.

Overall, in this chapter we demonstrated that synthetic gene circuits are a viable approach to stabilize chondrogenic phenotype and increase cartilage matrix accrual by hMdChs. However, clinical application of MSC-based cartilage repair requires implantation of engineered cartilage in hostile inflammatory joint environment and therapeutic success entails resistance to inflammation induced cartilage matrix catabolism. Therefore, it is necessary to evaluate the efficacy of shRUNX2 gene circuit to protect hMdChs from inflammation-induced cartilage matrix catabolism to validate it's feasibility for clinical application.

6.1.2 Aim 2: RUNX2 suppression protects hMdChs from inflammation-induced matrix loss

Inflammation is a key contributor towards progression of cartilage injury into PTOA. Inflammatory cytokines such IL-1, IL-6 and TNF-α inhibit MSC chondrogenesis and induce hypertrophic maturation in hMdChs by upregulating RUNX2 expression, resulting in increase in matrix metalloproteinase expression that degrades engineered cartilage and compromise its mechanical function[24,47,140,149]. Therefore, in this aim we investigated the effect of autoregulated RUNX2 suppression in hMdChs on inflammation-mediated cartilage matrix catabolism. Since inflammatory pathways act on hMdChs via both RUNX2 dependent and independent pathways, we chose high RUNX2 suppressing gene circuits to achieve maximum suppression. We observed that RUNX2 suppressing hMdChs resist both IL-1β and TNF-α-induced increase in RUNX2 activity compared to scramble controls. Moreover, RUNX2 suppressing hMdChs retained higher cartilage matrix compared to controls upon treatment with IL-1β. However, TNF-α did not induce significant matrix catabolism in any groups. Although we chose the cytokine concentrations based on the synovial fluid concentration of osteoarthritic knees, we might need higher TNF-α concentrations to induce measurable cartilage matrix loss in vitro within 72 hours. To evaluate the effect of RUNX2 suppression on IL-1β-induced hypertrophic maturation, we analyzed the expression of chondrogenic and hypertrophic markers. We observed that RUNX2 suppressing hMdChs retained higher expression of COLII and ACAN and resisted IL-β induced increase in RUNX2, COLX and MMP13.

Overall, work done in this chapter validates that inflammatory cytokines indeed upregulate RUNX2 activity in hMdChs and demonstrates that autoregulated RUNX2 suppression partially protects hMdChs from IL-1β-induced matrix catabolism by suppressing MMP13 expression. However, treatment with individual inflammatory cytokines does not recapitulate the complex

pathological environment of the injured joint where chondrocytes interact with multiple cell populations in the synovium and are exposed to a plethora of inflammatory and catabolic mediators. Therefore, there is a need to test the efficacy to autoregulated RUNX2 suppressing gene circuits to maintain hMdCh phenotype and promote cartilage matrix accumulation in culture models that mimic the injured joint microenvironment.

6.1.3 Aim 3: Autoregulated RUNX2 suppression inhibits pro-inflammatory crosstalk between hMdChs and inflammatory macrophages

Macrophages are the predominant immune cell type that mediate joint inflammation post injury. Sustained polarization of macrophages into pro-inflammatory M1-like phenotype has been implicated in onset and progression of PTOA. Pro-inflammatory macrophages secrete inflammatory cytokines and catabolic mediators that degrade cartilage matrix, inhibit hMSC chondrogenesis, and induce hypertrophic maturation in hMdChs. These cytokines induce hMdChs to secrete additional inflammatory cytokines and catabolic mediators, creating a pro-inflammatory feed forward loop that sustains joint inflammation by promoting continuous cartilage degradation. Therefore, in this chapter we utilized a conditioned media (CM)-based co-culture model to analyze the effect of autoregulated RUNX2 suppression in hMdChs on the pro-inflammatory crosstalk between hMdChs and inflammatory macrophages. We observed that inflammatory M1-like macrophage CM (M1CM) upregulated RUNX2 activity in hMdChs which was suppressed by RUNX2 suppressing cells. Moreover, high level of RUNX2 suppression was necessary to resist M1CM induced cartilage matrix catabolism. Furthermore, RUNX2 suppressing cells retained higher expression of ACAN and COLII and inhibited M1CM induced expression of inflammatory markers IL-6 and NFκB, and hypertrophic markers COLX and MMP13. Furthermore, double conditioned media (DCM) from M1CM treated RUNX2 suppressing hMdChs attenuated

macrophage inflammation by downregulating the expression of inflammatory markers and upregulating the expression of anti-inflammatory markers.

6.1.4 Impact

Inadequate repair of injured cartilage leads to post-traumatic osteoarthritis, a disease with tremendous social and economic burden on the society[5,34,172]. Mesenchymal stem cell-based cartilage regeneration is the next generation therapy for repairing injured cartilage and reduce the incidence of PTOA. However, poor stability of chondrogenic phenotype and inflammation-induced neocartilage degradation poses significant challenges towards clinical application of MSC-based cartilage repair. In this dissertation, I utilized a multidisciplinary approach by combining the fields of tissue engineering, synthetic biology, and immunology to address these challenges. I demonstrate the application of synthetic gene circuits that allow autoregulated RUNX2 suppression in hMSC derived chondrocytes to successfully overcome these challenges.

Autoregulated RUNX2 suppressing hMSCs have the potential to revolutionize cartilage repair as they rely on intracellular RUNX2 concentrations to regulate RUNX2 activity, allowing them to respond to stimuli without requiring exogenous intervention. The ability of RUNX2 suppressing hMdChs to successfully maintain chondrogenic phenotype, inhibit hypertrophic maturation and resist inflammation-induced cartilage matrix catabolism brings hMSCs one step closer to clinical application. Moreover, the work done in this dissertation demonstrates that autoregulated RUNX2 suppression not only stabilizes hMdChs chondrogenic phenotype and protect from inflammation-induced neocartilage catabolism but also alters their interaction with pro-inflammatory macrophages, resulting in phenotype shift towards inflammation resolving state. Macrophages are key mediators of PTOA and the imbalance of pro-inflammatory/anti-inflammatory macrophages has been attributed to the severity of OA. Therefore, autoregulated

RUNX2 suppression in hMdChs can disrupt the vicious cycle that sustains macrophage inflammation to potentially attenuate whole joint inflammation and create a joint environment conducive for cartilage healing (Fig, 6-1). Successful repair of injured cartilage by hMSCs along with resolution of joint inflammation can significantly delay if not prevent the onset of PTOA.

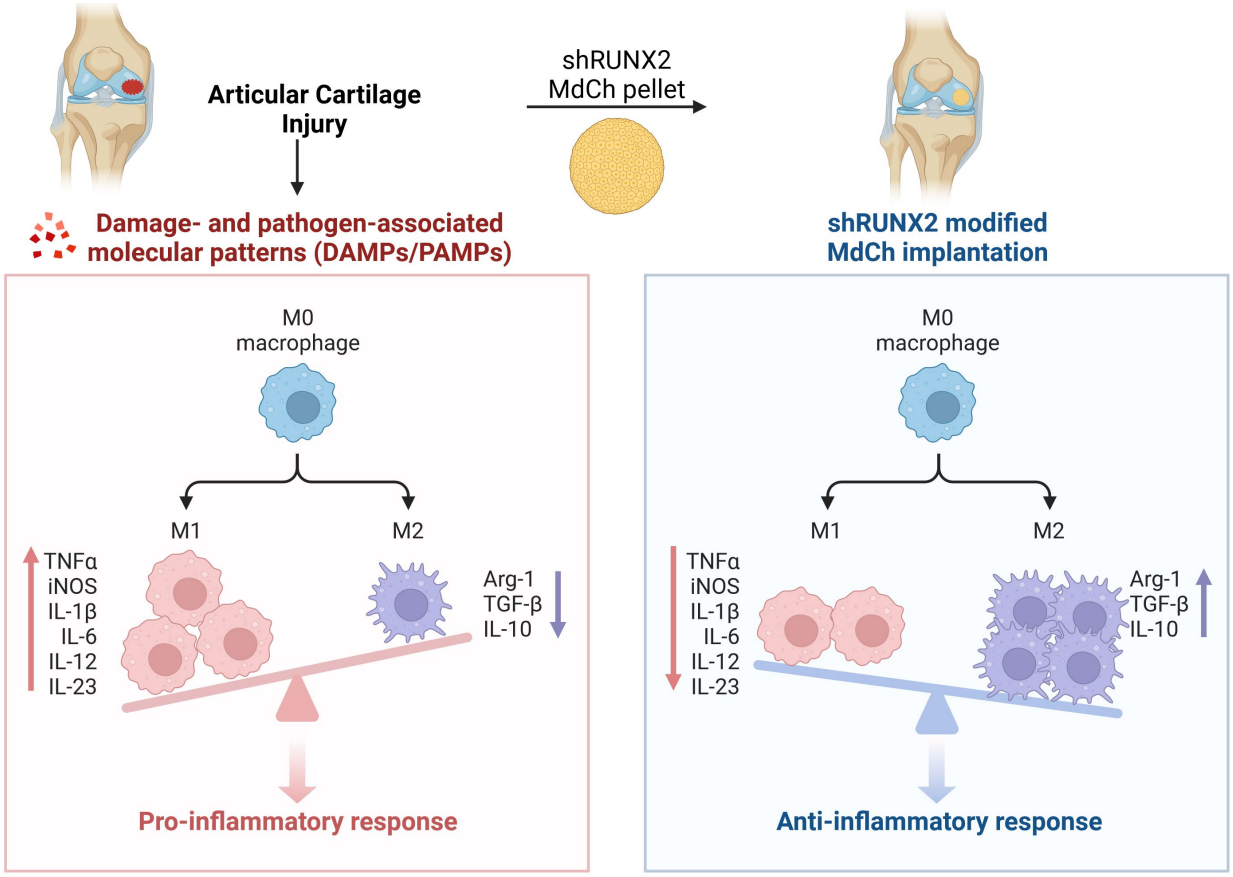

Figure 6-1 Strategy for successful MSC-based cartilage repair under inflammatory joint environment using autoregulated RUNX2 suppression. Image created using Biorender.com.

6.2 Future Directions

6.2.1 Double conditioned media analysis

In chapter 5, we found that double conditioned media (DCM) from RUNX2 suppressing hMdChs attenuates macrophage inflammation. We showed that RUNX2 suppression inhibits M1CM induced NFκB activation and we speculate that in the absence of NFκB, the response of

hMdChs to inflammatory stimulus might resemble the anti-inflammatory response of MSCs through secretion of anti-inflammatory cytokines and immunomodulatory exosome cargos[166,173,174]. Therefore, analyzing the composition of DCM could provide mechanistic understanding of RUNX2 mediated pro-inflammatory crosstalk between hMdChs and inflammatory macrophages and help develop therapeutic strategies that can be utilized in combination with the gene circuit to synergistically enhance the immunomodulatory effects and potentially prevent the onset of PTOA. Multiplex technologies like Luminex[175] can be utilized to analyze anti-inflammatory cytokines produced by RUNX2 suppressing hMdChs in response to M1CM. Moreover, exosome analysis using miRNAseq and mass spectrometry can be utilized to evaluate miRNAs and proteins shuttled by hMdChs in exosomes that modulate macrophage inflammation.

6.2.2 In vivo validation of the gene circuit

In this dissertation we successfully demonstrate the efficacy of the gene circuit to protect hMdChs from inflammation induced cartilage matrix catabolism and modulate hMdCh- pro-inflammatory macrophage crosstalk to attenuate macrophage inflammation in vitro. However, these studies do not include the contribution of fibroblast like synoviocytes, which is another cell type that is activated by inflammatory macrophages and significantly contributes towards PTOA and by producing inflammatory cytokines, catabolic mediators, and prostaglandins[41,150,176]. Moreover, the contribution of fat pad, systemic inflammation and loading stress also need to be incorporated[79]. Therefore, future studies testing the efficacy of the gene circuit modified hMdChs to repair injured cartilage in animal models are highly desirable. Rat cartilage defect repair model for cartilage injury[177] and the ACL rupture model[41,178] for joint injury can be utilized to validate the efficacy of autoregulated RUNX2 suppression in hMdChs to promote cartilage repair, maintain

chondrogenic phenotype and attenuate whole joint inflammation. In rat critical cartilage defect repair model, an arthrotomy is performed to create critical sized defect (diameter: 2mm, depth: 1mm) in articular cartilage, which is either left empty or filled with cells to induce repair[177]. Cartilage healing can be evaluated using a combination of microCT and histological analysis[179–181]. In ACL rupture model, non-invasive ACL rupture is utilized to induce injury and cells are injected in the joint to evaluate therapeutic effects. Joint degradation, inflammation and PTOA severity can be assessed using histological staining, immunofluorescence, and synovial fluid analysis[41,179].

6.2.3 Achieving zonal Cartilage organization

Articular cartilage is a heterogenous anisotropic tissue with specific zonal organization that contributes towards its mechanical function. Each zone consists of specific organization of collagen fibers, chondrocyte arrangement and matrix composition[1,30,182]. Researchers have utilized multiphasic scaffold systems to direct collagen fiber orientation to mimic specific zones[31,32,183]. By combining such scaffold systems with autoregulated RUNX2 suppressing hMSCs, we can significantly improve cartilage regeneration outcome by addressing challenges like unstable chondrogenic phenotype of hMdChs, calcified cartilage formation and poor integration with native tissue after in vivo implantation. For example, scaffolds directing horizontal, followed by random and longitudinal distribution of collagen fibers to mimic superficial, middle, and deep zone can be seeded with high RUNX2 suppressing MSCs to obtain stable hMdChs that mimic chondrocytes in the respective zones. Furthermore, another scaffold seeded with WT MSCs and treated with T3 and βGP can be used to create calcified cartilage to integrate with subchondral bone. By combining these scaffolds, an articular cartilage implant incorporating the zonal architecture can be generated to achieve superior mechanical properties and better integration with the host tissue compared to

hMdChs alone. Moreover, autoregulated RUNX2 suppression in hMdChs should also result in improved cartilage repair by stabilizing hMdCh phenotype and protecting from inflammation induced matrix catabolism.

Appendices

Appendix A- Protocol for MSC chondrogenesis

MATERIALS REQUIRED:

- High Glucose DMEM (Gibco, Cat# 11965-092 stored at 4 °C in cell culture refrigerator)
- FBS (Gibco, Cat# 26140-079, stored at -20 in cell culture freezer)
- ITS+ Premix (corning, cat# 354350)
- 1% Non-essential Amino Acids (Gibco, Cat# 11-140-050)
- L-proline (Sigma cat# P-0380),
- Ascorbic Acid 2-Phosphate
- Dexamethasone
- TGFβ1 (Shenandoah, cat# 100-39)
- Trypsin (Gibco, Cat# 25200-056, stored at 4 °C in cell culture refrigerator
- Phosphate Buffer Saline (PBS) at RT (Gibco, Cat# 10010-023, stored in cell culture shelf)
- 0.4% Trypan Blue (Gibco, Cat # 15250061)
- Lab supplies (sterile pipette tips, serological pipettes, conical tubes, tissue culture flasks, 96 well non treated U-Bottom plates and sterile lids etc.)
- Vacuum pump (connected to the cell culture hood)
- Hemocytometer

hMSC Chondrogenic Media:

H.DMEM (w/ 4.5 g Glucose/l), 1% (v/v) Anti-Anti, 1% (v/v) ITS+ Premix (corning, cat# 354350), 1% Non-essential Amino Acids (Gibco, 11-140-050), 40 ug/ml L-proline(Sigma cat# P-0380), 50 ug/ml Ascorbic Acid 2-Phosphate, 0.1 uM Dexamethasone, 10 ng/ml TGFβ1 (Shenandoah, cat# 100-39)

Neutralization media:

DMEM (either high glucose or low glucose) + 10% FBS +1% Anti-anti

SAFETY PRECAUTIONS:

- Make sure to work in BSL-2 hood when dealing with cells. Wear lab coat, safety glasses and gloves before beginning.
- After you are done, do a final clean and decontamination with 70% ethanol solution. All the waste material should be discarded in biohazard trash bins (lined with clear autoclave bags) next to the BSL-2 hood. Solid waste should be promptly decontaminated in the autoclave and disposed of in the trash.
- For media decontamination add 10% bleach to the waste media and let it sit for 15-20 minutes until the solution becomes colorless. Drain it in the sink and keep the water tap on for 10-15 minutes.

METHOD:

Step 1: Make hMSC chondrogenic media and neutralization media as described above.

Step 2: Trypsinization of hMSCs:

1. Aspirate the media out of the flask using a Pasteur pipette.
2. Add PBS to the flask and swirl it around to give it a wash (10 ml for T-175 and 5ml for T-75). Aspirate the PBS using Pasteur pipette.
3. Add trypsin to detach the cells (2ml for T-75 and 4ml for T-175) and move the flask to the incubator for 3 minutes.
4. Gently tap the flask and observe under microscope to make sure the cells have detached.
5. Add neutralization media to neutralize trypsin (4ml for T-75 and 8ml for T-175). Pipette the suspension up and down a couple of times and swirl it in the flask to make sure you get all the cells.
6. Transfer the suspension to a 15ml or 50 ml conical tube depending upon the total volume.
7. Wipe the hemocytometer with 70% ethanol
8. To a microcentrifuge tube add 40 µl 0.4% trypan blue solution.
9. Mix the cell suspension with a pipette and add 40 µl to the tube containing trypan blue. Mix it gently and wait for 1-2 minutes.

10. Add 10 µl of cell suspension to the hemocytometer and count the live cell population and dead cells.

    Dead cells do not have intact cell membrane, so trypan blue is able to enter the cell and stain the cytoplasm blue. Hence, blue cells are dead and are not counted towards the live cell population.

    Formula to count live cell population:

    Live cell number = Sum of number of live cells in 4 squares of hemocytometer * 2 * 2500 cells/ml = X

    The number 2 is to account for the dilution factor for trypan blue staining.
11. Depending upon the number of wells needed, count to total number of cells required. Always add one extra well to the calculation for account for pipetting error. Also make sure you have a control well for selection.

    We need 250,000 cells per pellet in one well of 96 well plate. If we require 20 pellets, we approximate for 21 pellets i.e. 5.25×10^6 cells.

    So, the volume of cell suspension for 5.25×10^6 cells = 5.25×10^6 / X ml.
12. Transfer the appropriate volume of the cell suspension in a conical tube and centrifuge the cells at 1200 rpm or 1000 rcf for 5 minutes.

Step 3: Seeding hMSCs to form pellets:

13. Aspirate the media and resuspend the pellet in appropriate volume of MSC chondrogenic media.

    For 1 well we need 200 µl cell suspension hence for 21 wells (21 pellets) we need 200 x 21 = 4.2ml cell suspension. Therefore, resuspend the pellet in 4.2ml of chondrogenic media.
14. Add 200 µl cell suspension per well of the 96 well U-Bottom plate.
15. Place parafilm around the plates to avoid spillage and contamination. Centrifuge the plate at 1640 rpm for 5 minutes to condense the cells at the bottom. Make sure to have respective balance plate with equal amounts of water or PBS in the wells.
16. Remove the parafilm and place the cell plates in incubator at 37°C, 5% CO_2 and 95% humidity. Let the cells condense further to form intact pellets for 72 hours. This is Day 0 of chondrogenesis.

17. After 72 hours change media (chondrogenic) every other day for however long chondrogenic culture needs to be done.

Appendix B- Differentiation and M1 polarization of THP-1 cells

MATERIALS REQUIRED:

- RPMI media
- FBS
- Anti- Anti (Gibco, Cat# 15240-062)
- PMA (Sigma, Cat# P8139-1MG)
- Human IFN-γ (Biolegend, Cat# 713906)
- LPS (Sigma, Cat# L4391-1MG)
- Betamercaptoethanol (Sigma, Cat# M3148-25ML)
- Phosphate Buffer Saline (PBS) at RT (Gibco, Cat# 10010-023)
- Lab supplies (sterile pipette tips, serological pipettes, conical tubes, tissue culture flasks etc.)
- Vacuum pump (connected to the cell culture hood)

SOLUTIONS:

THP-1 growth media:

Component	Concentration	Amount (for 50 ml)
RPMI	89%	44.5 ml
FBS (qualified)	10%	5 ml
Anti- Anti	1%	500 µl
Beta-mercaptoethanol (BME)	0.05mM	25 µl of 0.1M stock

Methods:

THP-1 culture

1. THP-1 is a monocytic leukemia cell line. The cells are cultured in suspension meaning that the cells will not adhere to the bottom of the flask.
2. For media changes, centrifuge the cells at 1200 rpm, discard the old spent media and resuspend the pellet in fresh growth media.
   Note: media can also be changed by adding fresh media to the cell suspension however, this will dilute the nutrients hence not recommended to be done frequently.

3. Cells become confluent at $1x10^6$cells/ml concentration. Do not let your cell numbers to go above 0.9-$1x10^6$cells/ml.

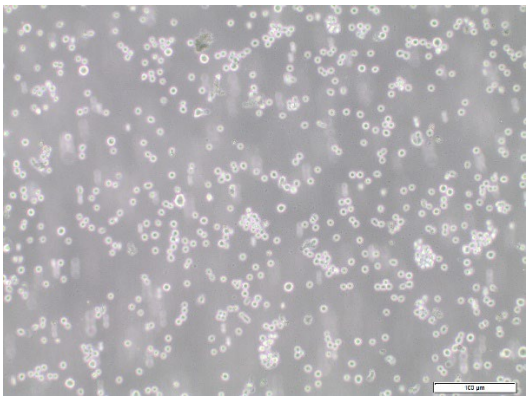

THP-1 differentiation into macrophage

1. Pre-warm the growth medium and thaw PMA aliquot.
2. Make THP-1 differentiation media by adding PMA to THP-1 growth media to the final concentration of 150nM.

   Stock is at 10,000X. Therefore for 10 ml media, add 1µl PMA stock to 10ml growth media.
3. Count the THP-1 cells using hemocytometer. To count live cells, take 40µl of cell suspension in a microcentrifuge tube and add 40 µl of trypan blue dye. Mix it well and let it sit for a minute.

   Take 10 µl of this solution and add to the hemocytometer. Dead cells will stain blue while alive cells will remain bright and clear. Count the live and dead cells in all the four squares. Also count the cells on the left and upper edges of the squares but not the right and bottom.

   Final cell concentration can be calculated as follows:

   Cell number = (Sum of cells in 4 squares/4) x 2 (dilution factor) x 10^4 cells/ml.
4. We seed 150,000 cells/ml of media per well.

   For a 6 well plate, we use 2ml media therefore we will add 150,000 x 2 = 300,000 cells per well

   Calculate the total number of cells needed. For example:

   if we need to differentiate macrophages in all the wells of a 6 well plate, we will need (6 + 1 extra) x 300,000 = 2.1 x 10^6cells.

   If we have X cells/ml then calculate the amount of cell suspension needed = $2.1x10^6$ /X ml.
5. Centrifuge the required volume of cell suspension at 1200 rpm for 5 minutes.
6. Discard the media and resuspend the cells in THP-1 growth media containing PMA.
7. Add the cell suspension to the well plate and transfer it to the incubator for 24 hours.

8. After 24 hours, the cells should attach to the surface of the plate. At this stage the monocytes have differentiated into macrophages *(refer to image below)* however they have not been polarized into pro or anti-inflammatory phenotypes yet. On a basal level the PMA differentiated macrophages do exhibit some pro-inflammatory phenotype.

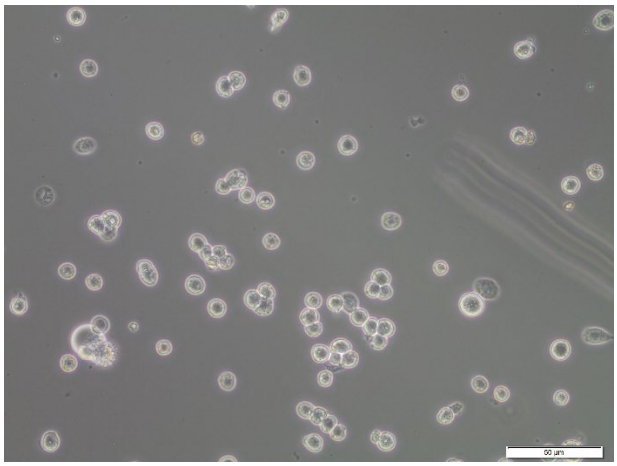

9. Discard the media and add fresh THP-1 growth media without PMA and incubate for another 24 hours.

   This rest period is necessary to increase viability before challenging cells with PMA for M1 polarization.

Inducing M1 polarization of THP-1 derived macrophage

10. After 24-hour rest period, the cells are ready to be polarized into pro-inflammatory M1 phenotype.
11. Make M1 polarization media by adding 10pg/ml LPS and 20ng/ml IFNγ to THP-1 growth media.
12. Remove growth media from THP-1 derived macrophages and add polarization media mentioned above. Incubate the cells with polarization media for 24 hours.
13. After 24 hours, macrophages will appear bigger in size and some cells will fuse to form giant cell like phenotype. Some cells will appear to have dendritic projections *(refer to image below)*. The cells have now been polarized into pro-inflammatory M1 macrophages.

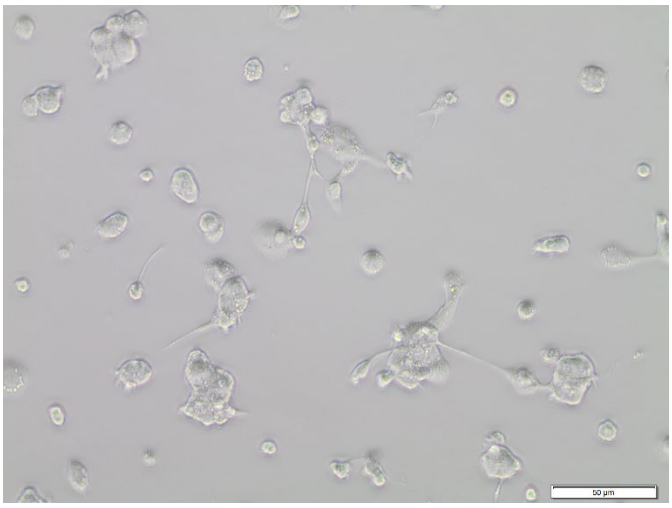

14. Change the media of the cells to THP-1 growth media.

Appendix C- Protocol for DMMB and DNA assay

www.qiagen.com/HB-0435

Material Required	Catalog Number	Storage Condition
Papain	Sigma, P4762	-20°C
L-Cysteine Hydrochloride	Sigma, 30120	Room Temperature
EDTA	Sigma, ED2SS	Room Temperature
Sodium phosphate (disodium anhydrous)	Sigma, S7907	Room Temperature
UltraPure Distilled Water	Invitrogen, 10977-015	Room Temperature
DMMB Assay		
1,9-Dimethylene Blue	Sigma, 341088	Room Temperature
Ethanol	Deacon Labs.	Room Temperature
Chondroitin-6-sulfate	Sigma, C4384	4°C
Glycine	Sigma, G8898	Room Temperature
NaCl	Sigma, S7653	Room Temperature
DNA Assay		
Hoechst 33342 Dye	Invitrogen, H3570	4°C
Calf Thymus DNA	Sigma, D4522	-20°C
EDTA	Sigma, EDS	Room Temperature
Trizma (Tris) Base	Sigma, T1503	Room Temperature

Solutions:

Digestion

1. Papain buffer (150 ml):
    a. Papain: 3.755 mg
    b. Cysteine: 47.28 mg
    c. EDTA (disodium dihydrate; FW 372.2): 111.66 mg
    d. Sodium phosphate (disodium anhydrous; FW 141.96): 1.06g
    e. Dissolve in 150 ml nuclease-free water, adjust pH to 6.5, and then filter sterilize with a 0.2 µm Nalgene filter.
    f. Store in aliquots at -20°C.
    1.
2. Base buffer (150 ml):
    a. Cysteine: 47.28 mg

b. EDTA (disodium dihydrate; FW 372.2): 111.66 mg
c. Sodium phosphate (disodium anhydrous; FW 141.96): 1.06g
d. Dissolve in 150 ml nuclease-free water, adjust pH to 6.5, and then filter sterilize with a 0.2 µm Nalgene filter.
e. Store at 4°C.

DMMB Assay

1. Dye Solution: Store up to 3 months
    a. Dissolve 16 mg DMMB into 5 ml 100 % ethanol
    b. Stir overnight in 20 ml capped glass vial, protect from light
    c. Bring volume to 800 ml with milli-Q water
    d. Add 2.37 g NaCl (0.04 M, final conc.)
    e. Add 3.04 g Glycine (0.04 M, final conc.)
    f. PH to 1.5 with concentrated HCl
    g. Bring the volume up to 1 L
    2.
2. Chondroitin Sulfate stock solution (12.5 mg/mL)
    a. Dissolve 25 mg of chondroitin sulfate in 2 mL of milli-Q water
    b. Store at -20°C -in 5 µl aliquots

DNA Assay

1. 10X TNE Buffer
    a. Measure 800 ml of Milli-Q water
    b. Dissolve 12.11 g Tris base
    c. Dissolve 3.72 g EDTA
    d. Dissolve 116.89 g NaCl
    e. Adjust pH to 7.4 with concentrated HCl
    f. Bring the volume up to 1000 ml with Milli-Q water
    g. Filter with 0.45 µm filter
    h. Store at 4°C up to 3 months
    3.
2. 1X TNE Buffer
    a. Dilute 10 ml 10X TNE with 90 ml Milli-Q water
3. Calf Thymus Stock Solution (200 ng/mL)
    a. Dissolve 0.5 mg Calf Thymus DNA into 1 ml DNAse, RNAse Free distilled water
4. 5000X Dye Stock Solution (10 mg/ml)
    a. Ready-to-use product: Hoechst 33342 (H3570), 10 mg/ml
5. 1X Dye Solution (2 ng/µl)
    a. Dilute with 20 µl stock dye with 100 ml 1X TNE buffer
    b. **Prepare fresh when performing the assay and protect from light**
    4.

Protocol: For hMSC pellets (250,000 cells/pellet)

Papain Digestion – One day before assay

1. Add 100 µl of papain buffer to each sample
2. Digest gels for 16 hrs at 65°C
3. Samples can be frozen at -20°C for later analysis after digestion

DMMB Assay

1. Prepare chondroitin sulfate standards at the following concentrations: 125, 62.5, 31.25, 15.625, 7.8125, 3.90625 µg/ml by making serial two-fold dilutions with papain buffer. Also, include a 0 µg/ml standard
2. Check the pH of the dye – readjust with HCl to 1.5 if too high
3. Run standards in duplicate and samples in triplicate (example plate pictured below)
4. Vortex samples, briefly spin down, and pipette 10 µl of standard or sample into each well of a NUNC 96-well assay plate
5. Each well requires 200 µl of die. Calculate the approximate amount of die needed and use a serological pipette to transfer that amount plus an extra 3 mL into a non-sterile media reservoir
6. Using a multi-channel pipette, add 200 µl of dye to each well
7. Cover plate with aluminum foil and take to BioTek Plate reader immediately following addition of the dye.
8. Protocol is named "DMMB ASSAY – 96WP"
    a. Absorbance is read at both **525nm** and **595 nm**

    b. A precipitate will form if the plate is allowed to sit.
9. Left over die should be disposed of as hazardous material

Plate #1	A	**B**	**C**	**D**	**E**	**F**	**G**	**H**	**I**	**J**	**K**	**L**
1	125.00 µg/ml	1	1	1	9	9	9	17	17	17	25	125.00 µg/ml
2	62.50 µg/ml	2	2	2	10	10	10	18	18	18	25	62.50 µg/ml
3	31.25 µg/ml	3	3	3	11	11	11	19	19	19	25	31.25 µg/ml
4	15.63 µg/ml	4	4	4	12	12	12	20	20	20	26	15.63 µg/ml
5	7.81 µg/ml	5	5	5	13	13	13	21	21	21	26	7.81 µg/ml
6	3.91 µg/ml	6	6	6	14	14	14	22	22	22	26	3.91 µg/ml
7	0 µg/ml	7	7	7	15	15	15	23	23	23		0 µg/ml

8	Blank	8	8	8	16	16	16	24	24	24		Blank

DNA Assay

1. Take a DNA stock aliquot and check concentration using Nanodrop.
2. Prepare DNA standards at the following concentrations: 20, 10, 5, 2.5, 1.25, 0.625 ng/µl by making serial two-fold dilutions with 1X TNE Buffer. Also, include a 0 ng/µl standard
3. Run standards in duplicate and samples in triplicate (example plate pictured above)
4. Vortex samples, briefly spin down, and pipette 10 µl of standard or sample into each well of a BLACK NUNC 96-well assay plate
5. Each well requires 190 µl of 1X dye solution. Calculate the approximate amount of die needed and create a 1X dye solution. **Make sure to keep the dye protected from light.**
6. Using a multi-channel pipette, add 190 µl of dye to each well
7. Cover plate with aluminum foil and take to BioTek Plate reader immediately following addition of the dye.
8. Protocol is named "DNA ASSAY – 96WP"
    a. Excitation is read at **355 nm** and emission is read at **460 nm**.

Bibliography

1. Sophia Fox, A. J., Bedi, A. & Rodeo, S. A. The Basic Science of Articular Cartilage: Structure, Composition, and Function. *Sports Health* **1**, 461 (2009).
2. Sovani, S. & Grogan, S. P. Osteoarthritis: Detection, pathophysiology, and current/future treatment strategies. *Orthopaedic Nursing* **32**, 25–36 (2013).
3. Hunter, D. J. & Bierma-Zeinstra, S. Osteoarthritis. *Lancet* **393**, 1745–1759 (2019).
4. Stevens, A. L., Wishnok, J. S., White, F. M., Grodzinsky, A. J. & Tannenbaum, S. R. Mechanical Injury and Cytokines Cause Loss of Cartilage Integrity and Upregulate Proteins Associated with Catabolism, Immunity, Inflammation, and Repair. *Mol Cell Proteomics* **8**, 1475 (2009).
5. Medvedeva, E. v. *et al.* Repair of Damaged Articular Cartilage: Current Approaches and Future Directions. *Int J Mol Sci* **19**, (2018).
6. Makris, E. A., Gomoll, A. H., Malizos, K. N., Hu, J. C. & Athanasiou, K. A. Repair and tissue engineering techniques for articular cartilage. *Nat. Rev. Rheumatol.* **11**, 21–34 (2015).
7. Schäfer, N. & Grässel, S. New refinements aim to optimize articular cartilage tissue engineering. *Nature Reviews Rheumatology 2023 19:2* **19**, 66–67 (2023).
8. Mackay, A. M. *et al.* Chondrogenic differentiation of cultured human mesenchymal stem cells from marrow. *Tissue Eng* **4**, 415–428 (1998).
9. Pittenger, M. F. *et al.* Multilineage potential of adult human mesenchymal stem cells. *Science (1979)* **284**, 143–147 (1999).

10. Yoo, J. U. *et al.* The chondrogenic potential of human bone-marrow-derived mesenchymal progenitor cells. *Journal of Bone and Joint Surgery - Series A* **80**, 1745–1757 (1998).

11. Barry, F., Boynton, R. E., Liu, B. & Murphy, J. M. Chondrogenic differentiation of mesenchymal stem cells from bone marrow: differentiation-dependent gene expression of matrix components. *Exp Cell Res* **268**, 189–200 (2001).

12. Pelttari, K. *et al.* Premature induction of hypertrophy during in vitro chondrogenesis of human mesenchymal stem cells correlates with calcification and vascular invasion after ectopic transplantation in SCID mice. *Arthritis Rheum* **54**, 3254–3266 (2006).

13. Nishimura, R. *et al.* Osterix regulates calcification and degradation of chondrogenic matrices through matrix metalloproteinase 13 (MMP13) expression in association with transcription factor Runx2 during endochondral ossification. *Journal of Biological Chemistry* **287**, 33179–33190 (2012).

14. Lu, H., Lin, Z., Yang, Z., Chen, M. & Zhang, K. Inhibition of RUNX2 expression promotes differentiation of MSCs correlated with SDF-1 up-regulation in rats. *Int J Clin Exp Pathol* **9**, 11388–11395 (2016).

15. Gouze, J. N. *et al.* Glucosamine modulates IL-1-induced activation of rat chondrocytes at a receptor level, and by inhibiting the NF-κB pathway. *FEBS Letters* vol. 510 166–170 Preprint at https://doi.org/10.1016/S0014-5793(01)03255-0 (2002).

16. Takahashi, N. *et al.* Elucidation of IL-1/TGF-β interactions in mouse chondrocyte cell line by genome-wide gene expression1. *Osteoarthritis and Cartilage* vol. 13 426–438 Preprint at https://doi.org/10.1016/j.joca.2004.12.010 (2005).

17. Studer, D., Millan, C., Öztürk, E., Maniura-Weber, K. & Zenobi-Wong, M. Molecular and biophysical mechanisms regulating hypertrophic differentiation in chondrocytes and mesenchymal stem cells. *Eur Cell Mater* (2012) doi:10.22203/eCM.v024a09.

18. Kondo, M., Yamaoka, K. & Tanaka, Y. Acquiring chondrocyte phenotype from human mesenchymal stem cells under inflammatory conditions. *Int J Mol Sci* **15**, 21270–21285 (2014).

19. Kraus, V. B. *et al.* Direct in vivo evidence of activated macrophages in human osteoarthritis. *Osteoarthritis Cartilage* **24**, (2016).

20. Wu, C. L., Harasymowicz, N. S., Klimak, M. A., Collins, K. H. & Guilak, F. The role of macrophages in osteoarthritis and cartilage repair. *Osteoarthritis and Cartilage* vol. 28 Preprint at https://doi.org/10.1016/j.joca.2019.12.007 (2020).

21. Chen, Y. *et al.* Macrophages in osteoarthritis: Pathophysiology and therapeutics. *Am J Transl Res* **12**, (2020).

22. Zhang, H., Cai, D. & Bai, X. Macrophages regulate the progression of osteoarthritis. *Osteoarthritis Cartilage* **28**, (2020).

23. Griffin, T. M. & Scanzello, C. R. Innate inflammation and synovial macrophages in osteoarthritis pathophysiology. *Clinical and experimental rheumatology* vol. 37 Preprint at (2019).

24. Wu, B., Kaur, G., Murali, S., Lanigan, T. & Coleman, R. M. A Synthetic, Closed-Looped Gene Circuit for the Autonomous Regulation of RUNX2 Activity during Chondrogenesis. *bioRxiv* (2021).

25. Okubo, Y. & Reddi, A. H. Thyroxine downregulates Sox9 and promotes chondrocyte hypertrophy. *Biochem Biophys Res Commun* **306**, 186–190 (2003).

26. Wu, B. *et al.* Phosphate regulates chondrogenesis in a biphasic and maturation-dependent manner. *Differentiation* (2017) doi:10.1016/j.diff.2017.04.002.

27. Mueller, M. B. & Tuan, R. S. Functional Characterization of Hypertrophy in Chondrogenesis of Human Mesenchymal Stem Cells. *Arthritis Rheum* **58**, 1377 (2008).

28. Goldring, M. B. & Otero, M. Inflammation in osteoarthritis. *Current Opinion in Rheumatology* Preprint at https://doi.org/10.1097/BOR.0b013e328349c2b1 (2011).

29. Muir, H. The chondrocyte, architect of cartilage. Biomechanics, structure, function and molecular biology of cartilage matrix macromolecules. *BioEssays* Preprint at https://doi.org/10.1002/bies.950171208 (1995).

30. Tee, C. A. *et al.* Perspective in Achieving Stratified Articular Cartilage Repair Using Zonal Chondrocytes. *https://home.liebertpub.com/teb* (2023) doi:10.1089/TEN.TEB.2022.0142.

31. Steele, J. A. M. *et al.* In vitro and in vivo investigation of a zonal microstructured scaffold for osteochondral defect repair. *Biomaterials* **286**, 121548 (2022).

32. Allard, S. A., Bayliss, M. T. & Maini, R. N. The synovium-cartilage junction of the normal human knee. Implications for joint destruction and repair. *Arthritis Rheum* **33**, 1170–1179 (1990).

33. Lieberthal, J., Sambamurthy, N. & Scanzello, C. R. Inflammation in joint injury and post-traumatic osteoarthritis. *Osteoarthritis Cartilage* **23**, 1825–1834 (2015).

34. Li, L., Lv, G., Wang, B. & Kuang, L. XIST/miR-376c-5p/OPN axis modulates the influence of proinflammatory M1 macrophages on osteoarthritis chondrocyte apoptosis. *J Cell Physiol* **235**, (2020).

35. Zhu, X. *et al.* Phenotypic alteration of macrophages during osteoarthritis: a systematic review. *Arthritis Research and Therapy* vol. 23 Preprint at https://doi.org/10.1186/s13075-021-02457-3 (2021).

36. Ellis, S., Lin, E. J. & Tartar, D. Immunology of Wound Healing. *Current Dermatology Reports* vol. 7 Preprint at https://doi.org/10.1007/s13671-018-0234-9 (2018).

37. Krzyszczyk, P., Schloss, R., Palmer, A. & Berthiaume, F. The role of macrophages in acute and chronic wound healing and interventions to promote pro-wound healing phenotypes. *Frontiers in Physiology* vol. 9 Preprint at https://doi.org/10.3389/fphys.2018.00419 (2018).

38. Shapouri-Moghaddam, A. *et al.* Macrophage plasticity, polarization, and function in health and disease. *Journal of Cellular Physiology* vol. 233 Preprint at https://doi.org/10.1002/jcp.26429 (2018).

39. Locati, M., Curtale, G. & Mantovani, A. Diversity, Mechanisms, and Significance of Macrophage Plasticity. *Annual Review of Pathology: Mechanisms of Disease* **15**, 123–147 (2020).

40. Knights, A. J. *et al.* Synovial fibroblasts assume distinct functional identities and secrete R-spondin 2 in osteoarthritis. *Ann Rheum Dis* (2022) doi:10.1136/ARD-2022-222773.

41. Han, D. *et al.* The emerging role of fibroblast-like synoviocytes-mediated synovitis in osteoarthritis: An update. *J Cell Mol Med* **24**, 9518 (2020).

42. Zhang, H. *et al.* Synovial macrophage M1 polarisation exacerbates experimental osteoarthritis partially through R-spondin-2. *Ann Rheum Dis* (2018) doi:10.1136/ANNRHEUMDIS-2018-213450.

43. Haraden, C. A., Huebner, J. L., Hsueh, M. F., Li, Y. J. & Kraus, V. B. Synovial fluid biomarkers associated with osteoarthritis severity reflect macrophage and neutrophil related inflammation. *Arthritis Res Ther* **21**, (2019).

44. Samavedi, S., Diaz-Rodriguez, P., Erndt-Marino, J. D. & Hahn, M. S. A Three-Dimensional Chondrocyte-Macrophage Coculture System to Probe Inflammation in Experimental Osteoarthritis. *Tissue Eng Part A* **23**, 101 (2017).

45. Lai-Zhao, Y., Klapak, D., Blackler, G., Gillies, E. & Appleton, T. Selective targeting of synovial macrophages in experimental post-traumatic knee osteoarthritis modulates articular chondrocyte physiology. *Osteoarthritis Cartilage* **28**, S202 (2020).

46. Houard, X., Goldring, M. B. & Berenbaum, F. Homeostatic mechanisms in articular cartilage and role of inflammation in osteoarthritis. *Curr Rheumatol Rep* (2013) doi:10.1007/s11926-013-0375-6.

47. Malemud, C. J. Biologic basis of osteoarthritis: State of the evidence. *Curr Opin Rheumatol* **27**, 289–294 (2015).

48. Liu, B., Zhang, M., Zhao, J., Zheng, M. & Yang, H. Imbalance of M1/M2 macrophages is linked to severity level of knee osteoarthritis. *Exp Ther Med* **16**, 5009–5014 (2018).

49. Fernandes, T. L. *et al.* Macrophage: A Potential Target on Cartilage Regeneration. *Frontiers in Immunology* vol. 11 Preprint at https://doi.org/10.3389/fimmu.2020.00111 (2020).

50. Dai, M., Sui, B., Xue, Y., Liu, X. & Sun, J. Cartilage repair in degenerative osteoarthritis mediated by squid type II collagen via immunomodulating activation of M2 macrophages, inhibiting apoptosis and hypertrophy of chondrocytes. *Biomaterials* **180**, 91–103 (2018).

51. Liang, C. *et al.* Engineered M2a macrophages for the treatment of osteoarthritis. *Front Immunol* **13**, (2022).

52. Rivera-Delgado, E. *et al.* Injectable liquid polymers extend the delivery of corticosteroids for the treatment of osteoarthritis. *Journal of Controlled Release* (2018) doi:10.1016/j.jconrel.2018.05.037.

53. Xie, J. W. *et al.* Alpha defensin-1 attenuates surgically induced osteoarthritis in association with promoting M1 to M2 macrophage polarization. *Osteoarthritis Cartilage* **29**, 1048–1059 (2021).

54. Mithoefer, K., Mcadams, T., Williams, R. J., Kreuz, P. C. & Mandelbaum, B. R. Clinical efficacy of the microfracture technique for articular cartilage repair in the knee: An evidence-based systematic analysis. *American Journal of Sports Medicine* **37**, 2053–2063 (2009).

55. Gobbi, A., Karnatzikos, G. & Kumar, A. Long-term results after microfracture treatment for full-thickness knee chondral lesions in athletes. *Knee Surgery, Sports Traumatology, Arthroscopy* **22**, 1986–1996 (2014).

56. Brittberg, M., Recker, D., Ilgenfritz, J. & Saris, D. B. F. Matrix-Applied Characterized Autologous Cultured Chondrocytes Versus Microfracture: Five-Year Follow-up of a Prospective Randomized Trial. *American Journal of Sports Medicine* **46**, 1343–1351 (2018).

57. Hangody, L. & Füles, P. Autologous osteochondral mosaicplasty for the treatment of full-thickness defects of weight-bearing joints: Ten years of experimental and clinical experience. *Journal of Bone and Joint Surgery* **85**, 25–32 (2003).

58. Nakagawa, Y., Mukai, S., Yabumoto, H., Tarumi, E. & Nakamura, T. Serial Changes of the Cartilage in Recipient Sites and Their Mirror Sites on Second-Look Imaging after Mosaicplasty. *American Journal of Sports Medicine* **44**, 1243–1248 (2016).

59. Liu, Y., Shah, K. M. & Luo, J. Strategies for Articular Cartilage Repair and Regeneration. *Front Bioeng Biotechnol* **9**, (2021).

60. Brittberg, M. *et al.* Treatment of Deep Cartilage Defects in the Knee with Autologous Chondrocyte Transplantation. *New England Journal of Medicine* **331**, 889–895 (1994).

61. Barbero, A. *et al.* Age related changes in human articular chondrocyte yield, proliferation and post-expansion chondrogenic capacity. *Osteoarthritis Cartilage* (2004) doi:10.1016/j.joca.2004.02.010.

62. Caron, M. M. J. *et al.* Redifferentiation of dedifferentiated human articular chondrocytes: Comparison of 2D and 3D cultures. *Osteoarthritis Cartilage* **20**, 1170–1178 (2012).

63. Goyal, D., Goyal, A., Keyhani, S., Lee, E. H. & Hui, J. H. P. Evidence-based status of second- and third-generation autologous chondrocyte implantation over first generation: A systematic review of level i and II studies. *Arthroscopy - Journal of Arthroscopic and Related Surgery* **29**, 1872–1878 (2013).

64. Kreuz, P. C. *et al.* Classification of graft hypertrophy after autologous chondrocyte implantation of full-thickness chondral defects in the knee. *Osteoarthritis Cartilage* **15**, 1339–1347 (2007).

65. Makris, E. A., Gomoll, A. H., Malizos, K. N., Hu, J. C. & Athanasiou, K. A. Repair and tissue engineering techniques for articular cartilage. *Nat Rev Rheumatol* **11**, 21–34 (2015).

66. Huang, B. J., Hu, J. C. & Athanasiou, K. A. Cell-based tissue engineering strategies used in the clinical repair of articular cartilage. *Biomaterials* **98**, 1–22 (2016).

67. Darling, E. M. & Athanasiou, K. A. Rapid phenotypic changes in passaged articular chondrocyte subpopulations. *Journal of Orthopaedic Research* **23**, 425–432 (2005).

68. Yang, K. G. A. *et al.* Impact of expansion and redifferentiation conditions on chondrogenic capacity of cultured chondrocytes. *Tissue Eng* **12**, 2435–2447 (2006).

69. Domm, C., Schünke, M., Christesen, K. & Kurz, B. Redifferentiation of dedifferentiated bovine articular chondrocytes in alginate culture under low oxygen tension. *Osteoarthritis Cartilage* **10**, 13–22 (2002).

70. Mackay, A. M. *et al.* Chondrogenic differentiation of cultured human mesenchymal stem cells from marrow. *Tissue Eng* (1998) doi:10.1089/ten.1998.4.415.

71. Miljkovic, N. D., Cooper, G. M. & Marra, K. G. Chondrogenesis, bone morphogenetic protein-4 and mesenchymal stem cells. *Osteoarthritis Cartilage* **16**, 1121–1130 (2008).

72. Johnstone, B., Hering, T. M., Caplan, A. I., Goldberg, V. M. & Yoo, J. U. In vitro chondrogenesis of bone marrow-derived mesenchymal progenitor cells. *Exp Cell Res* **238**, 265–272 (1998).

73. Miceli, M. *et al.* Preliminary Characterization of the Epigenetic Modulation in the Human Mesenchymal Stem Cells during Chondrogenic Process. *Int J Mol Sci* **23**, (2022).

74. Loo, S. & Wong, N. Advantages and challenges of stem cell therapy for osteoarthritis (Review). *Biomed Rep* **15**, (2021).

75. Shah, S., Esdaille, C. J., Bhattacharjee, M., Kan, H. M. & Laurencin, C. T. The synthetic artificial stem cell (SASC): shifting the paradigm of cell therapy in regenerative engineering. *Proc. Natl. Acad. Sci. USA* **119**, (2022).

76. Nishimura, R., Hata, K., Matsubara, T., Wakabayashi, M. & Yoneda, T. Regulation of bone and cartilage development by network between BMP signalling and transcription factors. *Journal of Biochemistry* vol. 151 247–254 Preprint at https://doi.org/10.1093/jb/mvs004 (2012).

77. Nishihara, A., Fujii, M., Sampath, T. K., Miyazono, K. & Reddi, A. H. Bone morphogenetic protein signaling in articular chondrocyte differentiation. *Biochem Biophys Res Commun* **301**, 617–622 (2003).

78. Madej Z, W., van Caam Y A, A., Davidson, E. B., Buma, P. & van der Kraan, P. M. Unloading results in rapid loss of TGFβ signaling in articular cartilage: role of loading-induced TGFβ signaling in maintenance of articular chondrocyte phenotype? (2016) doi:10.1016/j.joca.2016.05.018.

79. Tracy Ballock, R. *et al.* TGF-beta 1 prevents hypertrophy of epiphyseal chondrocytes: regulation of gene expression for cartilage matrix proteins and metalloproteases. *Dev Biol* **158**, 414–429 (1993).

80. Kozhemyakina, E., Lassar, A. B. & Zelzer, E. A pathway to bone: Signaling molecules and transcription factors involved in chondrocyte development and maturation. *Development (Cambridge)* **142**, 817–831 (2015).

81. Mandl, E. W. *et al.* Fibroblast growth factor-2 in serum-free medium is a potent mitogen and reduces dedifferentiation of human ear chondrocytes in monolayer culture. *Matrix Biology* **23**, 231–241 (2004).

82. Somoza, R. A. *et al.* Transcriptome-Wide Analyses of Human Neonatal Articular Cartilage and Human Mesenchymal Stem Cell-Derived Cartilage Provide a New Molecular Target for Evaluating Engineered Cartilage. *Tissue Eng Part A* **24**, 335–350 (2018).

83. Rowland, C. R. *et al.* Regulation of decellularized tissue remodeling via scaffold-mediated lentiviral delivery in anatomically-shaped osteochondral constructs. *Biomaterials* (2018) doi:10.1016/j.biomaterials.2018.04.049.

84. Browe, D. C. *et al.* Promoting endogenous articular cartilage regeneration using extracellular matrix scaffolds. *Mater. Today Bio.* **16**, 100343 (2022).

85. Rowland, C. R., Colucci, L. A. & Guilak, F. Fabrication of anatomically-shaped cartilage constructs using decellularized cartilage-derived matrix scaffolds. *Biomaterials* (2016) doi:10.1016/j.biomaterials.2016.03.012.

86. O'Shea, D. G., Curtin, C. M. & O'Brien, F. J. Articulation inspired by nature: a review of biomimetic and biologically active 3D printed scaffolds for cartilage tissue engineering. *Biomater Sci* (2022) doi:10.1039/d1bm01540k.

87. Ousema, P. H. *et al.* The inhibition by interleukin 1 of MSC chondrogenesis and the development of biomechanical properties in biomimetic 3D woven PCL scaffolds. *Biomaterials* (2012) doi:10.1016/j.biomaterials.2012.08.045.

88. Duval, E. *et al.* Hypoxia-inducible factor 1α inhibits the fibroblast-like markers type I and type III collagen during hypoxia-induced chondrocyte redifferentiation: Hypoxia not only induces type II collagen and aggrecan, but it also inhibits type I and type III collagen in the hypoxia-inducible factor 1α-dependent redifferentiation of chondrocytes. *Arthritis Rheum* **60**, 3038–3048 (2009).

89. Shang, J., Liu, H., Li, J. & Zhou, Y. Roles of Hypoxia During the Chondrogenic Differentiation of Mesenchymal Stem Cells. *Curr Stem Cell Res Ther* (2014) doi:10.2174/1574888x09666131230142459.

90. Thoms, B. L., Dudek, K. A., Lafont, J. E. & Murphy, C. L. Hypoxia Promotes the Production and Inhibits the Destruction of Human Articular Cartilage. *Arthritis Rheum* **65**, 1302–1312 (2013).

91. Wang, Y., Wu, S., Kuss, M. A., Streubel, P. N. & Duan, B. Effects of Hydroxyapatite and Hypoxia on Chondrogenesis and Hypertrophy in 3D Bioprinted ADMSC Laden Constructs. *ACS Biomater Sci Eng* **3**, 826–835 (2017).

92. Robins, J. C. *et al.* Hypoxia induces chondrocyte-specific gene expression in mesenchymal cells in association with transcriptional activation of Sox9. *Bone* **37**, 313–322 (2005).

93. Zhao, Z. *et al.* Mechanotransduction pathways in the regulation of cartilage chondrocyte homoeostasis. *J Cell Mol Med* **24**, 5408–5419 (2020).

94. Huang, C.-Y. C., Hagar, K. L., Frost, L. E., Sun, Y. & Cheung, H. S. Effects of Cyclic Compressive Loading on Chondrogenesis of Rabbit Bone-Marrow Derived Mesenchymal Stem Cells. *Stem Cells* (2004) doi:10.1634/stemcells.22-3-313.

95. Juhász, T. *et al.* Mechanical loading stimulates chondrogenesis via the PKA/CREB-Sox9 and PP2A pathways in chicken micromass cultures. *Cell Signal* (2014) doi:10.1016/j.cellsig.2013.12.001.

96. Yang, B. *et al.* YAP1 negatively regulates chondrocyte differentiation partly by activating the β-catenin signaling pathway. *International Journal of Biochemistry and Cell Biology* **87**, 104–113 (2017).

97. Farrell, M. J. *et al.* Functional properties of bone marrow-derived MSC-based engineered cartilage are unstable with very long-term in vitro culture. *J Biomech* (2014) doi:10.1016/j.jbiomech.2013.10.030.

98. O'Conor, C. J., Leddy, H. A., Benefield, H. C., Liedtke, W. B. & Guilak, F. TRPV4-mediated mechanotransduction regulates the metabolic response of chondrocytes to dynamic loading. *Proc Natl Acad Sci U S A* **111**, 1316–1321 (2014).

99. Nurminskaya, M. & Linsenmayer, T. F. Analysis of up-regulated genes during chondrocyte hypertrophy. *Ann N Y Acad Sci* **785**, 309–310 (1996).

100. Zheng, Q. *et al.* Type X collagen gene regulation by Runx2 contributes directly to its hypertrophic chondrocyte-specific expression in vivo. *Journal of Cell Biology* **162**, 833–842 (2003).

101. Mueller, M. B. *et al.* Hypertrophy in mesenchymal stem cell chondrogenesis: effect of TGF-beta isoforms and chondrogenic conditioning. *Cells Tissues Organs* **192**, 158–166 (2010).

102. Saito, T. *et al.* Transcriptional regulation of endochondral ossification by HIF-2α during skeletal growth and osteoarthritis development. *Nat Med* **16**, 678–686 (2010).

103. Kawato, Y. *et al.* Nkx3.2-induced suppression of Runx2 is a crucial mediator of hypoxia-dependent maintenance of chondrocyte phenotypes. *Biochem Biophys Res Commun* **416**, 205–210 (2011).

104. Yu, Z. G. *et al.* Interleukin-1 inhibits Sox9 and collagen type II expression via nuclear factor-κB in the cultured human intervertebral disc cells. *Chin Med J (Engl)* (2009) doi:10.3760/cma.j.issn.0366-6999.2009.20.016.

105. Alivernini, S. *et al.* Distinct synovial tissue macrophage subsets regulate inflammation and remission in rheumatoid arthritis. *Nat Med* **26**, 1295–1306 (2020).

106. Neumeier, J. & Meister, G. siRNA Specificity: RNAi Mechanisms and Strategies to Reduce Off-Target Effects. *Front Plant Sci* **11**, 2196 (2021).

107. Filipowicz, W. RNAi: The nuts and bolts of the RISC machine. *Cell* **122**, 17–20 (2005).

108. Medvedeva, E. v. *et al.* Repair of damaged articular cartilage: Current approaches and future directions. *International Journal of Molecular Sciences* Preprint at https://doi.org/10.3390/ijms19082366 (2018).

109. Kwon, H. Cartilage tissue engineering in the inflammatory milieu. *ProQuest Dissertations and Theses* (2014).

110. Arnold, M. A. *et al.* MEF2C Transcription Factor Controls Chondrocyte Hypertrophy and Bone Development. *Dev Cell* **12**, 377–389 (2007).

111. Amano, K., Densmore, M., Nishimura, R. & Lanske, B. Indian hedgehog signaling regulates transcription and expression of collagen type X via Runx2/Smads interactions. *Journal of Biological Chemistry* **289**, 24898–24910 (2014).

112. Kawane, T. *et al.* Dlx5 and Mef2 regulate a novel Runx2 enhancer for osteoblast-specific expression. *Journal of Bone and Mineral Research* vol. 29 1960–1969 Preprint at https://doi.org/10.1002/jbmr.2240 (2014).

113. Ilic, M. Z., Handley, C. J., Robinson, H. C. & Mok, M. T. Mechanism of catabolism of aggrecan by articular cartilage. *Arch Biochem Biophys* (1992) doi:10.1016/0003-9861(92)90144-L.

114. Leijten, J. C. H., Moreira Teixeira, L. S., Landman, E. B. M., van Blitterswijk, C. A. & Karperien, M. Hypoxia Inhibits Hypertrophic Differentiation and Endochondral Ossification in Explanted Tibiae. *PLoS One* **7**, e49896 (2012).

115. Gale, A. L., Mammone, R. M., Dodson, M. E., Linardi, R. L. & Ortved, K. F. The effect of hypoxia on chondrogenesis of equine synovial membrane-derived and bone marrow-derived mesenchymal stem cells. *BMC Vet Res* **15**, 1–11 (2019).

116. Markway, B. D., Cho, H. & Johnstone, B. Hypoxia promotes redifferentiation and suppresses markers of hypertrophy and degeneration in both healthy and osteoarthritic chondrocytes. *Arthritis Res Ther* **15**, 1–14 (2013).

117. Murphy, C. L. & Sambanis, A. Effect of oxygen tension and alginate encapsulation on restoration of the differentiated phenotype of passaged chondrocytes. *Tissue Eng* **7**, 791–803 (2001).

118. Robins, J. C. *et al.* Hypoxia induces chondrocyte-specific gene expression in mesenchymal cells in association with transcriptional activation of Sox9. *Bone* **37**, 313–322 (2005).

119. Meretoja, V. v., Dahlin, R. L., Wright, S., Kasper, F. K. & Mikos, A. G. The effect of hypoxia on the chondrogenic differentiation of co-cultured articular chondrocytes and mesenchymal stem cells in scaffolds. *Biomaterials* **34**, 4266–4273 (2013).

120. Meerbrey, K. L. *et al.* The pINDUCER lentiviral toolkit for inducible RNA interference in vitro and in vivo. *Proc Natl Acad Sci U S A* **108**, 3665–3670 (2011).

121. Siebler, T., Robson, H., Shalet, S. M. & Williams, G. R. Dexamethasone inhibits and thyroid hormone promotes differentiation of mouse chondrogenic ATDC5 cells. *Bone* **31**, 457–464 (2002).

122. Mello, C. C. & Conte, D. Revealing the world of RNA interference. *Nature* **431**, 338–342 (2004).

123. O'Brien, J., Hayder, H., Zayed, Y. & Peng, C. Overview of microRNA biogenesis, mechanisms of actions, and circulation. *Front Endocrinol (Lausanne)* **9**, (2018).

124. Lieberthal, J., Sambamurthy, N. & Scanzello, C. R. Inflammation in joint injury and post-traumatic osteoarthritis. *Osteoarthritis and Cartilage* Preprint at https://doi.org/10.1016/j.joca.2015.08.015 (2015).

125. Paul, J. *et al.* Donor-site morbidity after osteochondral autologous transplantation for lesions of the talus. *Journal of Bone and Joint Surgery - Series A* (2009) doi:10.2106/JBJS.H.00429.

126. Darling, E. M. & Athanasiou, K. A. Rapid phenotypic changes in passaged articular chondrocyte subpopulations. *Journal of Orthopaedic Research* (2005) doi:10.1016/j.orthres.2004.08.008.

127. Tan, Z. *et al. Synergistic co-regulation and competition by a SOX9-GLI-FOXA phasic transcriptional network coordinate chondrocyte differentiation transitions*. *PLoS Genetics* vol. 14 (2018).

128. Furumatsu, T., Tsuda, M., Taniguchi, N., Tajima, Y. & Asahara, H. Smad3 induces chondrogenesis through the activation of SOX9 via CREB-binding protein/p300 recruitment. *Journal of Biological Chemistry* (2005) doi:10.1074/jbc.M413913200.

129. Sekiya, I. *et al.* SOX9 enhances aggrecan gene promoter/enhancer activity and is up-regulated by retinoic acid in a cartilage-derived cell line, TC6. *Journal of Biological Chemistry* **275**, 10738–10744 (2000).

130. Akiyama, H., Chaboissier, M. C., Martin, J. F., Schedl, A. & de Crombrugghe, B. The transcription factor Sox9 has essential roles in successive steps of the chondrocyte differentiation pathway and is required for expression of Sox5 and Sox6. *Genes Dev* **16**, 2813–2828 (2002).

131. Mohanraj, B. *et al.* Chondrocyte and mesenchymal stem cell derived engineered cartilage exhibits differential sensitivity to pro-inflammatory cytokines. *Journal of Orthopaedic Research* (2018) doi:10.1002/jor.24061.

132. Thoms, B. L., Dudek, K. A., Lafont, J. E. & Murphy, C. L. Hypoxia promotes the production and inhibits the destruction of human articular cartilage. *Arthritis Rheum* **65**, 1302–1312 (2013).

133. Sitcheran, R., Cogswell, P. C. & Baldwin, A. S. NF-κB mediates inhibition of mesenchymal cell differentiation through a posttranscriptional gene silencing mechanism. *Genes Dev* (2003) doi:10.1101/gad.1114503.

134. Saito, T. *et al.* Transcriptional regulation of endochondral ossification by HIF-2α during skeletal growth and osteoarthritis development. *Nat Med* (2010) doi:10.1038/nm.2146.

135. Bédouet, L. *et al.* Synthesis of hydrophilic intra-articular microspheres conjugated to ibuprofen and evaluation of anti-inflammatory activity on articular explants. *Int J Pharm* (2014) doi:10.1016/j.ijpharm.2013.11.004.

136. Whitmire, R. E. *et al.* Self-assembling nanoparticles for intra-articular delivery of anti-inflammatory proteins. *Biomaterials* (2012) doi:10.1016/j.biomaterials.2012.06.101.

137. Kay, J. D. *et al.* Intra-articular gene delivery and expression of interleukin-1Ra mediated by self-complementary adeno-associated virus. *Journal of Gene Medicine* (2009) doi:10.1002/jgm.1334.

138. Agarwal, R. *et al.* Synthesis of self-assembled IL-1Ra-presenting nanoparticles for the treatment of osteoarthritis. *J Biomed Mater Res A* (2016) doi:10.1002/jbm.a.35601.

139. Lieberthal, J., Sambamurthy, N. & Scanzello, C. R. Inflammation in joint injury and post-traumatic osteoarthritis. *Osteoarthritis and Cartilage* Preprint at https://doi.org/10.1016/j.joca.2015.08.015 (2015).

140. Robinson, W. H. *et al.* Low-grade inflammation as a key mediator of the pathogenesis of osteoarthritis. *Nat Rev Rheumatol* **12**, 580–592 (2016).

141. Kapoor, M., Martel-Pelletier, J., Lajeunesse, D., Pelletier, J. P. & Fahmi, H. Role of proinflammatory cytokines in the pathophysiology of osteoarthritis. *Nat Rev Rheumatol* **7**, 33–42 (2011).

142. Molnar, V. *et al.* Cytokines and Chemokines Involved in Osteoarthritis Pathogenesis. *International Journal of Molecular Sciences 2021, Vol. 22, Page 9208* **22**, 9208 (2021).

143. Chen, Z. *et al.* The Immune Cell Landscape in Different Anatomical Structures of Knee in Osteoarthritis: A Gene Expression-Based Study. *Biomed Res Int* **2020**, (2020).

144. Orlowsky, E. W. & Kraus, V. B. The role of innate immunity in osteoarthritis: When our first line of defense goes on the offensive. *Journal of Rheumatology* **42**, 363–371 (2015).

145. Kalaitzoglou, E., Griffin, T. M. & Humphrey, M. B. Innate Immune Responses and Osteoarthritis. *Curr Rheumatol Rep* **19**, (2017).

146. Wehling, N. *et al.* Interleukin-1β and tumor necrosis factor α inhibit chondrogenesis by human mesenchymal stem cells through NF-κB-dependent pathways. *Arthritis and Rheumatism* vol. 60 801–812 Preprint at https://doi.org/10.1002/art.24352 (2009).

147. Hashimoto, K. *et al.* Regulated transcription of human matrix metalloproteinase 13 (MMP13) and interleukin-1β (IL1β) genes in chondrocytes depends on methylation of specific proximal promoter CpG sites. *J Biol Chem* **288**, 10061–10072 (2013).

148. Scanzello, C. R. Chemokines and inflammation in osteoarthritis: Insights from patients and animal models. *Journal of Orthopaedic Research* **35**, 735–739 (2017).

149. Kemble, S. & Croft, A. P. Critical Role of Synovial Tissue–Resident Macrophage and Fibroblast Subsets in the Persistence of Joint Inflammation. *Front Immunol* **12**, (2021).

150. Genin, M., Clement, F., Fattaccioli, A., Raes, M. & Michiels, C. M1 and M2 macrophages derived from THP-1 cells differentially modulate the response of cancer cells to etoposide. *BMC Cancer* **15**, (2015).

151. Compeau, P. E. C. *et al.* Cutadapt removes adapter sequences from high-throughput sequencing reads kenkyuhi hojokin gan rinsho kenkyu jigyo. *EMBnet J* **17**, (2013).

152. Kim, D., Langmead, B. & Salzberg, S. L. HISAT: A fast spliced aligner with low memory requirements. *Nat Methods* **12**, (2015).

153. Pertea, M. *et al.* StringTie enables improved reconstruction of a transcriptome from RNA-seq reads. *Nat Biotechnol* **33**, (2015).

154. Marini, F. & Binder, H. pcaExplorer: an R/Bioconductor package for interacting with RNA-seq principal components. *BMC Bioinformatics* **20**, (2019).

155. Love, M. I., Huber, W. & Anders, S. Moderated estimation of fold change and dispersion for RNA-seq data with DESeq2. *Genome Biol* **15**, 1–21 (2014).

156. Thomas, P. D. *et al.* PANTHER: A Library of Protein Families and Subfamilies Indexed by Function. *Genome Res* **13**, 2129 (2003).

157. Thomas, P. D. *et al.* Applications for protein sequence-function evolution data: mRNA/protein expression analysis and coding SNP scoring tools. *Nucleic Acids Res* **34**, (2006).

158. Ilic, M. Z., Handley, C. J., Robinson, H. C. & Mok, M. T. Mechanism of catabolism of aggrecan by articular cartilage. *Arch Biochem Biophys* (1992) doi:10.1016/0003-9861(92)90144-L.

159. Choi, M. C., Jo, J., Park, J., Kang, H. K. & Park, Y. NF-κB Signaling Pathways in Osteoarthritic Cartilage Destruction. *Cells* **8**, (2019).

160. Jimi, E., Fei, H. & Nakatomi, C. NF-κB Signaling Regulates Physiological and Pathological Chondrogenesis. *Int J Mol Sci* **20**, (2019).

161. Olivotto, E. *et al.* Differential requirements for IKKalpha and IKKbeta in the differentiation of primary human osteoarthritic chondrocytes. *Arthritis Rheum* **58**, 227–239 (2008).

162. Tamiya, H. *et al.* Analysis of the Runx2 promoter in osseous and non-osseous cells and identification of HIF2A as a potent transcription activator. *Gene* **416**, 53–60 (2008).

163. Wang, Y. *et al.* Mesenchymal stem cell–secreted extracellular vesicles carrying TGF-β1 up-regulate miR-132 and promote mouse M2 macrophage polarization. *J Cell Mol Med* **24**, (2020).

164. Zhang, F. *et al.* TGF-β induces M2-like macrophage polarization via SNAILmediated suppression of a pro-inflammatory phenotype. *Oncotarget* **7**, (2016).

165. Zhang, B. *et al.* Mesenchymal stem cells secrete immunologically active exosomes. *Stem Cells Dev* **23**, 1233–1244 (2014).

166. Ragni, E. *et al.* Secreted Factors and EV-miRNAs Orchestrate the Healing Capacity of Adipose Mesenchymal Stem Cells for the Treatment of Knee Osteoarthritis. *International Journal of Molecular Sciences 2020, Vol. 21, Page 1582* **21**, 1582 (2020).

167. Li, C. L., Li, W., Pu, G. Z., Wu, J. W. & Qin, F. Exosomes derived from miR-338-3p-modified adipose stem cells inhibited inflammation injury of chondrocytes via targeting RUNX2 in osteoarthritis. *J Orthop Surg Res* **17**, (2022).

168. Domenis, R. *et al.* Pro inflammatory stimuli enhance the immunosuppressive functions of adipose mesenchymal stem cells-derived exosomes. *Sci Rep* **8**, (2018).

169. Maldonado, M. & Nam, J. The role of changes in extracellular matrix of cartilage in the presence of inflammation on the pathology of osteoarthritis. *Biomed Res Int* **2013**, (2013).

170. Tamiya, H. *et al.* Analysis of the Runx2 promoter in osseous and non-osseous cells and identification of HIF2A as a potent transcription activator. *Gene* (2008) doi:10.1016/j.gene.2008.03.003.

171. Punzi, L. *et al.* Post-traumatic arthritis: Overview on pathogenic mechanisms and role of inflammation. *RMD Open* vol. 2 Preprint at https://doi.org/10.1136/rmdopen-2016-000279 (2016).

172. Prockop, D. J. & Youn Oh, J. Mesenchymal stem/stromal cells (MSCs): Role as guardians of inflammation. *Molecular Therapy* **20**, 14–20 (2012).

173. Mancuso, P., Raman, S., Glynn, A., Barry, F. & Murphy, J. M. Mesenchymal stem cell therapy for osteoarthritis: The critical role of the cell secretome. *Front Bioeng Biotechnol* **7**, (2019).

174. Stöcker, W. & Schlumberger, W. Luminex-Assay. in *Lexikon der Medizinischen Laboratoriumsdiagnostik* (2018). doi:10.1007/978-3-662-49054-9_1980-1.

175. Zhang, H. *et al.* Synovial macrophage M1 polarisation exacerbates experimental osteoarthritis partially through R-spondin-2. *Ann Rheum Dis* (2018) doi:10.1136/annrheumdis-2018-213450.

176. Katagiri, H., Mendes, L. F. & Luyten, F. P. Definition of a Critical Size Osteochondral Knee Defect and its Negative Effect on the Surrounding Articular Cartilage in the Rat. *Osteoarthritis Cartilage* **25**, 1531–1540 (2017).

177. Rzeczycki, P. *et al.* Cannabinoid receptor type 2 is upregulated in synovium following joint injury and mediates anti-inflammatory effects in synovial fibroblasts and macrophages. *Osteoarthritis Cartilage* **29**, 1720–1731 (2021).

178. Orth, P., Zurakowski, D., Wincheringer, D. & Madry, H. Reliability, reproducibility, and validation of five major histological scoring systems for experimental articular cartilage repair in the rabbit model. *Tissue Eng Part C Methods* **18**, 329–339 (2012).

179. Newton, M. D., Osborne, J., Gawronski, K., Baker, K. C. & Maerz, T. Articular cartilage surface roughness as an imaging-based morphological indicator of osteoarthritis: A preliminary investigation of osteoarthritis initiative subjects. *Journal of Orthopaedic Research* **35**, 2755–2764 (2017).

180. Maerz, T., Newton, M. D., Matthew, H. W. T. & Baker, K. C. Surface roughness and thickness analysis of contrast-enhanced articular cartilage using mesh parameterization. *Osteoarthritis Cartilage* **24**, 290–298 (2016).

181. Antons, J. *et al.* Zone-dependent mechanical properties of human articular cartilage obtained by indentation measurements. *J Mater Sci Mater Med* **29**, (2018).

182. Zhu, D., Tong, X., Trinh, P. & Yang, F. Mimicking Cartilage Tissue Zonal Organization by Engineering Tissue-Scale Gradient Hydrogels as 3D Cell Niche. *Tissue Eng Part A* **24**, 1 (2018).